Mass Spectrometry-Based Methods for Analyzing Oxidative Stress-Mediated Cellular ADP-Ribosylation

Dissertation

zur

Erlangung der naturwissenschaftlichen Doktorwürde

(Dr. sc. nat.)

vorgelegt der

Mathematisch-naturwissenschaftlichen Fakultät

der

Universität Zürich

von

Vera Bilan

aus

Russland

Promotionskomitee

Prof. Dr. Dr. Michael O. Hottiger

(Vorsitz und Leitung der Dissertation)

Prof. Dr. Bernd Wollscheid

Prof. Dr. Thierry Hennet

Prof. Dr. Gérard Hopfgartner

Zürich, 2017

“Unter all den stummen Erfahrungen sind diejenigen verborgen, die unserem Leben unbemerkt seine Form, seine Färbung und seine Melodie geben. Der Gegenstand der Betrachtung weigert sich stillzustehen, die Worte gleiten am Erlebten ab, und am Ende stehen lauter Widersprüche auf dem Papier.”

Pascal Mercier, «Nachtzug nach Lissabon»

SUMMARY

Mono- or poly-ADP-ribosylation of proteins in cells is mediated in response to different stress conditions, such as oxidative stress, DNA damage, or ionizing radiation, and is associated with the development of cancer as well as other pathological conditions. Biochemically, the ADP-ribose moiety of NAD^+ is transferred by intracellular diphtheria toxin-like ADP-ribosyltransferases (ARTDs) onto specific acceptor amino acids (MARylation) or to already attached ADP-ribose units (PARylation). Recently, the combination of selective ADP-ribosylation enrichment techniques with mass spectrometric analysis enabled the proteome-wide identification of ADP-ribosylated proteins in different cell types exposed to various stress conditions. However, an in-depth unbiased identification of all ADP-ribosylated proteins (i.e. the ADP-ribosylome) and their qualitative and quantitative changes during various stress conditions has been missing. Thus, the aims of the present thesis were to elucidate the changes in the cellular ADP-ribosylome under different degrees of oxidative stress.

First, we identified the basal as well as the oxidative stress-induced ADP-ribosylome in HeLa cells using a newly developed enrichment protocol based on the Af1521 macrodomain and subsequent mass spectrometry analysis of modified peptides. While the basal ADP-ribosylome mainly contained cytoplasmic proteins, the H_2O_2-induced ADP-ribosylome was mainly characterized by nuclear proteins with DNA and RNA binding properties. Second, we improved the mass spectrometric analysis by utilizing the unique features of ADP-ribose fragmentation to build an ADP-ribosylation specific method based on the combination of HCD and EThcD fragmentations. The high-quality spectra obtained with this method allowed us to identify a lysine-ADP-ribosylation motif. Third, we developed a targeted proteomics method based on parallel reaction monitoring (PRM) to quantify oxidative stress-induced ADP-ribosylation sites in various cell types. We identified two types of ADP-ribosylated proteins: stably ADP-ribosylated proteins maintaining a constant modification level independent of H_2O_2 treatment and H_2O_2-induced ADP-ribosylated proteins, which are significantly ADP-ribosylated upon H_2O_2. Upon treatment with low H_2O_2 concentrations, reduced ADP-ribosylation levels for certain acceptor sites were detected. Moreover, the analysis of ovarian cancer cells revealed variable basal and oxidative stress-induced ADP-ribosylation levels of defined proteins.

Together, the developed methods allow to reproducibly identify and assign ADP-ribose acceptor sites and to quantify the cellular ADP-ribosylome. The application of these mass spectrometry methods will improve understanding the function of cellular ADP-ribosylation in different pathological conditions.

ZUSAMMENFASSUNG

Mono- und poly-ADP-Ribosylierungen sind posttranslationale Proteinmodifikationen in Säugetierzellen, die während Stressreaktionen katalysiert werden können. Beispiele für solche Stressreaktionen sind oxidativer Stress, DNA-schäden, ionisierende Bestrahlung und die damit assoziierten pathologischen Veränderungen. Biochemisch wird ADP-Ribosylierung durch intrazelluläre Diptheria-Toxin ähnliche ADP-Ribosyltransferasen (ARTDs) katalysiert. Dabei wird die ADP-Ribose von NAD^+ auf eine spezifische Aminosäure eines Zielproteins (MARylation) oder ein bereits ADP-ribosyliertes Protein (PARylation) übertragen. Die selektive Anreicherung von ADP-ribosylierten Proteinen oder Peptiden in Kombination mit massenspektrometrischen Messungen führte kürzlich zur Identifikation von diversen ADP-Ribosylierungsstellen im Proteom (ADP-Ribosylom) bei verschiedenen Stressreaktionen in unterschiedlichen Zelltypen. Bis her fehlte allerdings die Identifikation von allen möglichen ADP-Ribosylierungsstellen sowie deren quantitative Veränderung während verschiedenen Stressreaktionen. Das Ziel der vorliegenden Arbeit war es, alle ADP-ribosylierten Proteine (d.h. das gesamte ADP-Ribosylom) während verschiedenen oxidativen Stressstärken zu identifizieren und zu quantifizieren.

In einem ersten Schritt wurde durch die Etablierung eines AF1521-basierten Anreicherungsprotokolls das basale sowie das H_2O_2-induzierte ADP-Ribosylom in HeLa Zellen bestimmt. Im Gegensatz zum basalen ADP-Ribosylom, welches hauptsächlich zytoplasmatische Proteine enthielt, setzte sich das H_2O_2-induzierte ADP-Ribosylom aus Kernproteinen zusammen, die DNA und RNA-Bindungseigenschaften besitzen. Zweitens wurde die massenspektrometrische Methode weiter optimiert. Hierzu wurden die Eigenschaften der ADP-Ribose-Fragmentierung genutzt und eine kombinierte HCD EThcD Fragmentierungsmethode etabliert. Es wurden hochqualitative Spektren aufgenommen, welche die Identifizierung eines Lysin-ADP-ribosylierungsmotivs ermöglichten. Drittens haben wir eine quantitative proteomweite Methode basierend auf dem Parallel Reaction Monitoring (PRM) entwickelt, um das H_2O_2-induzierte ADP-Ribosylom in verschieden Zelllinien zu untersuchen. Mit dieser Methode war es möglich, zwei Gruppen von ADP-ribosylierten Proteinen zu identifizieren: ADP-ribosylierte Proteine, die unabhängig von der H_2O_2-Behandlung konstant modifiziert waren und Proteine, bei denen ADP-Ribosylierung signifikant durch H_2O_2 induziert wurden. Bei sehr geringem oxidativen Stress wurde eine reduzierte ADP-Ribosylierung für gewisse untersuchte Modifikationsstellen beobachtet. Darüber hinaus konnten wir in verschiedenen Krebszelllinien variable basale und oxidativer Stress induzierte ADP-Ribosylierung bestätigen.

Zusammenfassend erlaubt uns die neu entwickelte Methode ADP-Ribose Akzeptorstellen zu identifizierung und zelluläre ADP-Ribosylierung reproduzierbar zu quantifizieren. Anhand dieser massenspektrometrischen Anwendung wird es zukünftig möglich sein, die Funktion von zellulärer ADP-Ribosylierung unter unterschiedlichen pathologischen Bedingungen zu untersuchen.

TABLE OF CONTENTS

ABBREVIATIONS

3-AB	3-aminobenzamide
ARH3	ADP-ribosylhydrolase 3
ART	ADP-ribosyltransferase
ARTC	ART cholera-toxin like
ARTD	ART diphtheria-toxin like
CID	collision-induced dissociation
DBD	DNA binding domain
DSB	double-strand break
ECD	electron capture dissociation
ETD	electron transfer dissociation
HA	hydroxylamine
HR	homologous recombination
ICAT	isotope-coded affinity tag
KO	knockout
m/z	mass to charge ratio
MAR	mono-ADP-ribose
MARylation	mono-ADP-ribosylation
MRM	multiple reaction monitoring
MS	mass spectrometry
NAM	nicotinamide
NHEJ	non-homologous end joining
PAR	poly-ADP-ribose
PARG	poly-ADP-ribose glycohydrolase
PARPi	poly-ADP-ribose polymerase inhibitor
PARylation	poly-ADP-ribosylation
PBD	PAR binding domain
PBZ	PAR binding zinc finger
PRM	parallel reaction monitoring
PTM	posttranslational protein modification
Q	quadrupole
ROS	reactive oxygen species
SILAC	stable isotope labeling by amino acids in cell culture
SRM	single reaction monitoring
SSB	single strand break
SVP	snake venom phosphodiesterase
WT	wildtype

1. INTRODUCTION

1.1. Protein posttranslational modifications - increasing protein complexity

Genome sequencing has identified 20’000-25’000 coding genes in the human genome [5]. Following the classical molecular biology paradigm, “one gene – one protein”, the number of different proteins in the cells equals the number of genes. However, the recent advantages in decoding and annotating the total protein content of human cells (i.e. the human proteome) [6, 7] revealed an overall higher complexity of the proteome compared to the genome. The term proteoform was, therefore, introduced to describe various protein forms of one gene [8]. This increased complexity of the proteome stems from two sources. First source is genome variability and RNA metabolism (e.g. alternative splicing, RNA editing, single-nucleotide polymorphisms) [9]. Second source is alterations in the protein structure coming either from proteolytic cleavage or chemical modification of the amino acid side chains termed protein posttranslational modification (PTM). Among the well-studied examples of PTMs are phosphorylation, acetylation, methylation, and ubiquitination.

Cells utilize PTMs, which dynamically regulate protein activity, localization, and interactions, to quickly respond to changing environmental conditions. The majority of PTMs function in modification cycles, involving sets of enzymes, which write, read and erase the modification. With over 300 different PTMs known, it may not be surprising that 5% of the human genome encodes proteins responsible for catalyzing the metabolism of PTMs [10]. The transient nature of PTMs enables them to act as a regulatory switch, activating or inactivating enzymes. The best-known example is phosphorylation, which regulates kinase activity in many signaling cascades. Around 30% of the proteome is expected to be phosphorylated at any given time point [11]. Together, these events can potentially generate about 50-60 proteoforms. Thus, the human proteome is estimated to consist of up to 1.5 million proteoforms [12], although the exact number remains elusive.

Understanding the PTMs cellular function and dynamics is an important task of molecular biology. However, the tools to study PTMs are limited and many PTMs were discovered using basic biochemical approaches applied to single isolated proteins [13]. The development of mass spectrometry-based proteomics boosted the analysis of PTMs [12].

1.2. ADP-ribosylation is a highly dynamic protein posttranslational modification

ADP-ribosylation is a highly dynamic, ancient, reversible PTM (Figure 1). Originally studied in bacteria as a mechanism of toxin action [14], ADP-ribosylation is also present in archaebacteria and eukaryotic cells. The reaction of ADP-ribosylation starts with the transfer of an ADP-ribose moiety from NAD^+ onto the target protein by specific enzymes (Figure 1, discussed in 2.3). This initiation reaction generates mono-

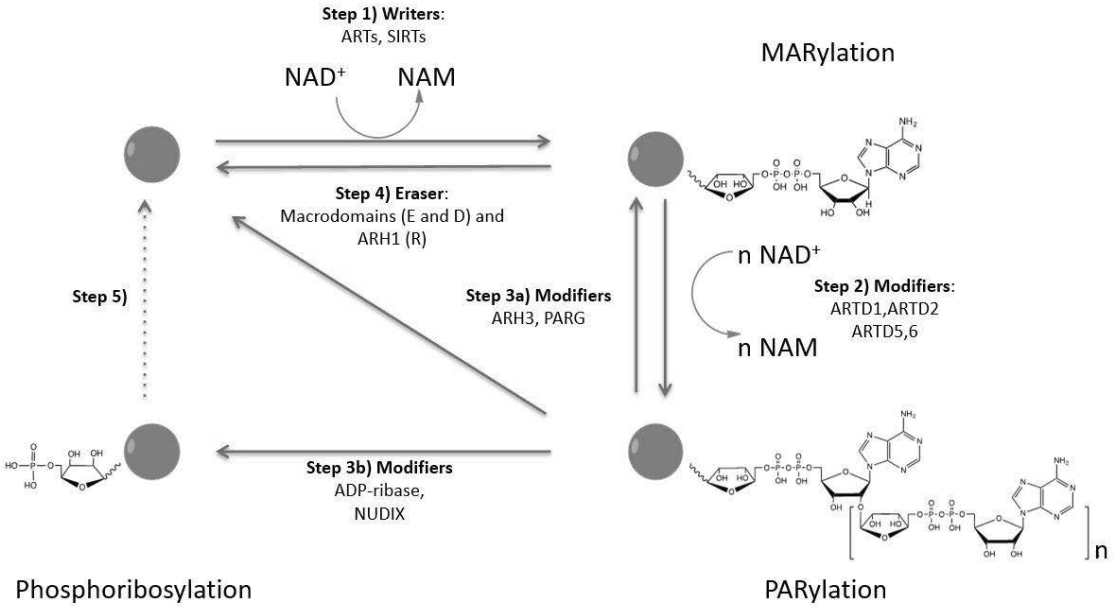

Figure 1. ADP-ribosylation cycle. 1. Initiation step – MARylation reaction 2. Elongation step – PARylation reaction. n is a number of ADP-ribose units attached to the MARylated protein and the number of consumed NAD^+ molecules. 3a. Degradation of PAR chains. 3b. Modification reaction - hydrolysis of pyrophosphate bond. Phosphoribose residue stays on the proteins. 4. Complete reversion of MARylation. The enzymes reversing the ADP-ribosylation and their specifically is indicated. 5. An unknown step of phosphoribose cleavage from modified proteins.

ADP-ribosylation (MARylation). Several enzymes can then extend MARylation and attach additional ADP-ribose units producing poly-ADP-ribosylation (PARylation). Whereas MARylation is widely observed within the entire taxon, PARylation is limited mainly to multicellular eukaryotes [15]. Moreover, the half-life of PAR is short compared to the relatively stable MAR [16].

The changes that PARylation triggers in modified proteins and cellular environment explain the transient nature of the modification. PAR is a large modification, sometimes exceeding the size of the modified protein. Carrying two negative charges per ADP-ribose unit, it can vastly change the physical properties of the modified proteins. Moreover, synthesis of PAR consumes NAD^+ molecules, an essential cofactor in energy metabolism. The NAD^+ pool can be almost completely

depleted at severe genotoxic stress [17]. In these cases, following ATP depletion leads to cell death [16].

Two types of chemical linkages between ADP-ribose and an acceptor site exist. An ester linkage connects the modification to acidic amino acids (aspartic and glutamic acids), whereas a ketamine bond is formed at lysines and arginines (Figure 2)

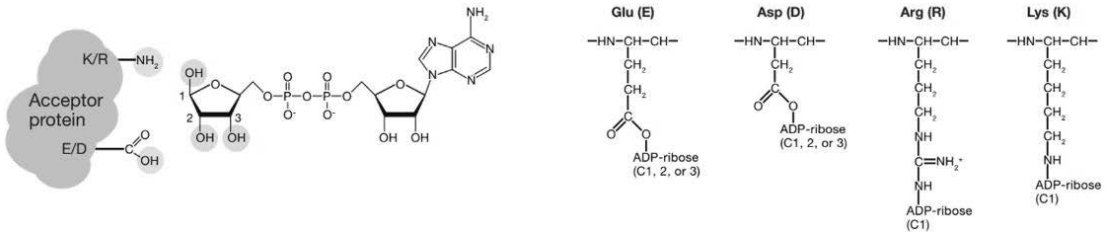

Figure 2. Chemical linkages between ADP-ribose and four best-studied acceptor sites. The numbers on the ribose ring indicate the stereo-specificity of a specific linkage. Adapted from [4].

[4]. Additionally, cysteine, diphthamide, phosphoserine, and asparagine serve as possible acceptor sites of ADP-ribosylation [18]. Interestingly, non-enzymatic conjugation of ADP-ribose to lysine formed via Amadori rearrangement, called glycation, exists, occurring at high pH values and high concentrations of free ADP-ribose [19]. The non-physiological conditions of the reaction make it arguable whether it occurs in cells.

1.3. ARTDs – intracellular writers of ADP-ribosylation

Several groups of enzymes catalyze ADP-ribosylation: ADP-ribosyltransferases (ARTs) and sirtuins 1 and 3. The ARTs family is subdivided into ARTDs (diphtheria toxin-like ARTs) and ARTCs (the structurally distinct cholera toxin-like ARTs) based on their structural similarity to bacterial toxins. ARTCs are located at the cellular membrane and mainly modify extracellular proteins [20], whereas ARTDs are located in different cellular compartments and responsible for the modification of intracellular proteins (Table 1) [15].

There are 17 members of ARTDs (also known as PARPs) in humans. The enzymes are grouped together based on their structural features [15]. Despite their similarity, ARTDs show various enzymatic activities. The majority of ARTDs only catalyze MARylation [21]. ARTD1 is the first studied enzyme with PARylation activity. The ability to produce PAR chains is associated with the characteristic H-Y-E motif within the catalytic domain [22]. Indeed, four enzymes with this motif perform PARylation: ARTD1, ARTD2, ARTD5 and 6.

Enzyme	Motif	Activity	Localization
ARTD1 (PARP1)	H-Y-E	PAR	nucleus
ARTD2 (PARP2)	H-Y-E	PAR	nucleus
ARTD3 (PARP3)	H-Y-E	MAR	nucleus, cytoplasm
ARTD4 (vPARP, PARP4)	H-Y-E	MAR	nucleus, exosome, cell membrane
ARTD5 (PARP5a, TNKS1)	H-Y-E	PAR	nucleus, Golgi, cytoplasm
ARTD6 (PARP5b, TNKS2)	H-Y-E	PAR	nucleus, Golgi, cytoplasm
ARTD7 (PARP15, BAL3)	H-Y-I	MAR	cytoplasm
ARTD8 (PARP14, BAL2)	H-Y-I	MAR	nucleus, cell membrane
ARTD9 (PARP9, BAL1)	Q-Y-T	inactive	nucleus, cytoplasm, cell membrane
ARTD10 (PARP10)	H-Y-I	MAR	nucleus, cytoplasm
ARTD11 (PARP11)	H-Y-I	MAR	nucleus, cytoplasm
ARTD12 (PARP12)	H-Y-I	MAR	cytoplasm
ARTD13 (PARP13, ZC3HAV1)	Y-Y-V	inactive	cytoplasm
ARTD14 (PARP7, tiPARP)	H-Y-I	MAR	nucleus, cytoplasm
ARTD15 (PARP16)	H-Y-I	MAR	cell membrane, endoplasmic reticulum
ARTD16 (PARP8)	H-Y-I	MAR	cytoplasm
ARTD17 (PARP6)	H-Y-I	MAR	cytoplasm

Table 1. Summary of ARTD family member's reported enzymatic activity, catalytic motif, and cellular localization. Modified from [21], [4].

ARTD1 is a 114 kDa nuclear protein consisting of a catalytic domain, a DNA binding domain (two Zn-finger motifs and one Zn finger domain), a nuclear localization signal, an automodification domain (including a BRCA1 C-terminal motif), and a WGR motif [23, 24]. PAR chains produced by ARTD1 can reach a total length of up to 200 units *in vitro* [25]. The elongation reaction is dependent on E988 in the catalytic domain of ARTD1. Mutation of E988, however, does not inactivate ARTD1 but limits its activity to MARylation [26]. This fact indicates an enzymatically different mechanism of the elongation reaction in comparison to the initiation reaction. Moreover, ARTD1 also branches the polymers every 20-40 ADP-ribose units [27, 28]. A 2"-1" O-glycosidic ribose bond connects ADP-ribose units in

an elongation reaction, whereas a 2”-1” glycosidic bond is formed upon branching. Indeed, the ARTD1 catalytic pocket can fit ADP-ribose in both orientations (rotation of 180^{o}) for elongation and branching [29]. However, the physiological function of branched polymers is still unclear.

ARTD5 and 6 (also known as tankyrases (TNKS) are the last ARTD enzymes with proven PARylation activity. However, they lack branching activity and produce only short linear PAR up to 20 units long [30]. They share a highly conserved structure, which is different from other ARTD members [31]. Although initially localized to the nucleus, ARTD5 and 6 are present in the cytoplasm, Golgi complex and transport vesicles [21, 32]. The activity of ARTD5 and 6 is linked to the regulation of protein turnover by ubiquitination [33].

The remaining ARTD family members catalyze MARylation (except ARTD9 and ARTD13, which are postulated to be inactive). Despite the fact that ARTD3 has the characteristic H-Y-E motif, it performs MARylation only [34]. The presence of R instead of M890 in the ARTD3 catalytic pocket partially explains the difference in the enzymatic activity of ARTD1 and ARTD3 [31]. Together with ARTD1 and ARTD2, ARTD3 is commonly referred to as a DNA-dependent ARTD. ARTD1 recognizes DNA via zinc-finger domains, whereas ARTD3 and ARTD2 have WGR domains allowing them to bind DNA and/or RNA [35]. Interestingly, the type of DNA template and specific DNA breaks define the activity of the enzymes [36]. The activation upon binding to DNA breaks defines their key function in DNA repair (discussed in more detail in 1.6.1).

Other ARTDs localize to various cellular compartments and have diverse domain organizations. ARTD4 is another enzyme with an H-Y-E motif and only MARylation activity. The inability of ARTD3 and ARTD4 to produce PAR indicates that additional structural differences discriminate between PARylation and MARylation activity. Interestingly, three enzymes, i.e. ARTD7, ARTD8 and ARTD9 possess macrodomains (described below) which enable them to bind ADP-ribosylated proteins [29]. However, due to the limited tools to study MARylation, the structure, activity, and function of these enzymes stay poorly understood.

1.4. ADP-ribose binding domains

In various cellular signaling events, PAR and MAR are recognized by different protein domains, so-called readers. Depending on the binding affinity, the readers are either specific for PAR or able to bind both PAR and MAR (Figure 3). The PAR binding

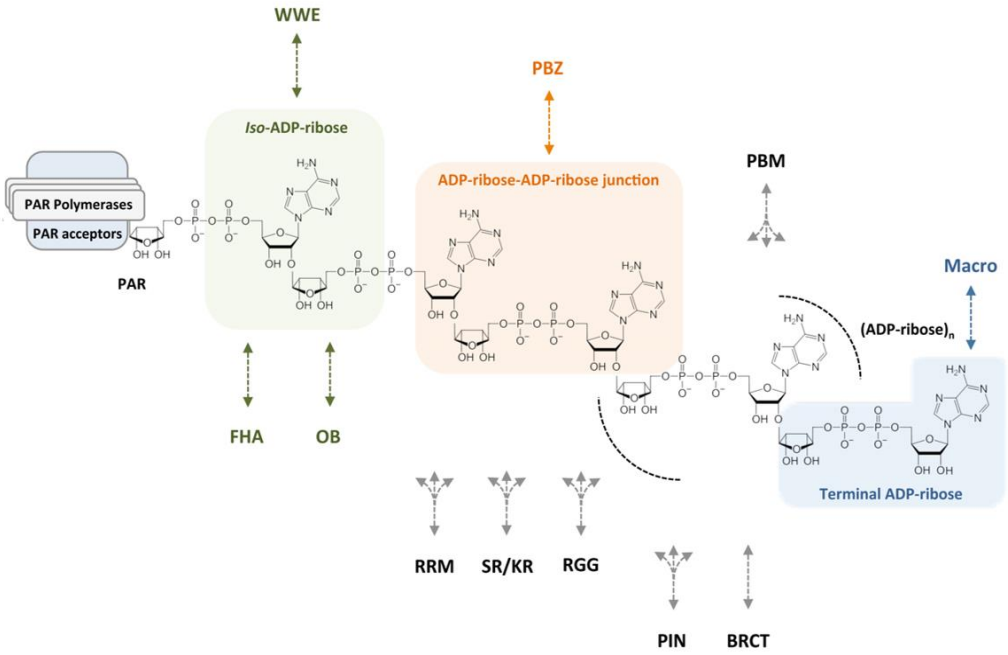

Figure 3. ADP-ribose binding domains. The colored areas on the ADP-ribose structure indicate the known affinity of the domains. Modified from [2].

domain, the PAR binding zinc finger (PBZ), and the WWE domain are specific PAR binders. The macrodomain is an example of a protein fold with both PAR and MAR binding affinity. The first discovered PAR-binding motif was the PAR binding domain. It is mainly present in proteins involved in DNA repair and chromatin remodeling [37]. The PAR binding zinc finger is another example of a domain which specifically binds PAR [38]. However, only two proteins involved in the DNA damage response i.e. APFL and CHFR, possess a PBZ domain [39].

The WWE domain functionally links ADP-ribosylation and ubiquitination since it is mainly found in ubiquitin ligases and several ARTD family members [40]. The domain received its name by the presence of three characteristic amino acids (W – tryptophan, E – glutamate). The domain functions through the recognition of an iso-ADP-ribose moiety, surrounding the α(1→2) O-glycosidic bonds [41] and can, thus, specifically interact with PAR but not MAR.

The macrodomain fold is a conserved domain of 130–190 amino acids [42, 43], which binds to various forms of ADP-ribose including free ADP-ribose [44]. This affinity toward different versions of ADP-ribose allows macrodomains to bind both PARylated and MARylated proteins. Ten macrodomains, e.g. histone variant macroH2A and O-acetyl-ADP-ribose deacetylase (MacroD1), are present in human cells. Interestingly, macrodomains were also identified in archaebacteria [45]. Moreover, archaebacterial protein Af1521 from *Archaeoglobus fulgidus* has one of the highest identified affinities to ADP-ribose (K_d of 130 nM) [44]. Based on this high affinity, Af1521 was successfully tested in pull-downs of ADP-ribosylated proteins from complex cellular mixes [46]. In addition to their PAR binding activity, some macrodomain-containing proteins including Af1521 hydrolyze and release ADP-ribose from MARylated proteins modified on glutamic and aspartic acids [47, 48]. Additional ADP-ribose binding domains, e.g. the OB-fold or the BRCT domain, have been discovered recently. However, for many of them, the binding affinity has not been extensively studied yet [2].

1.5. Erasers/Modifiers: reversing the modification

Degradation of PAR chains and removal of MAR from proteins complete the cycle of ADP-ribosylation. Depending on their activity, ADP-ribosylation catabolizing enzymes are grouped into three categories. The first group is active against PAR chains; the second group catabolizes MARylation: the last is modifying ADP-ribosylation (Table 2).

Two enzymes can hydrolyze PAR chains: PAR glycohydrolase (PARG, [49]) and PAR hydrolase (ARH3, [50]). PARG has five isoforms, produced from one gene by alternative splicing and localized to different cellular compartments [51]. The most abundant 110 kDa isoform of PARG is a nuclear enzyme responsible for the fast turnover of PAR upon DNA damage. Despite the relatively low abundance, PARG degrades PAR chains within minutes after a certain DNA damage stimulus [52]. PARG KO mice die during embryonic development, and even downregulation of PARG activity sensitizes cells to DNA damaging agents. These observations indicate an important function of PARG in stress responses and DNA repair [53]. PARG, as well as ARH3, possess endo- and exoglycosidase activity, however, are unable to cleave MAR from proteins (Figure 1). ARH1 was the first identified enzyme to

Enzyme	Isoforms/Proteins	Activity	Localization
PARG	111 kDa	Endo- and exoglycosidase, to PAR	nucleus
	102, 99, 60 kDa		cytoplasm
	55 kDa		mitochondria
ARH1	39 kDa	Glycosidase (specific to R), to MAR	cytoplasm
ARH3	39 kDa	Endo- and exoglycosidase, to PAR	nucleus, cytoplasm, mitochondria
Macrodomains	MacroD1/MDO1 35 kDa	Glycosidase (specific to D and E), to MAR	nucleus, cytoplasm
	MacroD2/MDO2 50 kDa		
	C6orf130/TARG 17 kDa		

Table 2. Summary of ADP-ribosylation hydrolases indicating their enzymatic activity and cellular localization. Modified from [16].

completely reverse the modification specifically from arginines [54]. As mentioned before, some of the macrodomains have the ability to cleave ADP-ribose from aspartic and glutamic acids. The enzyme responsible for removing MARylation from lysines is yet to be discovered.

Enzymes with phosphatase activity have the ability to modify ADP-ribosylation. Among the known examples are snake venom phosphodiesterase (SVP) and the NUDIX family. SVP is a phosphatase which cleaves the pyrophosphate bond between adenosine monophosphate and phosphoribose, leaving the latter attached to the protein [54]. The NUDIX family of pyrophosphatases consists of 24 genes in humans. NUDIX family analogs are found in *E. coli*, yeast, and archaebacteria. NUDT9 and NUDT14 have experimentally proven hydrolase activity against ADP-ribose, and NUDT6 has a similar predicted activity [55]. Recently, the *E. coli* enzyme EcRppH and human NUDT16 were shown to reverse ADP-ribosylation of proteins *in vitro* [56]. These enzymes may play a major role in the elimination of free ADP-ribose after oxidative stress and PAR degradation by PARG.

1.6. Function of ARTD1-mediated PARylation

The diversity of ARTD enzymes and their localization indicate the involvement of ADP-ribosylation in various cellular events. Little is still known about the function and regulation of MARylation. The few examples of studied MARylation signaling

include transcriptional regulation of STAT6 signaling (ARTD8 activity) [57] and regulation of inflammation via NF-κB Signaling (ARTD10 activity) [58]. The main obstacles in MARylation research are the limited number of available methods and poor understanding of ARTD activity, specifically stimuli, which trigger a response. On the other hand, stimuli inducing PAR are well known and include genotoxic and oxidative stress.

1.6.1. Role of ARTD1 in genome stability

ADP-ribosylation has a key function in DNA strand break repair, a fundamental cellular pathway ensuring genome stability. The type of generated DNA break defines a specific repair pathway. Single-strand break (SSB) repair is executed via base excision adducts. Double-strand breaks (DSB) are repaired via non-homologous end joining (NHEJ) or homologous recombination (HR) [59]. The HR pathway is error-free and preferred in cells, however, can be executed only during late S- and G2-phases, where sister chromatids are available as templates [60]. Accumulation of PAR was observed in response to various genotoxic agents (e.g. ionizing radiation, alkylating agents). Thus, ADP-ribosylation plays a role in all four repair pathways. ARTD1, ARTD2, and ARTD3 are the nuclear enzymes associated with DNA repair. ARTD1, however, is responsible for up to 90% of occurring PARylation [61]. ARTD1 recognizes and binds both SSB and DSB with its DNA binding (DB) domain [62]. Binding to DNA activates ARTD1 *in vitro* by inducing conformational rearrangements within the WGR domain [63] and, therefore, increasing its activity up to 500 fold. ARTD1 activation leads to the fast accumulation of PAR chains in the nucleus. Among the targets of ARTD1 are ARTD1 itself (auto-modification), histones, and topoisomerase I [17, 64]. Modification of histones leads to the accumulation of negative charges and the relaxation of the chromatin structure. This enables easy access of DNA repair proteins to the DNA breaks [65]. Another function of PAR in DNA repair is the recruitment of key DNA repair proteins to the site of the damage. E.g., recruitment of XRCC1 (in SSB repair) and ATM, Mre11, and Nbs1 (in HR) is dependent on PAR formation and ARTD1 activity [64, 66]. An XRCC1 PAR-binding domain was identified recently [67] and the presence of PAR binding protein sequences was hypothesized for ATM and Mre11 [64, 68]. Nevertheless, the exact mechanism of recruitment for other proteins has not been extensively studied.

Despite the major role of ARTD1 in genome stability, ARTD1 KO mice are viable and fertile, and show residual PAR formation upon genotoxic treatment [69], which can be explained by functional redundancy within the ARTD family. Moreover, the ARTD1 and ARTD2 double KO mice are not viable and die at the gastrulation stage [70]. Interestingly, HR still functions in an ARTD1$^{-/-}$ background. ARTD1$^{-/-}$ mice are not predisposed to tumor formation [71], and Rad51 foci are still formed in response to hydroxyurea in ARTD1$^{-/-}$ cells [72]. Nevertheless, inhibition of ARTD1 leads to an increase in HR [72] and micronuclei formation [73], confirming an important role of ARTD1 in genome stability. Interestingly, the double knockout of ARTD1 together with other DNA repair proteins (e.g. XRCC5 [74] or ATM [75]) is embryonically lethal, whereas single KO mouse models of these proteins are viable, indicating their synergistic key function in DNA repair.

1.6.2. Role of ARTD1 in oxidative stress

A well-known trigger of genomic instability is oxidative stress. Induction of PAR in the nucleus upon H_2O_2 treatment was detected long ago. However, the precise mechanism on how PARylation contributes to the oxidative stress response is still unclear. Oxidative stress is a cellular condition caused by a misbalance of reactive oxygen species (ROS) accumulation and their neutralization. Cellular ROS i.e. superoxide radicals (O_2^-), hydrogen peroxide (H_2O_2) and hydroxyl radicals (·OH) come from endogenous and exogenous sources [76]. Exogenous sources include UV light, smoke, and ionizing radiation. Endogenous ROS are produced in mitochondria and peroxisomes. Since production of ROS is an unavoidable product of cellular metabolism, cells are equipped with an antioxidant defense system. The antioxidant defense includes superoxide dismutase, catalase, and glutathione peroxidase, which neutralize $O_2\cdot^-$, and H_2O_2, respectively [77]. Pathological conditions like chronic inflammation and hypoxia induce the accumulation of ROS, which cannot be effectively inactivated via the antioxidant defense. ROS cause macromolecule oxidation, thereby damaging lipids, proteins and nucleic acids, i.e. DNA. ROS-induced DNA damage is mainly repaired via the BER pathway, whose execution depends on ARTD1 and PARylation. For a long time, oxidative stress-induced PARylation was thought to be associated with binding and activation of ARTD1 to sites of DNA damage. Recent studies, however, suggest new functions of ARTD1. Oxidative stress-induced DNA damage alone is not sufficient to induce PAR

formation. Moreover, activation of ARTD1 is dependent on the balance of PKCα dependent eviction of HMGB1 from the nucleus [78]. Euchromatic regions are believed to be highly sensitive to genotoxic stress and thus should have a high level of PARylation. However, stress-induced PARylation is present on heterochromatic regions [79]. PAR accumulation at heterochromatic regions potentially protects histone marks and induces chromatin relaxation, pointing at an epigenetic function of ARTD1 and PARylation in genotoxic stress [79]. These recent observations indicate the broad function of ARTD1 and PARylation in oxidative stress and further studies should be performed to fully understand it.

1.6.3. ARTD1-mediated PARylation functions beyond stress signaling

Besides its function in genotoxic stress signaling and oxidative stress, ARTD1 regulates transcription and cell differentiation. ARTD1 is enriched at the promoters of active genes and enhancers, indicating its function in regulation of gene expression [80]. PAR chains promote recruitment of several chromatin modifier proteins: members of the polycomb group, transcriptional repressor proteins, and deacetylase complexes [81]. Moreover, ARTD1 was also shown to bind nucleosomes with intact DNA [82]. Physiologically occurring DNA breaks can activate ARTD1, e.g. DNA breaks induced by topoisomerase II β [83]. Interestingly, similar functions were reported for other DNA-binding ARTDs. ARTD2 negatively regulates SIRT1 [84] and ARTD3 is enriched on developmental genes [85]. These observations point to a function of PARylation in transcriptional regulation. PARylation mediated by ARTD1 also regulates cell differentiation. E.g, maturation of adipocytes is dependent on ARTD1 binding to PPARγ2 [86]. Similarly, ARTD1 regulates differentiation of astrocytes, osteoclasts, and myocytes as well as immune cells [16].

1.7. ADP-ribosylation inhibitors as therapeutic agents

Due to the critical role of ADP-ribosylation in genomic stability, ARTDs activity is considered as a valuable target for therapeutic intervention. The first inhibitor targeting ARTDs (generally named as PARP inhibitors (PARPi)) was 3-aminobenzamide (3-AB) developed over 30 years ago by Purnell and colleagues [87]. Many developed PARPi have structural similarity to nicotinamide (NAM) (e.g. 3-AB or olaparib) and act via blocking the NAM binding pocket within the active site of ARTDs. Since ARTD family members are structurally very similar, these PARPi are

not specific. Indeed, the screening of a chemical library consisting of 185 compounds showed that 56% of tested PARPi also block ARTD2 and 3, and 36% ARTD4 [88]. The broad inhibition spectrum of these PARPi leads to problems with understanding their mechanism of action. Recently, new chemical structures have been developed, i.e. substances targeting the DBD of ARTD1, which potentially can increase the specificity of the drugs [89].

1.7.1. Mechanism of action of PARP inhibitors

The exact mechanism on how PARPi kill cancer cells is still debatable. Three theories were proposed. "Synthetic lethality" underlies the role of ARTD1 in DNA repair; the second theory postulates the trapping of inactivated ARTD1 on chromatin, and the last theory explains the mechanism by disturbances in NAD^+ metabolism.

The widely accepted PARPi action mechanism is the "synthetic lethality" theory. According to this theory, inactivation of two key genes in one specific pathway leads to cell death. However, inactivation of either gene alone is not lethal [90]. In cancer, HR is commonly inactivated. Upon ARTD1 inhibition, HR-deficient cancer cells accumulate DNA breaks that are either not repaired or inefficiently repaired in an error-prone way. Accumulation of unrepaired DNA breaks leads to genomic instability and subsequently to cell death [91].

In recent years, an alternative mechanism of PARPi action was suggested. Based on this alternative theory, PARPi trap ARTD1 at sites of DNA damage, and thus obstruct DNA repair and transcription [92]. Interestingly, the property of PARPi to trap ARTD1 does not correlate with their enzymatic inhibitory property [93]. Understanding of this mechanism can potentially help to identify new cancer types that are sensitive to PARPi.

Based on the last theory, the activity of ARTD1 regulates NAD^+ concentration in the nucleus. SIRT1, another NAD^+ consuming enzyme, is activated by increased levels of NAD^+ in $ARTD1^{-/-}$ cells [94]. This activation leads to the induction of transcription factors regulating mitochondrial biogenesis. Cancer cells shift their energy metabolism to glycolysis (known as the "Warburg effect"), bypassing slow oxidative phosphorylation pathway. Glycolysis provides a fast energy source for cancer cells, allowing their accelerated growth rate [95]. Indeed, the activation of mitochondria upon PARPi administration potentially restores their involvement in energy metabolism and thus kills energy-demanding cancer cells [96].

1.7.2. Cancer treatment options with PARP inhibitors

The attention to PARPi increased when two studies reported sensitivity of BRCA-deficient cancer cells to PARPi [97, 98]. Plenty of PARPi underwent clinical studies for cancer treatment. Recently, the third generation of PARPi was approved for monotherapeutic treatment of BRCA negative ovarian cancers and BRCA1/2 or ATM negative metastatic castration-resistant prostate cancers [99].

Due to the key function of BRCA1 and 2 in HR, mutations in BRCA1 and BRCA2 are associated with the development of various cancer types. E.g., women who carry BRCA1 or BRCA2 gene deletions have a 40% and 20% lifetime risk to develop ovarian cancer and breast cancer, respectively [100]. The prevalence of these mutations in ovarian cancer is around 10-15% [101], with certain types reaching up to 44% of diagnosed cases [102]. The cancer phenotype similar to BRCA1 or 2 deletions was termed "BRCAness". The BRCAness phenotype is associated with HR deficiency that can be caused by inactivation of the BRCA gene or with a loss-of-function mutation in other HR genes [103]. Based on the synthetic lethality theory, BRCAness cells should be sensitive to PARPi. However, due to various types of BRCA mutations, genomic instability of cancer cells, and complex regulation of cancer cells in general, the response to PARPi is hard to predict [103]. Thus, various screening methods (BRCA mutations screen, mutation signatures of HR-deficient cells) are used to screen and predict a patient's response to PARPi.

PARPi can also be administrated in a combination therapy together with other cancer therapeutic agents. For many combinations and in various cancer types, the severe side effects such as eutropenia, thrombocytopenia, and myelosuppression were observed [104, 105]. Nevertheless, some combinatorial therapies showed acceptable toxicity, e.g. a combination of olaparib with the microtubular toxin paclitaxel for the treatment of breast, non-small cell lung, and ovarian cancer [106]. An aggressive triple-negative breast cancer showed a response to PARPi administrated together with nicotinamide phosphoribosyltransferase inhibitors [107]. Despite the fact that triple negative cancers have a BRCAness phenotype, sensitivity to PARPi is dependent on the NAD^+ metabolism of these cells. At the moment, 52 clinical studies are evaluating the efficiency of PARPi in combination with conventional treatments [108]. Thus, further studies should elucidate the PARPi mechanism of action in cancer cells to identify sensitive cancer types and to better predict the outcome of a certain treatment.

1.8. Shotgun approach to study protein posttranslational modifications

The application of mass spectrometry to study the cellular proteome started in the early 1990s [109]. The "classical" approach to unravel the proteome is the shotgun method (also named bottom-up approach) [110]. In this approach, cellular proteins are first digested with trypsin or other proteases. The resulting peptide mix is further analyzed using liquid chromatography connected to a tandem mass spectrometer (LC-MS/MS). Subsequent bioinformatics analysis aims to correspond the acquired spectra with the theoretical fragmentation of peptides obtained from a protein database. For this complex analysis, several algorithms were developed, e.g. Mascot [111] and Andromeda [112]. The development of mass spectrometry-based proteomics allows the identification of several thousand proteins in one short MS/MS measurement [113, 114].

Analysis of PTMs brings an additional level of complexity to proteomic studies. The attachment of a chemical group shifts the molecular weight of the peptide, making it difficult to assign the correct sequence. The fact that PTMs are only present on a small number of peptides in the complex sample increases the complexity of the downstream bioinformatics analysis. PTMs change the physical and chemical characteristics of modified peptides, which can lead to a lower detection efficiency [12]. Depending on the size and localization of a modification, the protease digestion can be limited and incomplete, leading to miscleavages. Additionally, the abundance of PTMs in the cellular proteome is low, making it challenging to detect them in complex mixtures such as cell lysates. More abundant, non-modified peptides cover the lower signals of a modified peptides. To increase the identification level of PTMs, enrichment steps developed specifically for certain PTMs are necessary.

1.9. Enrichment strategies for ADP-ribosylation

In general, enrichment strategies developed for ADP-ribosylation can be divided into three categories: chemical enrichments (e.g boronic beads enrichment and phosphoenrichment methods), affinity-based enrichments (e.g. using protein-binding domains or antibodies), and click-chemistry methods in combination with special ADP-ribose labeling approaches.

1.9.1. Chemical enrichments

Okayama *et al*. first applied boronate beads for purification of ADP-ribosylated proteins from rat liver in 1978. In the study, H1 and H2B were identified as acceptors of ADP-ribosylation [115]. The mechanism of the enrichment is based on the formation of an ester linkage between the boronate group and the 1,2-cis-diol moiety of ADP-ribose under alkaline conditions (pH > 8). The release of the bond occurs at low pH values (pH < 6). However, such pH changes are not optimal due to the chemical sensitivity of the ADP-ribose linkage. Depending on the ADP-ribosylation linkage type, ADP-ribose can be lost from the protein during this enrichment procedure [116]. Recently, Zhang *et al*. suggested hydroxylamine (HA) elution as an alternative to pH change [117]. During the elution, HA attacks the ester bond formed between an aspartic or glutamic acid and ADP-ribose. As a result, released peptides gain a characteristic mass shift of +15.01 Da, which is detected by MS/MS (Figure 4A). Using this approach, Zhang *et al*. were able to identify 340 ADP-ribosylated

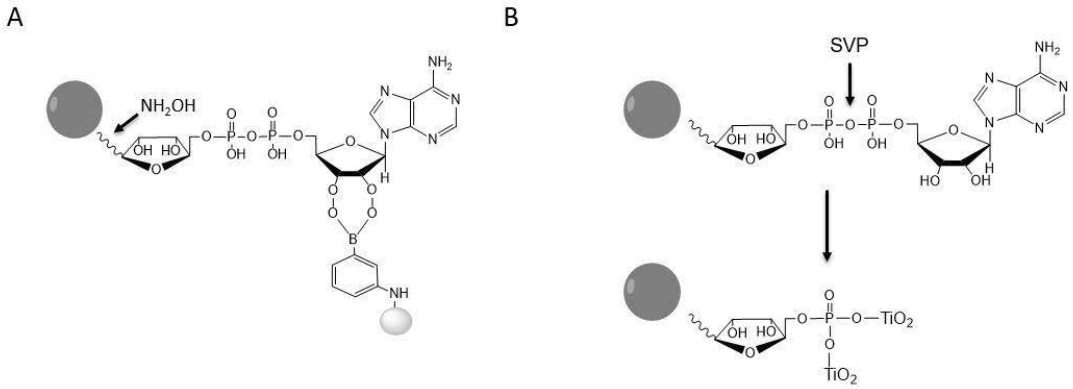

Figure 4. Enrichment of ADR-ribosylated proteins with chemical enrichment methods. A) Boronic beads enrichment with HA elution. The arrow points at the bond attacked by HA. B) Phosphoenrichment methods for the pull-down of ADP-ribosylation. In this example, TiO_2 binding is used for phosphoenrichment. The arrow indicates the bond cleaved by SVP.

proteins in HCT116 cells upon exposure to 1 mM H_2O_2. However, the study was performed in a $PARG^{-/-}$ background. The use of wildtype cells with this method significantly decreases the identification level of enriched peptides [117]. Moreover, the boronate beads also enrich glycoproteins due to the presence of ribose rings in their structure.

Due to the presence of phosphate groups in the ADP-ribose structure, PAR and MAR proteins can be enriched with phosphoenrichment techniques. Enrichments with TiO_2 or IMAC are well developed and standardized methods in phosphoproteomics

[118]. Indeed, ADP-ribosylated proteins have been identified in phosphoproteomics datasets [119]. Daniels *et al*. have further optimized phosphoenrichment methods for *in vitro* and *in vivo* ADP-ribosylated samples [120]. An SVP digest of peptides introduced before the enrichment aims at increasing the binding as well as decreasing the complexity of the modification (Figure 4B). However, in cellular samples, the use of this enrichment is limited due to the competition with the more highly abundant phosphopeptides.

1.9.2. Affinity purification with ADP-ribose binding domains

The first domain used for the enrichment of ADP-ribosylated proteins was the macrodomain Af1521 [46]. The combination of Af1521 enrichment with LC-MS/MS led to the identification of 235 ADP-ribosylation associated proteins in HeLa cells exposed to various stress conditions [121]. However, since the study has not assigned the ADP-ribosylated acceptor sites, it is not clear whether all identified proteins were ADP-ribosylated or only interacted with PAR, MAR or modified proteins.

1.9.3. Specific ADP-ribose labeling approaches

Various labeling methods were developed for several PTMs, allowing a specific enrichment via an introduced tag. To label ADP-ribosylation, various analogues of NAD^+ have been developed. It is hard to perform *in vivo* labeling of ADP-ribosylation, because NAD^+ analogues synthesized so far cannot penetrate cells due to their size. Thus, using NAD^+ analogues lacks the biologically relevant context, as the linkage to proteins is performed after disruption of the cellular compartments. All published methods so far are performed *in vitro* or using cellular lysates. Endogenously present ARTDs can catalyze the labeling with biotinylated NAD^+ [122], or 1,-N6-alkyne-NAD [123]. Another NAD^+ analogue, 8-Bu(3-yne) T-NAD^+, requires spiking engineered analog-sensitive ARTD enzymes, since it cannot be used as a substrate by endogenous enzymes [124]. Moreover, ARTDs inefficiently metabolize NAD^+ analogues, due to their bulky structure. The use of engineered ARTDs on the other side requires KO of the endogenous enzymes, which might perturb cell metabolism.

1.10. MS-based identification of ADP-ribosylation

The fragmentation of ADP-ribose was first tested using collision-induced dissociation (CID) [1]. Using CID, ADP-ribose fragments and produces characteristic ions (Figure 5). At the same time, fragmentation of ADP-ribose leads to the complete loss

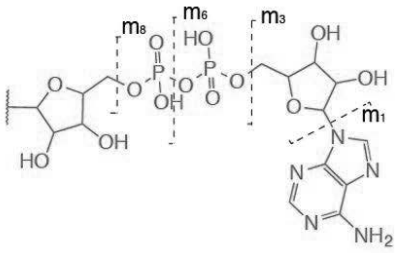

Ion	Fragment	Label
136.06	Adenine$^+$	m_1+
250.09	Adenosine-H_2O^+	m_3+
348.05	Adenosine-mono phosphate$^+$ (AMP$^+$)	m_6+
428.02	Adenosine-di phosphate$^+$ (ADP$^+$)	m_8+
542.07	ADP-ribose$^+$	m_{10}+

Figure 5. Fragmentation of ADP-ribose upon CID and HCD fragmentation. The table indicates the masses of generated fragments. Modified from [1].

of the modification from the peptide, leading to problems with the acceptor site assignment. Moreover, the fragmentation of the ADP-ribosylated peptide backbone using CID fragmentation is poor [1].

Alternatively to CID, electron capture dissociation (ECD) is a mild fragmentation method, which does not fragment ADP-ribose [1]. Thus, Hengel *et al*. proposed to use ECD and the later developed electron transfer dissociation (ETD) for the identification of ADP-ribosylated acceptor sites with MS/MS [54]. However, the systematic analysis of *in vitro* ADP-ribosylated ARTDs revealed that higher energy collisional dissociation (HCD), which was developed after CID, produced better results compared to ETD fragmentation [125]. Moreover, ADP-ribose marker ions can be used to tune the MS-method to selectively fragment only potentially ADP-ribosylated peptides increasing the number of identifications as well as the accuracy of the site assignments [125].

1.11. MS-based quantification methods using a shotgun approach

Quantitative analysis is critical for understanding PTM function. Protein abundance, site occupancy and PTM dynamics in cellular signaling can be addressed by the quantification of PTMs [12]. MS-based proteomics were not a quantitative approach originally. Different physicochemical properties of proteolytic peptides (size, charge, hydrophobicity), introduced substantial differences in their behavior in MS/MS measurements [12]. Nevertheless, several approaches were developed to overcome these shortcomings and allow quantitative studies. Quantitative MS measurements can

be performed either using standard shotgun methods or using specially developed targeted approaches.

1.11.1. Stable isotopes labeling methods

The classical method for shotgun quantification is the use of stable isotopes incorporated into peptides. The main principle of this quantification is the stable isotope dilution theory. Based on this theory, the endogenous and labeled peptides have identical chemical structures and thus identical MS behavior. Since MS allows to distinguish mass differences of these peptides, quantification is performed by comparing the signal intensities of endogenous and labeled peptides to each other. Thus, stable isotope labeling of proteins in combination with a proper enrichment technique can enable the relative quantification of PTMs under different experimental conditions [126].

Protein labeling is achieved either via metabolic labeling *in vivo* or chemical labeling after extraction of proteins. Additionally, stable isotopes can be added after sample preparation as internal standards (Figure 6). Metabolic labeling is an *in vivo*

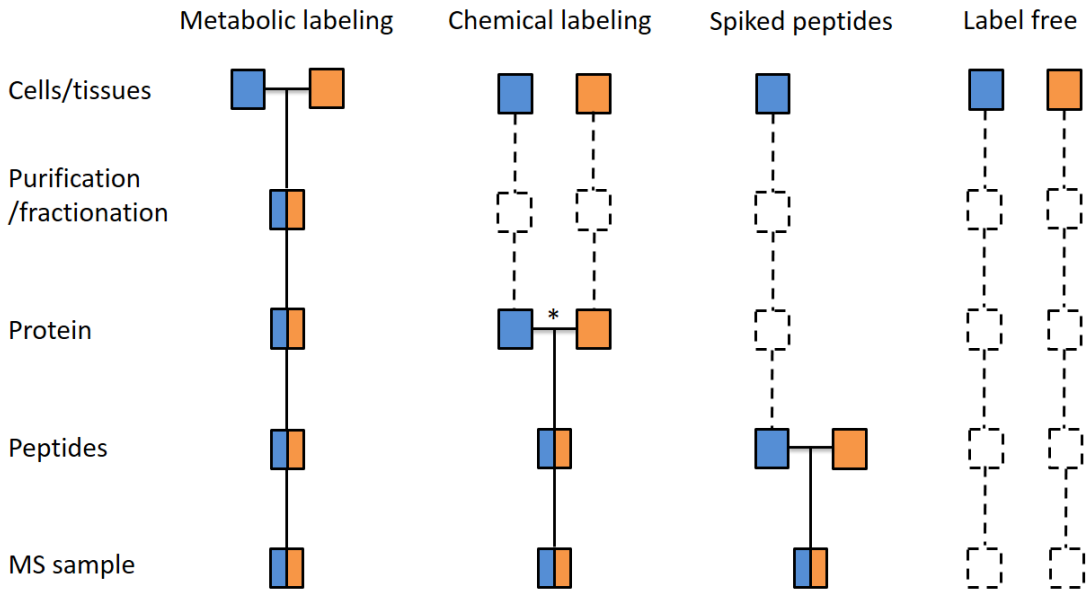

Figure 6. Shotgun MS-based quantification methods. Dashed figures and lines indicate the steps when samples are separately processed. Horizontal lines indicate the steps when samples are combined. The star indicates the earliest step where samples can be combined. Label-free samples are measured separately, and obtained data is combined during data analysis. Modified from [3].

labeling method, which allows the labeling of proteins directly in cells by growing them in the media containing labeling reagents [127, 128]. The best-known example is stable isotope labeling by amino acids in cell culture (SILAC) [129]. Usually, SILAC

utilizes radioactively labeled ^{3}C and/or ^{15}N-labeled arginine and lysine. When combined with the standard shotgun method using a trypsin digest, which cleaves peptides after Ks and Rs, this combination of isotopes enables the labeling of every peptide in the mix. However, due to the limited combination of available labeled amino acids, SILAC is hard to multiplex. One of the main advantages of metabolic labeling methods is that they provide a high measurement accuracy. The fact that the samples are combined immediately after the extraction procedure decreases the variability introduced by downstream processing steps (e.g. enrichment of PTMs).

Another approach to achieve isotope labeling is chemical labeling. In these methods, peptides are labeled with either light or heavy tags after protein extraction. The first developed method was using an Isotope-coded affinity tag (ICAT). ICAT uses a radioactively labeled reagent reactive against the cysteine (C) groups of the proteins. Additionally, the ICAT reagent contains a biotin-tag that is used to recover the labeled peptides using a pulldown with avidin beads [130]. However, the application of ICAT is limited to C-containing proteins. Moreover, unspecific background binding of avidin affinity purification is common. To overcome these drawbacks, several alternative methods like N-terminal labeling [128] and iTRAQ [131] were developed.

In addition to the aforementioned general protein labeling techniques, special PTM labeling methods i.e. for phosphoproteins have also been described [132, 133]. In contrast to SILAC, chemical labeling methods allow for easier multiplexing. However, the high cost of labeling reagents is a general limitation of all techniques using isotopes.

1.11.2. Label-free quantification methods

The development of instruments, which provide highly accurate and sensitive measurements, improved the reproducibility of shotgun measurements. Based on these improvements, label-free quantification methods become a valid alternative to quantification with labeled standards. An obvious advantage of the label-free approach is the simpler sample preparation, making it applicable to the analysis of various samples, from *in vitro* reactions to pathological biopsies [134]. However, the data analysis and interpretation should be approached with care due to a potentially high variability. Since standards are missing, cross sample variability is not assessed in this

type of measurements. Thus, several statistical tools have been developed allowing normalization of quantitative data after label-free measurements [135-137].

1.12. Targeted proteomics approaches

The main drawback of shotgun proteomics is its rather moderate reproducibility due to the data dependency of the MS/MS fragmentation. During the measurement, the instrument will select a number "n" (usually n = 10-12) of most abundant precursors from the MS spectra on which it will perform MS/MS fragmentation. This selection introduces a bias toward the most abundant peptide species. Additionally, dynamic exclusion is usually introduced to obtain an increased number of fragmented precursors. Applying this parameter, the instrument excludes already fragmented precursors from the following MS/MS fragmentations for a given period. Although good during the discovery phase, this parameter leads to an imprecise quantification of peptides since only a few scans of the same precursors are obtained [138].

To increase reproducibility of MS-based proteomics, targeted methods were developed. The basic principle of this kind of analysis is that the instrument will perform an MS/MS scan only on the selected targets. The mass spectrometer will only choose the precursors that have a similar m/z and a corresponding elution time of the peptide of interest for MS/MS fragmentation. In the targeted method, the precursor is monitored and fragmented several times (usually 10-12 times), which enables the precise quantification of the precursor [139]. These features enable a wide dynamic range and a low limit of detection making the methods well suited for the analysis of complex samples[140]. However, method development for targeted proteomics is still dependent on shotgun measurements since knowledge of the targets, and their fragmentation is essential for validating peptide identifications [138, 141].

The first targeted method was developed in the 80s and was named multiple reaction monitoring (also known as selected reaction monitoring (SRM)). Originally established for quantification and chemical structure elucidation of low molecular weight components [142], SRM was later adapted for proteomics [143]. SRM measurements are performed on triple quadrupole (Q) instruments, where the first (Q1) and the last quadrupole (Q3) serve as mass analyzers and the second quadrupole (Q2) is a collision cell. The precursor is quantified if the Q1-Q3 transition is similar to

the known fragmentation of the targeted peptide. In principle, 3-5 transitions per peptide are monitored [144] (Figure 7).

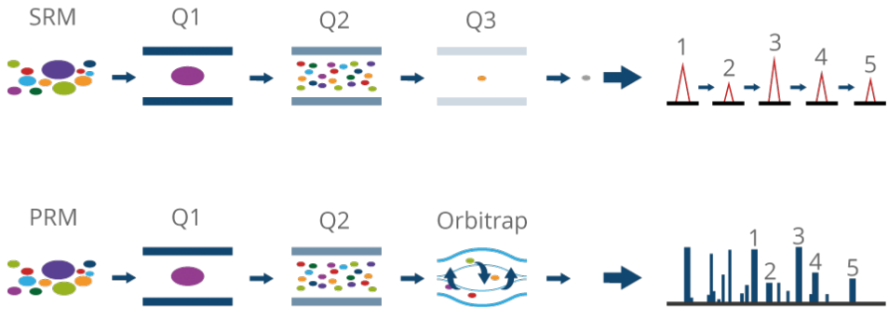

Figure 7. The principle of targeted proteomics methods. The SRM method is performed with QqQ and monitors pre-defined transitions (labeled with 1-5). The PRM method is performed with Orbitrap, allowing monitoring of all fragment ions from a selected precursor. Modified from [145].

The SRM method is an extremely useful tool for PTM quantification since it provides the sensitivity and allows the identification of PTMs even in complex samples. By optimizing Q1-Q3 transitions, it is possible to specifically target modified precursors. E.g., in the case of phosphorylation, targeting can be achieved by monitoring the common loss of phosphogroups upon HCD fragmentation [146]. Additionally, spiking heavy-labeled standards (analogs to the targeted peptides) allows absolute quantification of peptides and PTM sites [147]. However, the method development for SRM can be challenging since it is important to identify and validate the correct transitions for each targeted precursor to ensure specificity of the assay [148].

PRM measurements are performed on a benchtop quadrupole Orbitrap mass spectrometer. In this case, the role of Q3 is conducted by Orbitrap, which provides high resolution and high mass accuracy. Orbitrap mass spectrometer operating in PRM mode detects all fragment ions coming from the precursor, allowing easier validation of the peptide identity [149]. In this case, it is not necessary to pre-define the monitored transitions or to know the precise PTM localization site [139]. The relatively straightforward method development for PRM measurements led to a fast evolution of the technique. The high sensitivity of PRM allows the quantification of certain PTMs like ubiquitin in complex mixtures without prior enrichment [150]. Moreover, the acquisition of high-resolution spectra is useful for assignment of PTM modification sites [151].

2. AIMS OF THE PROJECT

Despite many efforts and the recent successes from several groups in identifying the ADP-ribosylome, a comprehensive understanding of ADP-ribosylation (e.g. identification of modified proteins and their acceptor sites as well as their dynamics) in oxidative stress remained to be determined. Thus, the goal of this PhD project was to develop rapid and highly reproducible MS-based assays for the quantification of certain ADP-ribosylated target proteins. The project had three major aims:

Aim 1: The identification of the oxidative stress-induced ADP-ribosylome. Using a shotgun proteomic approach, we aimed at identifying the cellular ADP-ribosylome and the specific ADP-ribose acceptor sites in oxidative stress. For that, the important step was to establish a reliable enrichment method. Additionally, optimization of MS/MS parameters specifically tailored for the analysis of ADP-ribose acceptor sites with high accuracy was essential.

Aim 2: The development of quantitative MS-based assays to monitor the relative concentrations of ADP-ribosylated proteins under oxidative stress conditions. The ADP-ribosylated peptides identified in the previous step were used for the development of quantitative methods based on the PRM approach.

Aim 3: The Confirmation and validation of identified oxidative stress markers in different cell types exposed to oxidative stress. The validation aimed to reveal those ADP-ribosylated markers that can be reliably used with extracts from various cell lines and under different experimental conditions. Considering the important function of ADP-ribosylation in oxidative stress, ADP-ribosylation of specific target sites might serve as a quantitative sensor for cellular stress.

3. RESULTS

3.1. Overview of a publication

3.1.1. Proteome-wide identification of the endogenous ADP-ribosylome of mammalian cells and tissue

Authors: Rita Martello[1], Mario Leutert[1], Stephanie Jungmichel[1], **Vera Bilan**, Sara C. Larsen, Clifford Young, Michael O. Hottiger & Michael L. Nielsen

[1] – equal contribution

Journal: Nature Communications DOI: 10.1038/ncomms12917

Contribution: I performed *in vitro* ADP-ribosylation assay with ARTD1 and ARTD10 (Figure 1D), the trans-modification *in vitro* ADP-ribosylation assay with ARTD1 and potential target candidates (including K-modification site mutants) (Figure 2C), and the glycation experiment with MALDI-TOF (Figure S2B and C).

3.2. Overview of submitted manuscripts

3.2.1. Combining HCD and EThcD fragmentations in a product dependent manner provides in-depth characterization of the cellular ADP-ribosylome

Authors: **Vera Bilan**[1], Mario Leutert[1], Paolo Nanni[1], Christian Panse and Michael O. Hottiger

[1] – equal contribution

Journal: Manuscript submitted

Contribution: Together with M.L., I performed the enrichment experiments and evaluated the obtained results. P.N. provided the technical support. C.P. helped with data analysis (Figure 1B and 2E). I wrote the manuscript and prepared all figures for publication. M.L and P.N. edited and revised the manuscript.

3.2.2. Quantitative analysis of protein ADP-ribosylation during oxidative stress by a label-free PRM approach

Authors: **Vera Bilan**, Nathalie Selevsek, Hans Kistemaker, Roxane Feurer, Dimitri Filippov, Michael O. Hottiger

Journal: Manuscript submitted

Contribution: I planned and performed all experiments (with technical input from N.S.). I analysed the obtained results, wrote the manuscript and prepared all figures for

publication. R.F. performed Af1521 pull down with modified HK326 peptide (Figure 1S). H.S and D.F synthesised HK326 peptides.

3.2.3. Identification of ADP-ribose acceptor sites on in vitro modified Proteins by Liquid Chromatography – Tandem Mass Spectrometry

Authors: Mario Leutert[1], **Vera Bilan[1]**, Peter Gehrig, and Michael O. Hottiger

[1] – equal contribution

Identification of ADP-ribose acceptor sites on in vitro modified Proteins by Liquid Chromatography – Tandem Mass Spectrometry

Book: Methods Mol Biol. 2016

Contribution: I helped to optimize the enrichment protocol, planned and evaluated the experiments. Together with M.L., I revised the manuscript.

3.2.4. In vivo proteome-wide identification of endogenous ADP-ribose acceptor sites by Liquid Chromatography – Tandem Mass Spectrometry

Authors: Sara C. Larsen[1], Mario Leutert[1], **Vera Bilan**, Rita Martello, Stephanie Jungmichel, Clifford Young, Michael O. Hottiger and Michael L. Nielsen

Book: Methods Mol Biol. 2016

Contribution: I helped to optimize the enrichment protocol, planned and evaluated the experiments.

3.1. Overview on a publication

3.1.1. Proteome-wide identification of the endogenous ADP-ribosylome of mammalian cells and tissue

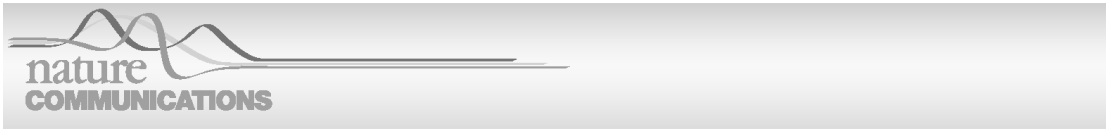

ARTICLE

Received 7 Apr 2016 | Accepted 15 Aug 2016 | Published xx xxx 2016

DOI: 10.1038/ncomms12917 OPEN

Proteome-wide identification of the endogenous ADP-ribosylome of mammalian cells and tissue

Rita Martello[1,*], Mario Leutert[2,3,*], Stephanie Jungmichel[1,*], Vera Bilan[2,3], Sara C. Larsen[1], Clifford Young[1], Michael O. Hottiger[2] & Michael L. Nielsen[1]

Although protein ADP-ribosylation is involved in diverse biological processes, it has remained a challenge to identify ADP-ribose acceptor sites. Here, we present an experimental workflow for sensitive and unbiased analysis of endogenous ADP-ribosylation sites, capable of detecting more than 900 modification sites in mammalian cells and mouse liver. In cells, we demonstrate that Lys residues, besides Glu, Asp and Arg residues, are the dominant in vivotargets of ADP-ribosylation during oxidative stress. In normal liver tissue, we find Arg residues to be the predominant modification site. The cellular distribution and biological processes that involve ADP-ribosylated proteins are different in cultured cells and liver tissue, in the latter of which the majority of sites were found to be in cytosolic and mitochondrial protein networks primarily associated with metabolism. Collectively, we describe a robust methodology for the assessment of the role of ADP-ribosylation and ADP-ribosyltransferases in physiological and pathological states.

[1] Faculty of Health Sciences, Department of Proteomics, The Novo Nordisk Foundation Centre for Protein Research, University of Copenhagen, DK-2200 Copenhagen, Denmark. [2] Department of Molecular Mechanisms of Disease, University of Zurich, Zurich CH-8057, Switzerland. [3] Molecular Life Science Program of the Life Science Graduate School, University of Zurich, Switzerland. * These authors contributed equally to this work. Correspondence and requests for materials should be addressed to M.L.N. (email: michael.lund.nielsen@cpr.ku.dk).

Protein ADP-ribosylation refers to the process where an ADP-ribose moiety is transferred from NAD^+ to the amino acid side-chains of target proteins (as mono-ADP-ribose, MAR) or to an already protein bound ADP-ribose to form poly-ADP-ribose (PAR). These modifications are primarily catalysed by a class of enzymes known as ADP-ribosyltransferases (ARTs), with certain Sirtuin deacetylases also being able to catalyse ADP-ribosylation[1]. The ARTs can be divided further into two major subclasses: ARTCs (cholera toxin-like) and ARTDs (diphtheria toxin-like, formerly called poly(ADP-ribose) polymerases (PARPs)), depending on their conserved structural features[2].

While MARylation has been reported to modulate GSK3β kinase activity and NF-κB signalling[3], little is known about the biological functions of this type of modification. In contrast, PARylation has emerged as a crucial post-translational modification (PTM) in cancer development[4]. PARylation is a transient PTM[5], whose rapid cellular degradation is predominantly carried out by PAR glycohydrolase (PARG)[6]. While PARylation is a key component of the DNA damage response (DDR) via its central role in the base excision repair pathway, many of the molecular details and processes affected by ARTs remain poorly understood. As a result, a detailed understanding of the molecular mechanisms and functions affected by ADP-ribosylation remains elusive.

In particular, the inventory of the amino acid residues modified by ADP-ribosylation remains incomplete. Current experimental evidence suggests that ADP-ribosylation primarily occurs on four different amino acids; Lys[7], Arg[8], Asp and Glu residues[9]. In addition, Cys residues were reported to be MARylated by certain ARTDs or bacterial toxins[10]. High-resolution mass spectrometry (MS) has become a valuable tool for comprehensive identification of PTMs[11]. However, current MS-based approaches for mapping ADP-ribosylation sites are biased towards modifications of only Glu and Asp[9], or they lack sensitivity due to co-enrichment of other PTMs (that is, phosphorylated peptides)[12].

Moreover, protein ADP-ribosylation is a low-abundant PTM that is rapidly degraded. To overcome this challenge cellular PARG knockdowns (siPARG) or knockouts have been developed[9,12]. Unfortunately, cellular absence of PARG leads to physiological alterations in cells, hepatocellular carcinoma in mice[13], progressive neurodegeneration[14] and excessive accumulation of PAR chains that are not rapidly degraded and promote cell death via parthanatos[15]. Consequently, strategies requiring knockdown of PARG constitute an improper setting for analysing physiological ADP-ribosylation and its associated mechanisms, thus rendering these methods inapplicable for *in vivo* analysis of tissues without genetic interventions[16]. Moreover, while ADP-ribosylation has been known for more than 50 years, the cellular stoichiometry of the modification has remained elusive, primarily due to the lack of methodologies that can elucidate such information[17].

Recently a chemical genetic discovery method for ARTD targets was reported[18], where the NAD^+ analogue 8-Bu(3-yne)T-NAD^+ was incubated with cell lysates from cells overexpressing mutated ARTDs sensitive to the analogue or cell lysates spiked with recombinant mutated ARTDs. However, as NAD^+ is impermeable to the cell membrane, this method requires either the lysis of cells or the isolation of organelles (that is, nuclei) followed by the complementation of exogenous 8-Bu(3-yne)T-NAD^+, which renders the identification of ARTD-specific substrates under different cellular conditions, and at physiological NAD^+ levels unattainable. Moreover, the ADP-ribose acceptor sites identified using this methodology were limited to Glu and Asp modifications[9].

To address these limitations, we have developed a protocol for the unbiased mapping of endogenous ADP-ribosylation sites in proteins. Our method led to the identification of more than 500 endogenous ADP-ribosylation sites in a single analysis and, as a result, provides an unprecedented in-depth analysis of protein ADP-ribosylation. Importantly, as the described workflow is applied under genetically unperturbed physiological conditions, we have used our methodology to analyse ADP-ribosylation sites in both cultured mammalian cells and mouse liver. Collectively, the workflow presented here represents a major advance in the detection of ADP-ribose acceptor sites and the identification of cellular processes regulated by ADP-ribosylation. Thus, facilitating a better understanding of the complex physiological and pathological processes that involve ADP-ribosylation, and the treatment of such conditions with PARP (that is, ADP-ribosylation) inhibitors.

Results

Identification of endogenous ADP-ribosylation sites. We have developed a technology for sensitive analysis of endogenous ADP-ribosylation sites in both cells and tissues that overcomes several of the above-mentioned limitations of current approaches. Briefly, proteins are isolated from cells, digested into peptides first using LysC and then trypsin. We then treat the cellular peptide digest with PARG, thereby converting all PARylated amino acids to their MARylated counterparts[19]. While this prevents discriminating whether the modification was originally PARylation or MARylation, the conversion is crucial for feasible MS analysis. Furthermore, this has the advantage that MARylated peptides can be unbiasedly enriched with an ADP-ribose-specific domain[20]. In contrast to previously described methodologies[21], enrichment at the peptide level with Af1521 in combination with prior PARG treatment has not been performed before. Subsequently, the enriched ADP-ribosylated peptides and their acceptor sites are identified using a high-resolution Orbitrap mass spectrometer (Q Exactive HF). As no pre-fractionation steps are employed, the described workflow analyses ADP-ribosylated peptides from a single sample requiring only a few hours of sensitive LC-MS operation[22]. All peptides are fragmented using higher-energy collisional dissociation (HCD) ensuring high p.p.m. accuracy on both the precursor and fragment ions[23]. Furthermore, ADP-ribosylated peptide identification is aided by diagnostic ions originating from the fragmentation of the ADP-ribose group linked to the peptide[24,25] (Supplementary Fig. 1a). Superior advancements over current methodologies are as follows: First, sample preparation without ARTD, NAD^+ or PARG level perturbation[9,18] allows analysis of both cells and tissues under physiological conditions. This will allow us to broaden our understanding of the mammalian ADP-ribosylation complexity, and facilitating comparisons across any cellular condition, cell type and, even, species. To substantiate this, we have applied our established method to HeLa cells exposed to hydrogen peroxide (H_2O_2)-induced oxidative stress (Fig. 1a), and to normal mouse liver samples. Second, using the Af1521 macro domain to enrich ADP-ribosylated peptides, which has favourable binding preferences and relatively high ADP-ribose affinity with a Kd of ~0.13 μM (ref. 26), allowed unbiased modified amino acid analysis. Third, we have ensured prevention of lysis-induced ADP-ribosylation artefacts, as previously reported[20], thus facilitating assessment of the ADP-ribosylome during actual physiological conditions.

Identification of the H_2O_2-induced ADP-ribosylome. To benchmark our methodology, we treated HeLa cells with 500 μM H_2O_2, which induces PAR formation through oxidative stress

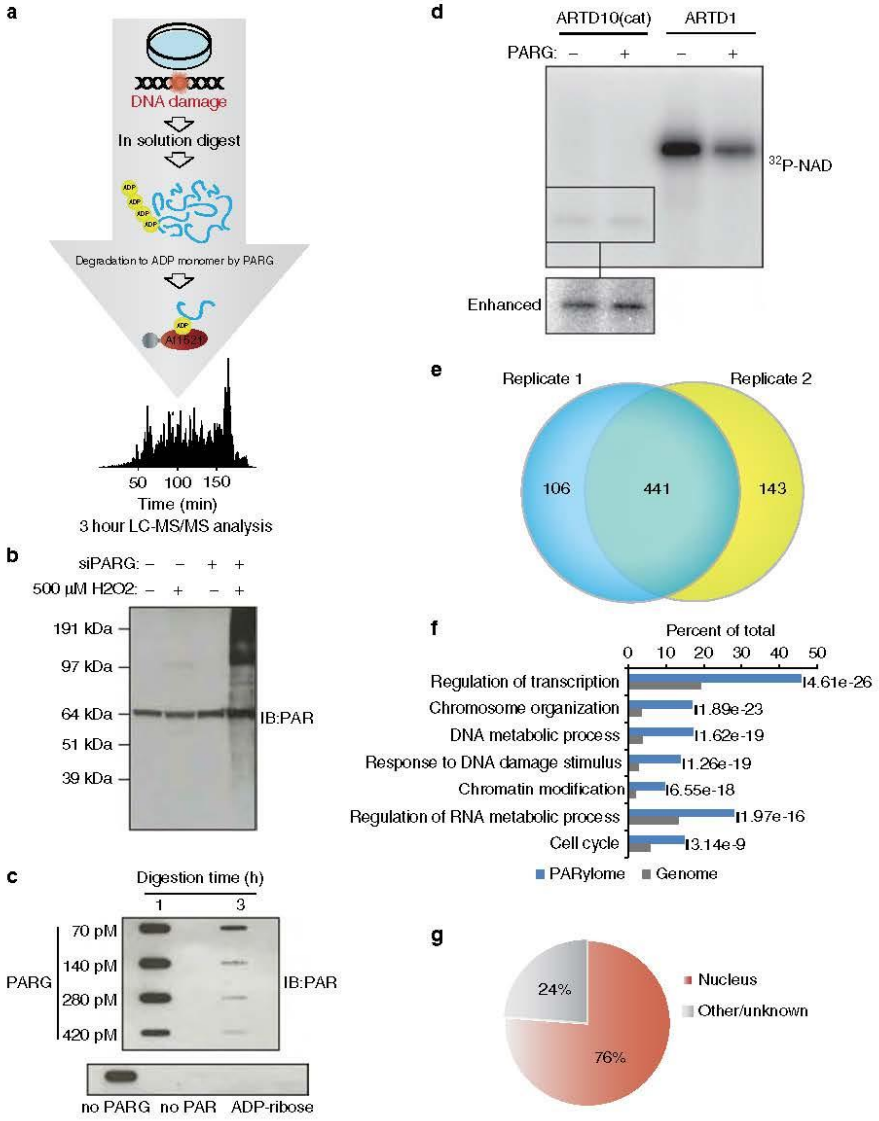

Figure 1 | Proteome-wide identification of endogenous ADP-ribosylation sites in human cell culture. (**a**) Schematic representation of the peptide-based enrichment strategy. HeLa cells were treated with genotoxic stress and digested into peptides. Tryptic digested peptides were treated with PARG enzyme to convert multimeric ADP-ribosylation into monomeric counterparts, and subsequently ADP-ribosylated peptides were enriched using GST-Af1521 macrodomain. Enriched peptides were analysed by high-resolution LC-MS/MS on an Orbitrap Q-Exactive HF instrument and the data was further processed by bioinformatic software tools. (**b**) Comparison of HeLa cells exposed with 500 µM H_2O_2. During cellular knock-down of PARG enzyme (siPARG) an abundant PAR signal is observed, while under physiological conditions the PAR signal is significantly weaker (compare second lane with fourth lane on gel). Previous methods for characterizing ADP-ribosylation solely worked under siPARG conditions while the methodology described here is applicable to physiological conditions. (**c**) Optimization of the incubation time and amount of PARG enzyme required for converting multimeric ADP-ribosylated peptides into monomeric counterparts. (**d**) Validation experiment that confirms PARG treatment does not remove MAR from investigated peptides. (**e**) Venn diagram of identified ADP-ribosylation sites identified in two biological replicate analyses. A strong overlap in identified sites signifies high reproducibility in the developed method. (**f**) GO functional annotation of significantly regulated proteins in the combined data set reveal strong enrichment of proteins involved in DNA repair processes compared with annotated GO genes across the entire human genome (indicated *P*-values<0.005). (**g**) GO term annotation enrichment for cellular distribution of proteins harbouring ADP-ribosylation sites.

signalling. Under physiological conditions (non-siPARG conditions), H_2O_2 treatment induces PAR levels only faintly detectable by immunoblot (Fig. 1b), while cellular knock-down of PARG via small interfering RNA (siPARG) causes strong PAR formation (Fig. 1b). This demonstrates the requirement for improved sensitivity in studying ADP-ribosylation under unperturbed physiological conditions.

To ensure complete catalysis of PARylated into MARylated peptides we next assessed the amount of PARG required to catalyse a fixed amount of PAR. Previously, PAR levels in HeLa cells have been reported to range up to 0.1 amol per cell during H_2O_2 treatment[27]. Thus, we incubated 10 μM of purified PAR with increasing concentrations of PARG and assessed the temporal efficiency of the catalysis by immune-slot blot (Fig. 1c). Since the most efficient catalysis was observed when PAR was treated with PARG for 3 h, we concluded that this enzyme ratio allowed enzymatic catalysis of PARylated peptides into MARylated peptides during our enrichment procedure.

As some macrodomains can exhibit hydrolase activity on MAR moieties[28,29], we performed the Af1521 enrichment procedure at 4 °C and incubated samples for only two hours. Moreover, all subsequent sample handling steps were performed at 4 °C, which collectively prevents hydrolase activity of the Af1521 macro domain[20]. To confirm that PARG exerted no enzymatic hydrolase activity on MAR (ref. 19) in our workflow, we assessed whether PARG removes ADP-ribosylation from automodified ARTD1 (also PARP1) or ARTD10 (formerly PARP10; Fig. 1d), which are known PARylated and MARylated substrates[30], respectively.

Using autoradiography assays, hydrolysis of the attached radioactive [^{32}P]-PAR of the protein substrates was monitored (Fig. 1d), revealing that PARG was indeed able to convert PAR chains on ARTD1 into MAR, while no reaction was observed regarding the auto-MARylation of ARTD10 (Fig. 1d). These results confirmed that PARG hydrolase activity would not affect enrichment of MAR residues.

To evaluate the reproducibility of the methodology, we performed replicate enrichment experiments in HeLa cells. Following MS analysis, there was a 75% overlap of the high-confident ADP-ribose acceptor sites identified (localization scores >0.60) between replicates (Fig. 1e). Thus, this indicates high reproducibility in the established approach, which compares well with the reproducibility obtained in other proteomic experiments (Supplementary Note 1)[31]. From three replicates, we have identified 739 ADP-ribosylation sites (Localization score >0.60) on 480 proteins after H_2O_2 treatment (Supplementary Data 1), with the majority of identified proteins containing a single modification site (Supplementary Fig. 1b). To corroborate our identification analysis, we performed a separate MS analysis employing the complementary fragmentation technique electron transfer dissociation (ETD)[32], which confirmed the localization of several identified sites (Supplementary Fig. 1c,d; Supplementary Data 2).

Functional analysis using gene ontology (GO) confirmed that the identified proteins participate in biological processes known to involve ADP-ribosylation activity, including transcription, chromosome organization and response to DNA damage stimulus[33,34] (Fig. 1f). Reassuringly, we find that 76% of the ADP-ribosylated proteins localize to the nucleus (Fig. 1g), in line with the cellular localization of ARTD1 and ARTD2 (also PARP2). Moreover, the cellular abundance profile of identified ADP-ribosylation protein targets supports the notion that our methodology is not biased towards abundant proteins (Supplementary Fig. 1e). Collectively, these results confirm the feasibility and reproducibility of this novel proteomics approach for identifying the endogenous ADP-ribosylation sites in cultured HeLa cells.

Identification of Lys residues as endogenous acceptor sites. As the Af1521 macro domain binds to the ADP-ribose moiety[26] our methodology allows for unbiased detection of any ADP-ribose acceptor site. In support of this, no discernable difference was observed when the amino acid distribution of ADP-ribosylation sites was compared with the amino acid distribution of the same residues across the proteome (Fig. 2a). Among the identified ADP-ribosylation sites, we observed a significant portion of modifications residing on Lys residues, including the previously confirmed ARTD1 modification site K498 (ref. 7). ADP-ribosylation of Lys residues has been suggested as an artefact related to the release of ADP-ribose moieties during PARG cleavage of PAR chains[17]. This suggestion was made based on observations that ADP-ribose was found to non-enzymatically attach to Lys, Arg and Cys residues in a glycation process[35]. However, the incorporation rate (stoichiometry) achieved in this study, which utilized large amounts of histone proteins for *in vitro* reactions, were estimated to be below 2%, suggesting that this is an inefficient reaction[35]. To investigate whether PARG treatment of PAR chains causes glycation in our experimental setup, we performed a quantitative experiment using Stable Isotope Labelling by Amino acids in Cell culture (SILAC)[36]. Herein 'Heavy' SILAC cell lysates were treated with free PAR chains before PARG degradation, while 'Light' SILAC cell lysates were left untreated (Supplementary Fig. 2a). Since no PAR-inducing stress was exerted on these cells, identification of ADP-ribosylation sites exhibiting increased SILAC ratios would be indicative of chemical reactions caused by free ADP-ribose released by PARG. Here we identified 39 ADP-ribosylation sites equally distributed across Lys, Arg, Glu and Asp residues, and no increased SILAC ratios were observed for identified modification sites. These findings strongly suggest that PARG treatment does not lead to random glycation of Lys or Arg residues (Fig. 2b and Supplementary Data 3). To substantiate our findings, we performed a 'reverse' SILAC experiment where only light SILAC cells were treated with free PAR chains, which resulted in a similar outcome (Fig. 2b). These results confirm that ADP-ribose moieties released on PARG treatment are unlikely to cause relevant *in vitro* artefacts and, combined with the overall reproducibility of ADP-ribosylation site identification (Fig. 1e), suggest that the identified ADP-ribosylation sites were not derived from non-enzymatic glycation.

In addition, an *in vitro* experiment utilizing a synthesized histone H2B-like peptide (NH_2-PQPAKSAPAPKKG-OH) incubated with free ADP-ribose was performed analogous to previously reported experiments[35]. Briefly, the non-modified H2B peptide was incubated with 1 mM ADP-ribose at 37 °C at pH 9 or 7.5 for two time points (1 h or overnight incubation). Glycation levels were then determined using time-of-flight (TOF) MS (Supplementary Fig. 2b). On incubation with free ADP-ribose, only small levels of glycation were observed, dependent on pH and incubation time (Supplementary Fig. 2b). Tandem mass spectrometry (MS/MS) confirmed that glycation took place at Lys residues (Supplementary Fig. 2c), corroborating earlier observations that free ADP-ribose is able to modify Lys residues by non-enzymatic glycation. However, our data reveal that glycation occurs primarily at high pH and requires non-physiological concentrations of free ADP-ribose. In contrast, PARG-released ADP-ribose was not able to induce similar artefacts at detectable levels. Moreover, the non-enzymatic glycation of ADP-ribose occurred primarily on several Lys residues within the short H2B-peptide, which is in stark contrast to the different ADP-ribosylation sites observed in cell culture (Supplementary Fig. 1b). Collectively, these results strongly suggest that the ADP-ribosylation sites observed in our cell culture analysis were not caused by glycation.

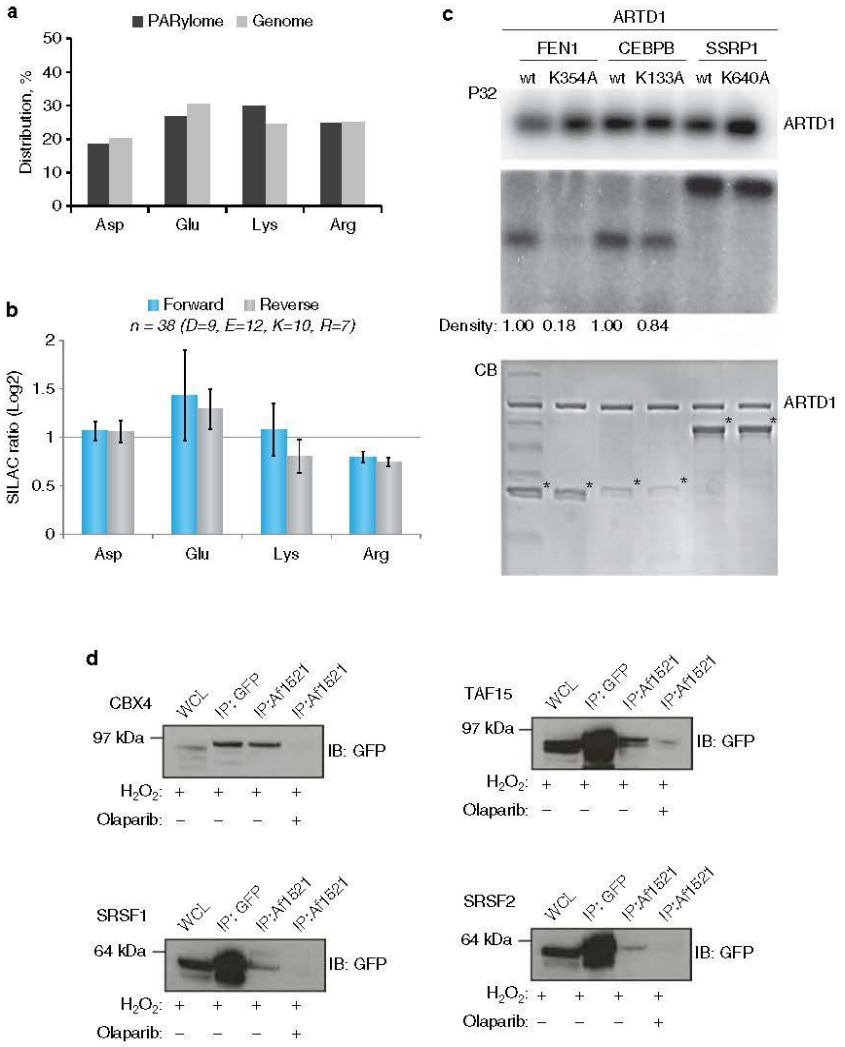

Figure 2 | Lysine residues are *in vivo* targets of ADP-ribosylation in human cells. (**a**) Distribution of ADP-ribosylation acceptor sites compared with their distribution in the genome. (**b**) Assessment of peptide glycation by free ADP-ribose. Distribution of Log2 transformed SILAC ratios, and ADP-ribosylation acceptor sites, from forward and reverse SILAC experiments as outlined in Supplementary Fig. 2a. No increased SILAC ratios were observed for the different acceptor sites when cells were treated with PAR, supporting the notion, that the observed modifications are not derived from glycation. (**c**) *In vitro* PARylation of identified protein targets. Purified full-length human ARTD1 was incubated with recombinantly expressed proteins in the presence of ^{32}P-NAD$^+$ and double-stranded DNA oligomer. Samples were resolved by SDS–PAGE, stained with Coomassie (CB; lower panel) and ^{32}P-incorporation was detected by autoradiography (P32; upper panel). (**d**) HeLa cells stably expressing SRSF1, SRSF2 CBX4 or TAF15 as GFP-fusion proteins were treated with H_2O_2 and PARP (that is, ADP-ribosylation) inhibitor olaparib as control experiment. Lysates were subjected to Af1521 WT pull-down or GFP-immunoprecipitation and subsequently analysed by immunoblotting with GFP antibody. Error bars are 95% confidence intervals with $n = 4$.

To further validate Lys residue ADP-ribosylation *in vivo*, we biochemically confirmed the Lys modification sites identified on FEN1, CEBPB and SSRP1 in cells using an *in vitro* PARylation assay. To this end, recombinant proteins for these target substrates were purified as wild type (WT) and potentially modification-deficient mutant variants, with the latter harbouring K-to-A mutations at Lys residues that we found to be modified (K354A for FEN1, K133A for CEBPB and K640A for SSRP1) (Supplementary Data 1). All proteins were incubated with purified ARTD1 in the presence of [^{32}P]-NAD$^+$ and a DNA fragment to measure the incorporation of NAD$^+$ radioactivity by autoradiography[37]. Activation of ARTD1 was confirmed by a

strong automodification (Fig. 2c, upper panel). Using ARTD1 we detected strong ADP-ribosylation signals for all three WT protein candidates, confirming that these are ADP-ribosylation substrates. When Fen1, CEBPB or SSRP1 were trans-modified with either ARTD1, ARTD1 + PJ34, ARTD1 Y907A/C908R (catalytically dead) or ARTD1 E988K (1.25% of wild-type activity; only monomers are added), modification of the substrates was not observed (Supplementary Fig. 3), confirming that glycation is not a problem in our *in vitro* assays.

However, in our data set we observed several other ADP-ribosylation sites in this protein, although these had lower localization scores. These findings suggest that the K640 modification may only contribute a low percentage of the total ADP-ribosylation levels for SSRP1. Conversely, for the K133A mutant of CEBPB9, we observed a 16% decrease in the ADP-ribosylation signal. Analogously, when K354 was mutated to Ala in FEN1, a reduction in total PAR signal was also observed, thus confirming that this residue constitutes an ADP-ribosylation site. Altogether, these findings demonstrate that Lys residues are indeed specific targets of ADP-ribosylation. In addition, we confirmed SRSF1, SRSF2, TAF15 and CBX4 as *in vivo* ADP-ribosylated protein substrates using western blot (WB) analysis (Fig. 2d). These targets were selected for three reasons: TAF15 is a known ADP-ribosylated substrate during oxidative stress[9,20] and serves to demonstrate the ability of the methodology to confirm known targets. For SRSF1, the identified modification sites were observed with localization scores of 0.5, and therefore do not constitute *bona fide* high-confident sites (Supplementary Data 1). Importantly, we demonstrate that the data obtained could still be used to infer that SRSF1 is an ADP-ribosylation target substrate as WB confirmed the MS results. Finally, both SRSF2 and CBX4 are novel ADP-ribosylation targets harbouring high-confident modifications sites.

ADP-ribosylation and PAR formation dynamics correlate. Since the established enrichment approach requires PARG enzymatic conversion of ADP-ribosylated acceptor sites into their MARylated counterparts, we examined the dynamics of the H_2O_2-induced ADP-ribosylation sites identified using SILAC. For this, Light SILAC cells were stimulated for only a few seconds with 500 μM H_2O_2 (~0 min), while heavy SILAC cells were treated with the same concentration of H_2O_2 for various durations (0, 5, 10, 30, 60 and 120 min) (Supplementary Fig. 4a). Using this approach, we investigated the effect oxidative stress (H_2O_2 treatment) has on the abundance of ADP-ribosylation sites determined by quantitative MS: if the identified ADP-ribosylation site is induced on oxidative stress, then the relative SILAC peptide intensity ratio between light and heavy peaks will be higher in the heavy isotope encoded sample, thereby exhibiting an increased SILAC ratio. Following MS analysis of H_2O_2-treated SILAC samples, we extracted and compared the temporal SILAC ratios of identified ADP-ribosylation sites, and observed the highest SILAC ratios at early time points (5 and 10 min H_2O_2 treatment) (Fig. 3a). To examine whether changes in SILAC ratios correlate with the dynamics of cellular PAR formation, we compared the SILAC readout signal (Fig. 3a) to the PAR signals analysed by immunofluorescence in the same cells. Although the employed antibody primarily recognizes only longer PAR chains, the employed approach constitutes a widely used methodology to evaluate relative differences (that is, dynamic changes) in cellular PAR formation[38–40] (Fig. 3b; Supplementary Fig. 4b). From triplicate IF experiments a good temporal and kinetic correlation between the measured SILAC ratios (Fig. 3a) and PAR IF signals was observed (Fig. 3b), with both analyses exhibiting the highest increase at 5–10 min of H_2O_2 treatment. Moreover, the dynamic changes observed are similar to results obtained from immuno-slot-blot analysis of PAR formation (Supplementary Fig. 4c), and to those reported in mouse embryonic fibroblasts treated with 100 μM H_2O_2. Also in these experiments a peak of PAR formation was observed after 5 min, with subsequent turnover after 15–20 min (ref. 39). Collectively, these data show that the upregulation of ADP-ribosylation sites determined by SILAC ratios correlates with the increase in PAR formation using IF analysis.

Determination of endogenous ADP-ribosylation stoichiometry. Today, large-scale proteomics experiments have been very successful in determining the relative abundance of PTMs between different cellular states[11]. However, an inherent challenge in PTM analyses is the estimation of stoichiometry, referred to as the fraction of a given protein modified with a particular PTM at a given amino acid. To obtain stoichiometry information, we used the information gathered in our H_2O_2-treated SILAC experiments (Fig. 3a and Supplementary Data 1), and combined it with data characterizing general protein regulation during H_2O_2 treatment[41]. Briefly, ADP-ribosylated peptides have opposite ratios of their unmodified counterparts, which can be used to calculate the absolute stoichiometry of modified sites from any two SILAC states. This calculation is made under the assumption that the sum of modified and unmodified peptides remains constant between SILAC states[41]. From a single experiment, we obtained stoichiometry values for 55 ADP-ribosylation sites, revealing that half of the ADP-ribosylation sites have less than 11% stoichiometry on H_2O_2 treatment (that is, the fraction of a given modification site occupied by ADP-ribosylation; Supplementary Fig. 4d). In line with the overall transient nature of the modification, these findings suggest a tight enzymatic regulation of ADP-ribosylation stoichiometry. Moreover, several of the arginine residue ADP-ribosylation sites were measured with high stoichiometry (Supplementary Fig. 4e, Supplementary Data 4). Whether these represent protein targets modified by ARTs other than ARTD1 and 2, or represent MARylation rather than PARylation remains to be determined.

Comparing this ADP-ribosylome to Asp/Glu ADP-ribosylomes. With the wide range of ADP-ribosylated proteins identified, we sought to compare our list of modified proteins with the previously reported proteins ADP-ribosylated at Asp/Glu (ref. 9). Although these analyses were conducted in different cell lines and under different physiological conditions, we found that 36 per cent of the reported Asp/Glu ADP-ribosylated proteins were also modified in our data set (Fig. 3c). Similarly, 38% of the targets identified in our previous report using the Af1521 domain for identification of ADP-ribosylated proteins[20] were also identified with the current methodology (Supplementary Fig. 4f). This overlap increased to 52 per cent when only H_2O_2-induced ADP-ribosylation substrates were compared, supporting the notion that differences in the substrates identified do not stem from the methodologies but from differences in cellular conditions (Supplementary Fig. 4f). Similarly, when comparing our data set with an *in vitro* analysis where 8-Bu(3-yne)T-NAD^+ was incubated with cell lysates and mutated analogue-sensitive ARTDs[42] an overlap of only 30% was observed (Fig. 3d). These findings suggest that *in vivo* and *in vitro* strategies target different ARTD substrates.

To further investigate the comparability of the different enrichment strategies, we performed SILAC experiments in which the PARP inhibitor olaparib was introduced before

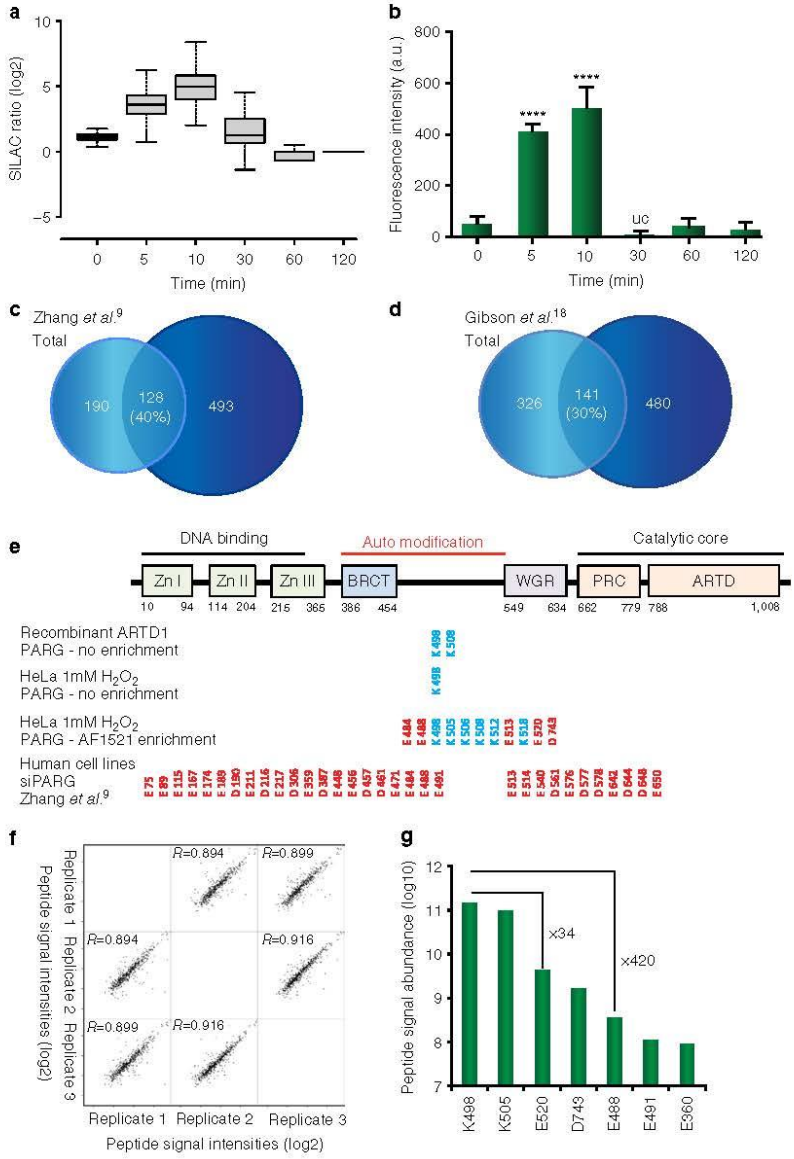

Figure 3 | SILAC ratios of ADP-ribosylation sites. (**a**) Boxplot analysis of logarithmized H/L SILAC ratios from six SILAC experiments representing HeLa cells treated with H_2O_2 in a temporal manner (see Supplementary Fig. 2a). Strongest regulation of ADP-ribosylation sites is observed when cells are treated for 5–10 min of genotoxic stress. (**b**) Densiometric evaluation of IF analysis of HeLa cells treated with H_2O_2 for different time points. The strongest abundance in PAR signal is observed after 5–10 min treatment of H_2O_2, in good correlation with observed increase in SILAC ratios on MS analysis (Fig. 2a). Experiments were performed in triplicates. (**c**) Venn diagram depicts overlap between identified ADP-ribosylated proteins compared with previously reported Asp and Glu ADP-ribosylated proteins. (**d**) Venn diagram depicts overlap between identified ADP-ribosylated proteins compared with previously reported Asp and Glu ADP-ribosylated proteins using an *in vitro* strategy. (**e**) Comparison of identified ARTD1 ADP-ribosylation sites across different experiments as indicated. (**f**) Multi-scatter plot of measured peptide signal intensities from triplicate ADP-ribosylation experiments. A strong Pearson correlation signifies high reproducibility in the measured abundance of ADP-ribosylated peptide species. (**g**) Abundance measurement for seven ADP-ribosylation sites, demonstrating that lysine residue K498 is abundantly modified in ARTD1. Error bars are 95% confidence intervals with $n=3$.

oxidative stress and compared the outcome with the analogous ADP-ribosylome experiment[9]. In two SILAC experiments, both light and heavy SILAC cells were treated with H_2O_2, while only light SILAC cells were treated with olaparib (1 μM or 10 μM)[43]. A strong Pearson correlation in SILAC ratios between the experiments ($R=0.69$) signifies that the ADP-ribosylation sites identified were similarly affected by the employed olaparib concentrations (Supplementary Fig. 4g). Using the STRING database of physical and functional interactions[44], we found that the proteins harbouring ADP-ribosylation sites regulated by olaparib were strongly connected with ARTD1 and ARTD2 (Supplementary Fig. 5a). Moreover, the regulated proteins were also strongly associated with biological processes known to involve ARTDs (Supplementary Fig. 5b) and therefore most probably constitute ADP-ribosylated candidates.

Next, we compared the protein distribution of identified modification sites between this data set and the above-mentioned methodology. In the Asp/Glu ADP-ribosylome[9], a total of 1,048 ADP-ribosylation sites residing on 320 proteins were identified, which corresponds to 3.3 modifications per identified substrate. In contrast, our combined data set includes 958 ADP-ribosylation sites on 565 proteins, or 1.7 modifications per identified substrate. Considering that only half of the identified sites in our data set reside on Glu or Asp residues (Fig. 2a), the boronic acid approach, which employs non-physiological siPARG conditions, identifies more ADP-ribosylation sites per identified substrate. Notably, this increase is analogous to the observed increase in overall PAR signal on siPARG treatment (Fig. 1b).

We then compared the ADP-ribosylation sites only identified on ARTD1. In the Asp/Glu ADP-ribosylome analysis by Zhang *et al.*, a total of 37 ADP-ribosylation sites were reported for ARTD1 (Fig. 3e), of which 23 resided on Glu residues, which corresponds to 31% of the total number of Glu within human ARTD1. In contrast, the Af1521 analysis only identified ADP-ribosylation in a total of 11 amino acid acceptor sites across all experiments (Fig. 3e). To investigate whether the differences in the number of identified ADP-ribosylation sites might be abundance-driven, we performed an analysis of HeLa lysates without Af1521 enrichment. In addition, we performed a similar analysis with recombinant ARTD1, where automodified ARTD1 was treated with PARG but not enriched by Af1521. From these experiments, we solely found K498 to be modified in the non-enriched HeLa sample, whereas both K498 and K505 were identified on recombinant ARTD1 (Fig. 3e). These data suggest that certain Lys residues within the auto-modification domain of ARTD1 are most abundantly present in the analysed samples, which is similar to previous mutational observations for ARTD1 (ref. 7). We observed a strong reduction in the *in vitro* PAR signal when the three lysine residues within the automodification domain of ARTD1 (K498R, K521R and K524R)[7] were mutated. Thus, indicating that these sites are indeed relevant for automodification of ARTD1 and supporting our observations that K498 is a major PAR acceptor site of ARTD1.

To quantify ARTD1 modification sites in more detail, we next compared the peptide signal abundance between replicate Af1521 analyses (Fig. 1e). To this end, the intensity values for all identified peptide sequences were compared across replicate samples. A strong Pearson correlation between replicates ($R>0.89$) demonstrates that the measured peptide signal intensities can be used as a reliable measure for modification site abundance (Fig. 3f). To further investigate quantification of ADP-ribosylation sites, we performed abundance assessment for seven modification sites on ARTD1 that were reliably identified in two out of the three replicate experiments (Fig. 3g). The analysis revealed that ADP-ribosylation located on lysine K498 yielded the strongest signal abundance. Although peptides from the same protein might exhibit different 'flyability'[45], an observed 34-fold and 420-fold difference in signal intensity compared with nearby modification sites residing on glutamic acids E520 and E488, respectively, suggests that K498 is an abundant auto-modification site on ARTD1. Besides, ADP-ribosylation on K498, both E488 and E491 reside on comparable tryptic peptide sequences within ARTD1, so that the observed differences in abundance cannot be attributed to different peptide ionization propensities. We observed that quantified ADP-ribosylation sites preferentially reside within the auto-modification domain of ARTD1 under physiological conditions (Fig. 3g,e).

Analysing endogenous ADP-ribosylation sites in mouse liver. Tissues can contain many different cell types that display a wide range of protein concentrations, which poses challenges to proteomic identification and the analysis of PTMs. Moreover, many tissues contain a broad range of different mono-ARTs, including members of the ARTD family, SIRTs and ARTCs (ref. 46). To further explore the general applicability of the new method, we characterized the endogenous ADP-ribosylome of mouse liver, a tissue that has already been described to regulate cellular processes in an ADP-ribosylation-dependent manner[47]. Three C57BL/6 mice were killed before their livers were collected and frozen in liquid nitrogen. The tissue was then ground up and processed as described for the HeLa cells (Fig. 4a). In triplicate analyses, we identified 901 modified peptides with unique ADP-ribosylation acceptor sites, of which 414 were identified in at least two different liver samples (Fig. 4b, Supplementary Data 5). The distribution of ADP-ribosylation sites was similar to the cell culture analysis, with 70% of identified proteins harbouring only one modification site (Fig. 4c). Strikingly, the majority (86%) of identified ADP-ribosylation acceptor sites in the mouse liver were Arg, while Lys, Asp and Glu were detected only at very low levels compared with HeLa cells (Fig. 4d). Notably, several Lys residues modified with ADP-ribosylation were also found on cytoplasmic proteins in this analysis (Supplementary Data 5), providing evidence that lysine residues being *in vivo* targets of ADP-ribosylation under physiological conditions.

GO analysis of the modified proteins revealed a high enrichment in mitochondrial, cytoplasmic, nuclear and membrane proteins (Fig. 4e). Among the identified ADP-ribosylated proteins, we found several previously reported ADP-ribosylated proteins. These included ARTD12 (formerly PARP12), which has been described to have MAR and auto-ADP-ribosylation activity; ARTC2, which is a GPI-anchored arginine-specific MARylating enzyme that can be shed and circulated in the blood; and glutamate dehydrogenase 1, which is known to be regulated through ADP-ribosylation by SIRT4 (refs 48,49). In agreement with experiments done in HeLa cells, we also found that histone H2B and several RNA helicases were modified. These results indicate that the established enrichment protocol can readily be employed to investigate the non-induced ADP-ribosylomes of tissues, which include both intra- and extra-cellular ADP-ribosylated proteins.

Discussion

Here, we describe the establishment of a robust and highly reproducible technology for the first unbiased proteome-wide view of a mammalian ADP-ribosylome, which includes the exact identification of endogenous ADP-ribose acceptor sites under different physiological conditions in cells and for the first time also in organ tissue. We show that PARG treatment of peptides before enrichment with Af1521, allows specific identification of ADP-ribosylated amino acids and highly sensitive identification

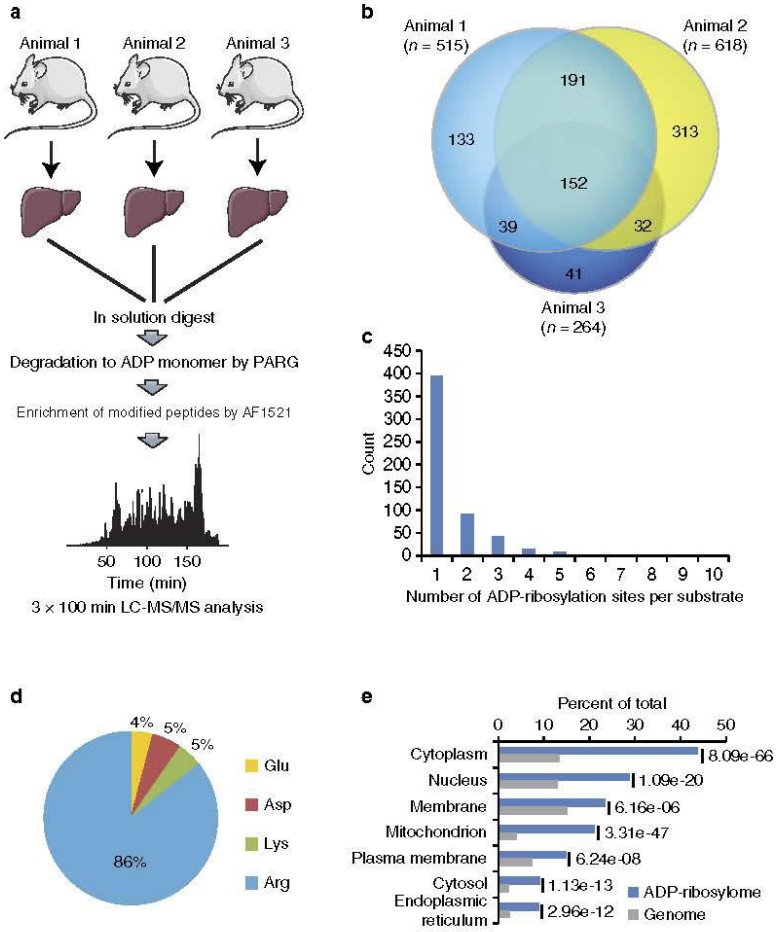

Figure 4 | Proteome-wide identification of endogenous ADP-ribosylation sites in mammalian tissue. (**a**) Experimental setup for mammalian liver tissue analysis. In total, liver samples derived from three mice were investigated and prepared as indicated. Mouse images were adapted from the Servier Image Bank under the Creative Commons licences CC-BY. (**b**) Venn diagram of identified ADP-ribosylation sites from three liver samples. A strong overlap between analysed sampled signifies good reproducibility in the identified ADP-ribosylation sites across investigated tissue samples. (**c**) Distribution of ADP-ribosylation sites across proteins. (**d**) Distribution of ADP-ribosylated amino acids. The majority (86%) of identified sites reside on arginine residues indicative of differential ART activity compared with cell culture analysis (Fig. 1g). (**e**) GO term annotation enrichment for cellular distribution of proteins identified in liver samples harbouring ADP-ribosylation sites.

of the corresponding proteins. And we demonstrate that the detected modifications are not derived from non-enzymatic glycation and, contrary to previous claims[50], Af1521 does not hydrolyse the modification under the applied conditions. Besides, this method supports the identification of ADP-ribosylated proteins without complementing cell lysates or organelles with NAD^+ analogues and mutated ARTDs (ref. 18) and is, consequently, able to analyse the ADP-ribosylome under different cellular conditions derived from endogenous ARTD protein and NAD^+ levels in both cells and tissue.

The streamlined methodology led to the identification of more than 900 endogenous ADP-ribosylation sites belonging to more than 500 proteins in both culture and tissue cells. Our results suggest that this methodology could be used in combination with high-throughput screening techniques to identify endogenous proteins affected by ADP-ribosylation and/or those modulated by ADP-ribosylation inhibitors (also called PARP inhibitors). ARTD1 is a key regulator within the DDR (ref. 33), which has recently become a highly attractive target for cancer therapy[51,52]. Although not specific for ARTD1, several ADP-ribosylation inhibitors have been approved or are currently being evaluated in clinical trials as mono-therapeutic or combination therapy agents. Our ability to now analyse the endogenous ADP-ribosylome from different cancer cells or tissues constitutes a promising approach that should advance of our understanding of ADP-ribosylation in a clinical setting.

FEN1 is a structure-specific nuclease with 5′-flap endonuclease and 5′–3′ exonuclease activities involved in DNA replication and repair, and ARTD1 recruits FEN1 to DNA damage intermediates[53]. The K354 reside of FEN1 becomes acetylated through the acetyltransferase p300, which reduces the DNA-binding activity of FEN1 (ref. 54), while ubiquitylation of the same lysine mediates the proteosomal degradation of FEN1 during G2/M phase[55]. These PTM-based regulatory mechanisms support the notion that ADP-ribosylation at K354 might relate to a currently uncharacterized regulatory function of FEN1. The observed ADP-ribosylation of the SUMO-protein ligase CBX4 suggests nuclear cross-talk between PARylation and SUMOylation, which might be more widely occurring than previously anticipated. Such cross-talk could be analogous to previously reported ADP-ribosylation-dependent ubiquitylation (PARdu)[56]. In fact, CBX4 is known to mediate SUMO conjugation in the DDR, and the recruitment of CBX4 to sites of DNA lesions is dependent on ADP-ribosylation[57]. Thus, our observation that CBX4 becomes ADP-ribosylated during oxidative stress strongly suggests that we have identified a previously uncharacterized DDR regulatory mechanism controlled by PARylation-dependent SUMOylation (PARsu).

The presented methodology is suitable for the identification of key endogenous ADP-ribosylation events in biological processes. We find that ADP-ribosylated proteins are on average less modified under physiological conditions than reported under siPARG treatment[9], which suggests that deregulation of PARG alters physiological ADP-ribosylation homoeostasis (Fig. 1b)[13,39]. Moreover, our MS analysis supports that Lys residues K498 and K505 are major acceptor sites in ARTD1, which follows previous mutational analysis of ADP-ribosylation sites on ARTD1 (ref. 7). Our analysis indicates that under physiological conditions ARTD1 is activated *in cis*[58], contradicting the observed *in trans* activation of ARTD1 under siPARG treatment[9].

Comparison of the SILAC and IF data obtained from HeLa cells revealed that the dynamic changes induced by H_2O_2 for these two data sets correlate well with each other. The relative increase in peptide abundance may thus suggest that the ADP-ribosylation sites detected reflect PARylation, at least partially. However, since the methodology described here cannot discriminate between MAR and PAR, each regulated ADP-ribosylation site will require follow-up experiments do determine whether they are indeed PARylated or MARylated.

The importance of tissue-specific protein ADP-ribosylation mapping is underscored by the substantial differences in ADP-ribosylation observed between cell culture and tissue (that is, liver). In mouse liver tissue the majority of ADP-ribosylated proteins localize to compartments containing enzymes with MAR activity, such as ARTD10, ARTD8, ARTC and SIRT4, suggesting that these proteins are primarily MARylated rather than PARylated (Fig. 4e). These observations are further supported by the increased levels of modified Arg residues, and membrane and extracellular proteins, which might stem from ARTC activity. Moreover, our data substantiates initial studies where ADP-ribosylation was observed on Arg residues within rat liver proteins[59]. From the analysed liver extracts, ARTD1 was not found to be auto-ADP-ribosylated, highlighting the fact that the enzyme is mainly inactive under normal, non-stressed conditions.

Our organ analysis of ADP-ribosylation provides evidence that the modification is involved in multiple physiological functions. For example, KEGG pathway analysis reveals that proteins involved in actin cytoskeleton and endoplasmic reticulum regulation are enriched in ADP-ribosylation (Supplementary Fig. 5c). These pathways have previously been associated with ADP-ribosylation[60,61], but the mechanism by which the modifications are catalysed (that is, ARTDs or ARTCs (ref. 62)) remains to be investigated. NAD^+ can be released on necrosis or mechanic stress in tissue, which in turn likely activates ARTCs during organ collecting[63]. Considering that ARTCs have lower affinity for NAD^+ compared with ARTD1, this renders ARTCs more prone to activation following NAD^+ release during tissue collecting. Moreover, we find that proteins involved in metabolic processes, oxidative-reduction processes and mitochondrial content are distinctly enriched in ADP-ribosylation targets (Fig. 4e and Supplementary Fig. 5f), which suggests these processes may be influenced by the modification. While the exact mechanisms are not well understood, inhibition of ARTDs is known to enhance these processes[64]. With ARTD1 activation known to affect cellular metabolism *via* direct PARylation events, transcriptional reprogramming, or alterations in cellular NAD^+ levels[64], our tissue analysis supports the hypothesis that metabolic consequences on ADP-ribosylation inhibition might occur via alterations in NAD^+ levels[65]. This is based on ARTD1 being an avid NAD^+ consumer, and that ADP-ribosylation inhibition increases the cellular levels of NAD^+ available for other ARTDs (ref. 65), in a manner reminiscent of the reported interplay between ARTD1 activity and deacetylase SIRT1 (ref. 66). Furthermore, with immortalized cell lines exhibiting mitochondria and metabolic processes deficiencies[67], hereby rendering them impractical for ADP-ribosylation inhibition/activation and cellular metabolism investigations, highlights that methodologies allowing proteomics-based whole tissue analyses are required to investigate this antagonistic interplay in more detail.

In conclusion, our novel methodology allows for the unbiased and sensitive characterization of ADP-ribosylation sites under physiological conditions, while the data presented here extends current ADP-ribosylation knowledge and highlights the widespread occurrence of the modification. Although the methodology presented cannot currently distinguish between MARylated and PARylated peptide species, adjustment of the binding reaction stringency and combining the enrichment with specific MAR-binding domains, will most likely facilitate dissecting peptide MAR- versus PARylation in a more specific manner[68]. Importantly, the approach presented supports comprehensive and quantitative evaluation of the mammalian ADP-ribosylome of cell lines and tissue samples. Thus, allowing downstream interrogation of disease pathways in which ARTs are implicated.

Methods

Cell culture and transfection. HeLa cells were grown in Dulbecco's modified Eagle's medium (D-MEM; Invitrogen) supplemented with 10% foetal bovine serum and penicillin/streptomycin (100 U ml^{-1}) (Gibco). Stable HeLa-Kyoto cells expressing CBX4, SRSF1 and FUS tagged with C-terminal GFP under the control of an endogenous promoter were generated by transfecting BAC transgenes and were kindly provided by Prof Anthony Hyman (Max Planck Institute, Dresden). Selection was maintained by adding 400 μg ml^{-1} G418 (Sigma Aldrich) to the culture medium. SILAC HeLa cells were grown in SILAC D-MEM (Invitrogen) supplemented with 10% dialyzed foetal bovine serum, L-glutamine, penicillin/streptomycin, and either L-lysine and L-arginine, L-lysine 4,4,5,5-D4 and L-arginine-U-13C6, or L-lysine-U-13C6-15N2 and L-arginine-U-13C6-15N4 (Cambridge Isotope Laboratories)[36]. The siRNA oligonucleotides against endogenous PARG (ID: 4390826) was purchased from Ambion as well as Negative Control siRNA#1. SiRNA transfections were performed using Lipofectamine RNAiMAX (Invitrogen) according to the manufacturer's protocol and lysed 48 h after transfection. All HeLa cells used for experiments were tested negative for mycoplasma.

Sample preparation. Cells were stimulated with H_2O_2 (Sigma Aldrich) for 10 min in PBS at 37 °C, collected by washing with ice-cold PBS and lysed in modified RIPA buffer (50 mM Tris pH 7.5, 400 mM NaCl, 1 mM EDTA, 1% Nonidet P-40, 0.1% Na-deoxycholate), protease inhibitor mixture (Roche) supplemented with 2 mM Na-orthovanadate, 5 mM NaF, 5 mM Glycero-2-phosphate, 1 μM ADP-HPD (Millipore) and 40 μM PJ-34 (Enzo Life Sciences) and cleared by high-speed centrifugation. Proteins were precipitated by adding fourfold excess volumes of

ice-cold acetone and stored at −20 °C overnight. Subsequently, proteins were solubilized in a urea solution (6 M urea/2 M thiourea/10 mM HEPES pH 8.0). Protein concentrations in lysates were measured using Bradford assay (Bio-Rad). Next, proteins were reduced by adding dithiothreitol to a final concentration of 1 mM, and alkylated with chloroacetamide at 5.5 mM. Proteins were digested using endoproteinase Lys-C (1:100 w/w) and modified sequencing grade trypsin (1:100 w/w) after a fourfold dilution in 50 mM ammonium bicarbonate solution. Protease digestion was terminated by slow addition of trifluoroacetic acid to pH 2. Precipitates were removed by centrifugation for 10 min at 3,000*g*. Peptides were purified using reversed-phase Sep-Pak C18 cartridges (Waters). Peptides were eluted off the Sep-Pak with 50 and 80% acetonitrile.

GST-protein expression and purification of Af1521. BL21 was used for long transformation. Briefly, 1 µl of cooled plasmid was added to BL21 and left on ice for 15 min. Bacteria were heat shocked at 42 °C for 45 sec, incubated for 1 min on ice and then mixed with SOC for 40 min at 37 °C. Bacteria were streaked onto Amp-plates and left overnight at 37 °C. The following day a single colony was inoculated in LB media and grown overnight at 37 °C. The starter culture was diluted and grown to an OD600 of 0.55–0.65. Protein expression was induced by adding IPTG to final concentration of 0.5 mM and incubated for 5–6 h. Bacteria were spun down and pellet frozen at −80 °C.

The bacterial pellet was thawn and incubated for 20 min in lysis buffer (50 mM Tris–HCl, pH 7.5, 150 mM NaCl, 1 mM MgCl2, 1 mM dithiothreitol, 1 × Bug Buster (Novagen), 1 µl ml^{-1} Benzonase (Sigma Aldrich), 200 µg ml^{-1} lysozyme (Sigma Aldrich), protease inhibitor mixture (Roche)). After breaking cells by vortexing with glass beads, cell debris was pelleted by centrifugation. The cleared lysate was incubated for 4 h at 4 °C rolling with equilibrated glutathione sepharose 4B (Sigma Aldrich). Beads were washed four times in wash buffer (50 mM Tris–HCl, pH 7.5, 150 mM NaCl and 1 mM dithiothreitol), resuspended in wash buffer and kept at 4 °C for up to 3 weeks.

Enrichment of ADP-ribosylated peptides. After eluting off Sep-Pak, appropriate amounts of IP buffer (50 mM Tris–HCl, pH 8, 10 mM MgCl2, 250 µM dithiothreitol and 50 mM NaCl) was added before the acetonitrile and the volume was reduced by vacuum centrifugation. PAR complexity was reduced by incubation with PARG (4.2 µg per sample) for 3 h at 37 °C. The peptide mixture was cooled down before it was incubated rotating for 2 h at 4 °C with the purified Af1521 macro domain. The peptides were washed three times in ice-cold IP buffer followed by one wash in water, and modified peptides were eluted with 2 × 100 µl 0.15% TFA in Milli-Q water. Peptide eluates were desalted on reverse phase C18 StageTips[69].

Mass spectrometric analysis. All MS experiments were performed on a nanoscale EASY-nLC 1000 UHPLC system (Thermo Fisher Scientific) connected to an Orbitrap Q-Exactive Exactive equipped with a nanoelectrospray source (Thermo Fisher Scientific). Each sample was eluted off the StageTip, auto-sampled and separated on a 15 cm analytical column (75 µm inner diameter) in-house packed with 1.9-µm C18 beads (Reprosil Pur-AQ, Dr Maisch) using a 3 h gradient ranging from 5 to 64% acetonitrile in 0.5% formic acid at a flow rate of 200 nl min^{-1}. The effluent from the high-performance liquid chromatography was directly electrosprayed into the mass spectrometer. The Q Exactive Plus mass spectrometer was operated using data-dependent acquisition, with all samples being analysed using a 'sensitive' acquisition method[22] and a normalized collision energy of 28. Back-bone fragmentation of eluting peptide species were obtained using HCD which ensured high-mass accuracy on both precursor and fragment ions.

Mass spectrometry analysis of ADP-ribosylation sites by ETD. ETD spectra of ADP-ribosylated peptides were acquired on an Orbitrap Fusion Lumos mass spectrometer (Thermo Scientific) operating in positive ion mode. Full MS scans (m/z 300–1,500) were performed at 120,000 resolution (m/z 200) in the Orbitrap, with the AGC target set at 4e5. Precursor selection was prioritized on the basis of highest charge state followed by highest intensity. Peptides (charge states from 3 + to 6 +) were selected by the quadrupole (1.3 m/z isolation window) before reaction with fluoranthene radical anions (ETD reagent target 4e5). ETD reaction times were set at 1.7τ for each charge state. MS/MS spectra were acquired using a normal ion trap scan rate with a maximum injection time of 50 ms (AGC target 2e5). A Venn diagram comparing identified protein targets derived from the ETD with HCD analysis is shown in Supplementary Fig. 6a.

***In vitro* TOF-MS analysis of H2B peptide sequence**. 1 µg of HK326 peptide (PQPAKSAPAPKKG) was incubated with 1 mM ADP-ribose in 50 mM sodium phosphate buffer (pH 7.5 and pH 9.5) for 1 h or overnight at 37 °C. Samples were desalted using Reversed-phase m-C18 ZipTips (for MALDI-MS) and eluted with MALDI matrix solution (a-cyano-4-hydroxycinnamicacid in 0.3 mM di-ammonium hydrogen citrate (Fluka), 60% acetonitrile in H_2O) directly on the target plate. MALDI analyses were performed on a 4800 MALDI TOF/TOF system in linear mode.

Identification of peptides and proteins. All raw data analysis was performed with MaxQuant software suite version 1.3.0.5 supported by the Andromeda search engine[70]. Data were searched against a concatenated target/decoy (forward and reversed) version of the UniProt Human fasta database encompassing 71,434 protein entries (downloaded from www.uniprot.org on 2013-07-03). Mass tolerance for searches was set to maximum 7 p.p.m. for peptide masses and 20 p.p.m. for HCD fragment ion masses. Data were searched with carbamidomethylation as a fixed modification and protein *N*-terminal acetylation, methionine oxidation and mono-ADP-ribosylation (m/z 541,06110: C10H13N5O9P2) on lysine, arginine, glutamic and aspartic acids as variable modifications. A maximum of three mis-cleavages was allowed while requiring strict trypsin specificity, and only peptides with a minimum sequence length of seven were considered for further data analysis. Peptide assignments were statistically evaluated in a Bayesian model on the basis of sequence length and Andromeda score. Only peptides and proteins with a false discovery rate of <1% were accepted, estimated on the basis of the number of accepted reverse hits, and false discovery rate values were finally estimated separately for modified and unmodified peptides. Protein sequences of common contaminants such as human keratins and proteases used were added to the database. For SILAC quantification a minimum of two ratio-counts was required.

GFP, strep and methylated protein precipitations. Cells expressing the tagged versions of the proteins of interest were collected by washing with PBS and lysed in modified RIPA buffer (50 mM Tris pH 7.5, 400 mM NaCl, 1 mM EDTA, 1% Nonidet P-40, 0.1% Na-deoxycholate), protease inhibitor mixture (Roche) supplemented with 2 mM Na-orthovanadate, 5 mM NaF, 5 mM Glycero-2-phosphate, 1 µM ADP-HPD (Millipore) and 40 µM PJ-34 (Enzo Life Sciences). Lysates were diluted in modified RIPA without salt and then cleared by high-speed centrifugation.

GFP-immunoprecipitaion was performed with 20 µl GFP-Trap_A agarose beads (Chromotek). 1 mg of protein mixtures were incubated for 2 h rotating at 4 °C before washing and subsequent elution with 2 × Laemmli sample buffer (Thermo Fisher Scientific) at 90 °C. Pull down of ADP-ribosylated proteins was performed similarly but using 200 µl crosslinked Af1521 macro domain and 2 mg of protein mixtures.

Western blotting. The following antibodies were used in this study: rabbit polyclonal PAR 1:1,000 (ALX-210–890A, Enzo Life Science) and mouse monoclonal GFP 1:1,000 (11814460001, Roche).

Total cell lysates together with the eluates were resolved on 4–12% gradient SDS–PAGE gels (Thermo Fisher Scientific) and proteins were transferred onto nitrocellulose membranes (Sigma Aldrich). Membranes were blocked using 5% BSA solution in PBS supplemented with Tween-20 (0.1%). Secondary antibodies coupled to horseradish peroxidase (Jackson ImmunoResearch Laboratories) were used for immunodetection. The detection was performed with Novex ECL Chemiluminescent Substrate Reagent Kit (Invitrogen). For slot blot analysis, PAR polymer (Trevigen) was incubated with different concentrations of PARG and spottet directly onto PVDF membranes (Millipore) using the slot blot chamber (Fisher Scientific) according to manufacturer's protocol. Cropped WBs presented in Fig. 2d have been included as uncropped scans in Supplementary Fig. 6b.

Immunofluorescence microscopy. HeLa cells were seeded on coverslips and the following day stimulated for indicated time points with H_2O_2. After washing with PBS, cells were fixed in methanol/acetic acid solution and incubated for 5 min at 37 °C. Coverslips were blocked in 5% milk powder, transferred to a humid chamber and incubated with rabbit polyclonal PAR (Enzo Life Science) for 1 h at 37 °C and with secondary antibody Alexa Fluor 488 (Invitrogen) for 1 h at 37 °C, stained with DAPI for 2 min, washed in PBS and mounted. Images were acquired on a DFC345 FX microscope (Leica) and analysed using ImageJ.

Immuno-slot-blot. For the immuno-slot-blot analysis, HeLa cells were treated and lysed as described in sample preparation, and proteins were vacuum aspirated onto a Hybond P 0.2 PVDF (Amersham Biosciences) using a slot-blot manifold (Amersham Biosciences). The membrane was blocked with 5% milk powder in 10 mM Tris–HCL (pH 8.0), 150 mM NaCl and 0.05% (v/v) Tween 20 (TBST buffer) and incubated with polyclonal PAR antibody (Enzo Life Science) diluted 1:1,000 in 5% milk powder in TBST for 1 h at RT and with secondary antibody IRDye 800CW goat anti-rabbit IgG (LI-COR) 1:15,000 in TBST for 1 h at RT. Signals were detected by the Odyssey infrared imaging system (LI-COR) and the immunoblot signal was quantified using GelEval (FrogDance Software).

***In vitro* radiography assay**. 10 pmol of ARTD1 and ARTD10 were automodified with 100 nM NAD^+ for 10 min at 37 °C, respectively, hereby inducing short PAR chains on ARTD1 and MAR on ARTD10 through auto-catalysis[29]. Samples were filtered through G50 columns to remove excess amount of unincorporated NAD^+, and subsequently treated with 10 pmol PARG for additional 1 h at 37 °C. Using autoradiography assays the hydrolysis of attached radioactive 32P-NAD^+ of the protein substrates were subsequently monitored. For transmodification reactions,

50 pmol of target protein was incubated with 10 pmol ARTD1 for 10 min at 37 °C. The reaction was stopped by adding Laemmli buffer and boiling for 5 min at 95 °C. After separation of samples by SDS–PAGE, the radiolabelled ADP-ribosylation signal was determined by GelEval (FrogDance Software).

Preparation of mouse liver extracts. Male 9-week-old C57BL/6 mice were maintained on a 12-h light–dark cycle with regular unrestricted diet. Mice were killed in a CO_2 chamber. Excised livers were washed in PBS and shock frozen in liquid nitrogen. Ice-cold modified RIPA buffer (supplemented with PARP-, PARG- and protease inhibitors as described before) was added to the shock frozen livers and they were lysed operating the Tissue Lyser II (Qiagen) device at 30 HZ for 4×30 s. The lysate was further sonicated until it became fluid and all liver pieces were dissolved. The lysate was cleared by high-speed centrifugation and processed similar as described for the cell culture samples. 20 mg of liver protein was used as starting material for the digest.

Bioinformatic analyses. Statistical analysis and hierarchical clustering was performed using the Perseus software suite (Max Planck Institute of Biochemistry, Department of Proteomics and Signal Transduction, Munich). Significantly enriched Gene Ontology terms were determined using the Functional Annotation Tool of the DAVID Bioinformatics database. Protein interaction networks were analysed using the interaction data from the STRING database (v. 9.05) and visualized using Cytoscape (v. 2.8.3). Protein abundance assessment was performed using a deep proteome reference data set for HeLa cells. All Venn diagrams were generated using the online Venny program (http://bioinfogp.cnb.csic.es/tools/venny/).

Comments related to animal study. C57BL/6J mice were bread at the animal facility of the University of Zurich. No randomization or blinding were used for these studies, and no animals had to be excluded. All animal experiments were carried out in accordance with the Swiss and EU ethical guidelines and have been approved by the local animal experimentation committee of the Canton of Zurich under licence #2012207 and following the 3R guidelines.

Data availability. The mass spectrometry proteomics data have been deposited to the ProteomeXchange Consortium via the PRIDE partner repository[71] with the data set identifier PXD004245. The additional data that support the findings of this study are available from the corresponding author on request.

References

1. Rack, J. G. *et al.* Identification of a class of protein ADP-ribosylating sirtuins in microbial pathogens. *Mol. Cell* **59,** 309–320 (2015).
2. Hottiger, M. O., Hassa, P. O., Luscher, B., Schuler, H. & Koch-Nolte, F. Toward a unified nomenclature for mammalian ADP-ribosyltransferases. *Trends Biochem. Sci.* **35,** 208–219 (2010).
3. Peijs, K. L. *et al.* ARTD10 substrate identification on protein microarrays: regulation of GSK3beta by mono-ADP-ribosylation. *Cell Commun. Signal.* **11,** 5 (2013).
4. Rouleau, M., Patel, A., Hendzel, M. J., Kaufmann, S. H. & Poirier, G. G. PARP inhibition: PARP1 and beyond. *Nat. Rev. Cancer* **10,** 293–301 (2010).
5. Polo, S. E. & Jackson, S. P. Dynamics of DNA damage response proteins at DNA breaks: a focus on protein modifications. *Genes Dev.* **25,** 409–433 (2011).
6. Meyer-Ficca, M. L., Meyer, R. G., Coyle, D. L., Jacobson, E. L. & Jacobson, M. K. Human poly(ADP-ribose) glycohydrolase is expressed in alternative splice variants yielding isoforms that localize to different cell compartments. *Exp. Cell Res.* **297,** 521–532 (2004).
7. Altmeyer, M., Messner, S., Hassa, P. O., Fey, M. & Hottiger, M. O. Molecular mechanism of poly(ADP-ribosyl)ation by PARP1 and identification of lysine residues as ADP-ribose acceptor sites. *Nucleic Acids Res.* **37,** 3723–3738 (2009).
8. Vandekerckhove, J., Schering, B., Barmann, M. & Aktories, K. Clostridium perfringens iota toxin ADP-ribosylates skeletal muscle actin in Arg-177. *FEBS Lett.* **225,** 48–52 (1987).
9. Zhang, Y., Wang, J., Ding, M. & Yu, Y. Site-specific characterization of the Asp- and Glu-ADP-ribosylated proteome. *Nat. Meth.* **10,** 981–984 (2013).
10. McDonald, L. J. & Moss, J. Enzymatic and nonenzymatic ADP-ribosylation of cysteine. *Mol. Cell. Biochem.* **138,** 221–226 (1994).
11. Olsen, J. V. & Mann, M. Status of large-scale analysis of post-translational modifications by mass spectrometry. *Mol. Cell. Proteomics.* **12,** 3444–3452 (2013).
12. Daniels, C. M., Ong, S. E. & Leung, A. K. Phosphoproteomic approach to characterize protein mono- and poly(ADP-ribosyl)ation sites from cells. *J. Proteome. Res.* **13,** 3510–3522 (2014).
13. Min, W., Cortes, U., Herceg, Z., Tong, W. M. & Wang, Z. Q. Deletion of the nuclear isoform of poly(ADP-ribose) glycohydrolase (PARG) reveals its function in DNA repair, genomic stability and tumorigenesis. *Carcinogenesis* **31,** 2058–2065 (2010).
14. Hanai, S. *et al.* Loss of poly(ADP-ribose) glycohydrolase causes progressive neurodegeneration in Drosophila melanogaster. *Proc. Natl Acad. Sci. USA* **101,** 82–86 (2004).
15. Yu, S. W. *et al.* Apoptosis-inducing factor mediates poly(ADP-ribose) (PAR) polymer-induced cell death. *Proc. Natl Acad. Sci. USA* **103,** 18314–18319 (2006).
16. Cuzzocrea, S. *et al.* Role of poly(ADP-ribose) glycohydrolase in the development of inflammatory bowel disease in mice. *Free Radic. Biol. Med.* **42,** 90–105 (2007).
17. Daniels, C. M., Ong, S.-E. & Leung, A. K. L. The promise of proteomics for the study of ADP-Ribosylation. *Mol. Cell* **58,** 911–924 (2015).
18. Gibson, B. A. *et al.* Chemical genetic discovery of PARP targets reveals a role for PARP-1 in transcription elongation. *Science* **353,** 45–50 (2016).
19. Slade, D. *et al.* The structure and catalytic mechanism of a poly(ADP-ribose) glycohydrolase. *Nature* **477,** 616–620 (2011).
20. Jungmichel, S. *et al.* Proteome-wide identification of poly(ADP-Ribosyl)ation targets in different genotoxic stress responses. *Mol. Cell* **52,** 272–285 (2013).
21. Sylvestersen, K. B., Young, C. & Nielsen, M. L. Advances in characterizing ubiquitylation sites by mass spectrometry. *Curr. Opin. Chem. Biol.* **17,** 49–58 (2013).
22. Kelstrup, C. D., Young, C., Lavallee, R., Nielsen, M. L. & Olsen, J. V. Optimized fast and sensitive acquisition methods for shotgun proteomics on a quadrupole orbitrap mass spectrometer. *J. Proteome. Res.* **11,** 3487–3497 (2012).
23. Rosenthal, F., Nanni, P., Barkow-Oesterreicher, S. & Hottiger, M. O. Optimization of LTQ-orbitrap mass spectrometer parameters for the identification of ADP-Ribosylation Sites. *J. Proteome. Res.* **14,** 4072–4079 (2015).
24. Hengel, S. M. & Goodlett, D. R. A review of tandem mass spectrometry characterization of adenosine diphosphate-ribosylated peptides. *Int. J. Mass. Spectrom.* **312,** 114–121 (2012).
25. Tao, Z., Gao, P. & Liu, H. W. Identification of the ADP-ribosylation sites in the PARP-1 automodification domain: analysis and implications. *J. Am. Chem. Soc.* **131,** 14258–14260 (2009).
26. Karras, G. I. *et al.* The macro domain is an ADP-ribose binding module. *Embo J.* **24,** 1911–1920 (2005).
27. Martello, R., Mangerich, A., Sass, S., Dedon, P. C. & Burkle, A. Quantification of cellular poly(ADP-ribosyl)ation by stable isotope dilution mass spectrometry reveals tissue- and drug-dependent stress response dynamics. *ACS Chem. Biol.* **8,** 1567–1575 (2013).
28. Jankevicius, G. *et al.* A family of macrodomain proteins reverses cellular mono-ADP-ribosylation. *Nat. Struct. Mol. Biol.* **20,** 508–514 (2013).
29. Rosenthal, F. *et al.* Macrodomain-containing proteins are new mono-ADP-ribosylhydrolases. *Nat. Struct. Mol. Biol.* **20,** 502–507 (2013).
30. Kleine, H. *et al.* Substrate-assisted catalysis by PARP10 limits its activity to mono-ADP-ribosylation. *Mol. Cell* **32,** 57–69 (2008).
31. Tabb, D. L. *et al.* Repeatability and reproducibility in proteomic identifications by liquid chromatography-tandem mass spectrometry. *J. Proteome. Res.* **9,** 761–776 (2010).
32. Coon, J. J., Shabanowitz, J., Hunt, D. F. & Syka, J. E. Electron transfer dissociation of peptide anions. *J. Am. Soc. Mass Spectrom.* **16,** 880–882 (2005).
33. Bryant, H. E. *et al.* PARP is activated at stalled forks to mediate Mre11-dependent replication restart and recombination. *Embo J.* **28,** 2601–2615 (2009).
34. Kraus, W. L. & Lis, J. T. PARP goes transcription. *Cell* **113,** 677–683 (2003).
35. Cervantes-Laurean, D., Jacobson, E. L. & Jacobson, M. K. Glycation and glycoxidation of histones by ADP-ribose. *J. Biol. Chem.* **271,** 10461–10469 (1996).
36. Ong, S. E. *et al.* Stable isotope labeling by amino acids in cell culture, SILAC, as a simple and accurate approach to expression proteomics. *Mol. Cell. Proteomics.* **1,** 376–386 (2002).
37. Messner, S. *et al.* PARP1 ADP-ribosylates lysine residues of the core histone tails. *Nucleic Acids Res.* **38,** 6350–6362 (2010).
38. Shah, G. M. *et al.* Approaches to detect PARP-1 activation *in vivo*, *in situ*, and *in vitro*. *Methods Mol. Biol.* **780,** 3–34 (2011).
39. Cortes, U. *et al.* Depletion of the 110-kilodalton isoform of poly(ADP-ribose) glycohydrolase increases sensitivity to genotoxic and endotoxic stress in mice. *Mol. Cell. Biol.* **24,** 7163–7178 (2004).
40. Andersson, A. *et al.* PKCalpha and HMGB1 antagonistically control hydrogen peroxide-induced poly-ADP-ribose formation. *Nucleic Acids Res.* (2016).
41. Olsen, J. V. *et al.* Quantitative phosphoproteomics reveals widespread full phosphorylation site occupancy during mitosis. *Sci. Signal.* **3,** ra3 (2010).
42. Gibson, B. A. & Kraus, W. L. Small molecules, big effects: a role for chromatin-localized metabolite biosynthesis in gene regulation. *Mol. Cell.* **41,** 497–499 (2011).
43. Garnett, M. J. *et al.* Systematic identification of genomic markers of drug sensitivity in cancer cells. *Nature* **483,** 570–575 (2012).
44. Szklarczyk, D. *et al.* STRING v10: protein-protein interaction networks, integrated over the tree of life. *Nucleic Acids Res.* **43,** D447–D452 (2015).

45. Steen, H., Jebanathirajah, J. A., Springer, M. & Kirschner, M. W. Stable isotope-free relative and absolute quantitation of protein phosphorylation stoichiometry by MS. *Proc. Natl Acad. Sci. USA* **102,** 3948–3953 (2005).
46. Butepage, M., Eckei, L., Verheugd, P. & Luscher, B. Intracellular mono-ADP-Ribosylation in signaling and disease. *Cells* **4,** 569–595 (2015).
47. Asher, G. *et al.* Poly(ADP-ribose) polymerase 1 participates in the phase entrainment of circadian clocks to feeding. *Cell* **142,** 943–953 (2010).
48. Vyas, S. *et al.* Family-wide analysis of poly(ADP-ribose) polymerase activity. *Nat. Commun.* **5,** 4426 (2014).
49. Menzel, S. *et al.* Nucleotide-induced membrane-proximal proteolysis controls the substrate specificity of T Cell Ecto-ADP-Ribosyltransferase ARTC2.2. *J. Immunol.* **195,** 2057–2066 (2015).
50. Daniels, C. M., Ong, S.-E. & Leung, A. K. L. Phosphoproteomic approach to characterize protein mono- and poly(ADP-ribosyl)ation sites from Cells. *J. Proteome. Res.* **13,** 3510–3522 (2014).
51. Garber, K. PARP inhibitors bounce back. *Nat. Rev. Drug. Discov.* **12,** 725–727 (2013).
52. Vyas, S. & Chang, P. New PARP targets for cancer therapy. *Nat. Rev. Cancer.* **14,** 502–509 (2014).
53. Kleppa, L. *et al.* Kinetics of endogenous mouse FEN1 in base excision repair. *Nucleic Acids Res.* **40,** 9044–9059 (2012).
54. Hasan, S. *et al.* Regulation of human flap endonuclease-1 activity by acetylation through the transcriptional coactivator p300. *Mol. Cell.* **7,** 1221–1231 (2001).
55. Guo, Z. *et al.* Sequential posttranslational modifications program FEN1 degradation during cell-cycle progression. *Mol. Cell* **47,** 444–456 (2012).
56. Zhang, Y. *et al.* RNF146 is a poly(ADP-ribose)-directed E3 ligase that regulates axin degradation and Wnt signalling. *Nat. Cell Biol.* **13,** 623–629 (2011).
57. Chou, D. M. *et al.* A chromatin localization screen reveals poly (ADP ribose)-regulated recruitment of the repressive polycomb and NuRD complexes to sites of DNA damage. *Proc. Natl Acad. Sci. USA* **107,** 18475–18480 (2010).
58. Langelier, M. F., Planck, J. L., Roy, S. & Pascal, J. M. Structural basis for DNA damage-dependent poly(ADP-ribosyl)ation by human PARP-1. *Science* **336,** 728–732 (2012).
59. Moss, J. & Stanley, S. J. Amino acid-specific ADP-ribosylation. Identification of an arginine-dependent ADP-ribosyltransferase in rat liver. *J. Biol. Chem.* **256,** 7830–7833 (1981).
60. Aktories, K. *et al.* Botulinum C2 toxin ADP-ribosylates actin. *Nature* **322,** 390–392 (1986).
61. Jwa, M. & Chang, P. PARP16 is a tail-anchored endoplasmic reticulum protein required for the PERK- and IRE1alpha-mediated unfolded protein response. *Nat. Cell Biol.* **14,** 1223–1230 (2012).
62. Aktories, K. & Barbieri, J. T. Bacterial cytotoxins: targeting eukaryotic switches. *Nat. Rev. Micro.* **3,** 397–410 (2005).
63. Koch-Nolte, F., Fischer, S., Haag, F. & Ziegler, M. Compartmentation of NAD^+-dependent signalling. *FEBS Lett.* **585,** 1651–1656 (2011).
64. Bai, P. & Canto, C. The role of PARP-1 and PARP-2 enzymes in metabolic regulation and disease. *Cell Metab.* **16,** 290–295 (2012).
65. Houtkooper, R. H., Canto, C., Wanders, R. J. & Auwerx, J. The secret life of NAD^+: an old metabolite controlling new metabolic signaling pathways. *Endocr. Rev.* **31,** 194–223 (2010).
66. Bai, P. *et al.* PARP-1 inhibition increases mitochondrial metabolism through SIRT1 activation. *Cell Metab.* **13,** 461–468 (2011).
67. Pan, C., Kumar, C., Bohl, S., Klingmueller, U. & Mann, M. Comparative proteomic phenotyping of cell lines and primary cells to assess preservation of cell type-specific functions. *Mol. Cell. Proteomics.* **8,** 443–450 (2009).
68. Bartolomei, G., Leutert, M., Manzo, M., Baubec, T. & Hottiger, M. O. Analysis of chromatin ADP-Ribosylation at the genome-wide level and at specific loci by ADPr-ChAP. *Mol. Cell* **61,** 474–485 (2016).
69. Rappsilber, J., Ishihama, Y. & Mann, M. Stop and go extraction tips for matrix-assisted laser desorption/ionization, nanoelectrospray, and LC/MS sample pretreatment in proteomics. *Anal. Chem.* **75,** 663–670 (2003).
70. Cox, J. & Mann, M. MaxQuant enables high peptide identification rates, individualized p.p.b.-range mass accuracies and proteome-wide protein quantification. *Nat. Biotechnol.* **26,** 1367–1372 (2008).
71. Vizcaino, J. A. *et al.* The PRoteomics IDEntifications (PRIDE) database and associated tools: status in 2013. *Nucleic Acids Res.* **41,** D1063–D1069 (2013).

Acknowledgements

We thank members of the NNF-CPR for fruitful discussions and careful reading of the manuscript. Ms Monika Fey is acknowledged for the expression and purification of recombinant human PARG (University of Zurich) and Paolo Nanni for technical support for the MS measurements (FGCZ, University of Zurich). Stephan Christen and Deena Leslie Pedrioli provided editorial assistance and critical input during the writing (University of Zurich). The work carried out in the laboratory of MLN was in part supported by the Novo Nordisk Foundation Center for Protein Research; the Novo Nordisk Foundation (grant number NNF14CC0001 and NNF13OC0006477); the Lundbeck Foundation (Grant number R171-2014-1496); The Danish Council of Independent Research, grant number DFF 4002-00051 (Sapere Aude) and grant agreement number DFF 4183-00322A. ADP-ribosylation research in the laboratory of MOH is funded by the Kanton of Zurich, the University Research Priority Program (URPP) in Translational Cancer Biology at the University of Zurich, and the Swiss National Science Foundation (grant 310030B_138667).

Author contributions

R.M., S.J. and M.L.N. developed the method and M.L., V.B. and M.O.H. provided critical inputs. R.M., S.J., M.L., V.B. and S.C.L. performed HeLa MS experiments. M.L. and V.B. performed *in vitro* ADP-ribosylation assays, R.M. and V.B. performed the *in vitro* glycation analysis, and M.L. performed the liver tissue analysis. R.M. performed IF experiments and S.C.L performed validation by WBs. S.C.L. and C.Y. performed ETD measurements. M.O.H. and M.L.N. wrote the paper.

Additional information

Supplementary Information accompanies this paper at http://www.nature.com/naturecommunications

Competing financial interests: The authors declare no competing financial interests.

Reprints and permission information is available online at http://npg.nature.com/reprintsandpermissions/

How to cite this article: Martello, R. *et al.* Proteome-wide identification of the endogenous ADP-ribosylome of mammalian cells and tissue. *Nat. Commun.* **7,** 12917 doi: 10.1038/ncomms12917 (2016).

Supplementary Materials

Supplementary Figure Legends

Supplementary Figure 1

(a) HCD tandem mass spectrum of peptide sequence GKSGAALSK, identifying Lysine K498 as ADP-ribosylated acceptor site. Identification of ADP-ribosylated peptides are greatly aided by the diagnostic ions generated by the ADP-ribosylation group of the modified peptide (Labeled as “Ribose”, “Adenosine”, “AMP”, “ADP”, “-ADPR”, “-ADP”, “-AMP”, “-Adenosine”.

(b) Distribution of identified ADP-ribosylation sites per protein

(c) ETD tandem mass spectrum of peptide sequence GKSGAALSK, idenfying Lysine K498 as ADP-ribosylated acceptor site. Further corroborating the ability of HCD for mapping of ADP-ribosylation sites.

(d) ETD tandem mass spectrum of peptide sequence LPVSSKPGK.

(e) Abundance distribution of the human HeLa proteome (white bars); the distribution of the annotated human nuclear HeLa proteome (red bars); and the distribution of identified ADP-ribosylated factors (blue bars).

Supplementary Figure 2

(a) Experimental design of SILAC experiment to determine if PARG digestion is able to induce in vitro glycation. Briefly, heavy labeled SILAC cells were treated with purified PAR while light SILAC cells were left untreated. Both cell conditions were subsequently treated with PARG, mixed 1:1 and ADP-ribosylated peptides analysed by LC-MS/MS. If PARG digestion is able to cause in vitro glycation we would expect identification of SILAC regulated ADP-ribosylation sites.

(b) In vitro glycation analysis of H2B peptide sequence PQPAKSAPAPKKG at different time-points and pH.

(c) Tandem mass spectrum that map in vitro glycations products to lysine residues within the investigated H2B peptide, PQPAKSAPAPKKG.

Supplementary Figure 3

In vitro PARylation analysis of identified protein targets FEN1, CEBPB and SSRP1. Various inactive mutant versions of purified full-length human ARTD1 (Y907A, C908R or E988K) was incubated with recombinantly expressed proteins in the presence of 32P-NAD and double-stranded DNA oligomer. Samples were resolved by SDS-PAGE, stained with Coomassie (CB; lower panels) and 32P-incorporation was detected by autoradiography (P32; upper panels).

For all investigated PARP1 mutants no ADP-ribosylation was detected, confirming that the ADP-ribosylation observed (Figure 2c) is catalyzed by wild-type PARP1 and not a glycation product.

Supplementary Figure 4

(a) Experimental design used for quantitative evaluation of ADP-ribosylation sites (SILAC ratios). Light SILAC condition was exposed shortly to H_2O_2 while heavy SILAC was exposed as indicated. A quantitative analysis revealed that measured SILAC ratios are most increased following 5-10 stimulation with H_2O_2.

(b) Immunoflourescence (IF) imaging of cells treated with H_2O_2 for indicated time-points (0 min, 5 min, 10 min, 30 min, 1 hour, 2 hours), and immunostained with PAR-specific antibody or DAPI as indicated. Strongest PAR signal is observed after 5-10 minute treatment of H_2O_2.

(c) Left: Immuno-slot blot analysis of PAR formation in HeLa cells treated with H_2O_2 for indicated time-points (0 min, 5 min, 10 min, 30 min, 1 hour, 2 hours). Right: Strongest PAR signal is observed after 5-10 minute treatment of H_2O_2.

B) Densiometric evaluation of immune-slot blot analysis. The strongest abundance in PAR signal is observed after 5-10 minutes treatment of H_2O_2. Data represent mean +/- SD of n=3 independent analyses.

(d) Distribution of ADP-ribosylation occupancy in cells exposed to H_2O_2 for 10 minutes. Fifty percent of all ADP-ribosylation sites have occupancy of 11% or more.

(e) Distribution of amino acid occupancies across identified ADP-ribosylation sites in cells exposed to H_2O_2 for 10 minutes. Occupancy is determined for both heavy (Blue bars) and light (Red bars) SILAC conditions, which correspond to treated and untreated conditions, respectively. Collectively arginine residues are observed harboring the highest occupancy.

(f) Venn diagram between identified ADP-ribosylated substrates and previously identified PARylated substrates derived from Jungmichel et al, 2013.

(g) Scatter plot show correlation of logarithmized H/L ratios from Olaparib treated SILAC experiments as indicated.

Supplementary Figure 5

(a) Protein interaction networks of regulated ADP-ribosylation sites upon Olaparib treatment. Data was combined from two SILAC experiments where cells were treated with two different inhibitor concentrations (1 µM and 10 µM Olaparib). Network interaction data was extracted from the STRING database and visualized using Cytoscape.

(b) GO functional annotation of significantly regulated proteins from Olarapib SILAC experiments as compared to annotated GO genes in the entire genome (indicated p-values < 1.5e-17). Strong enrichment for biological processes known to be targeted by PARP is observed.

(c) GO biological processes annotation of tissue-derived ADP-ribosylation factors compared to annotated GO genes across the entire human genome.

(d) KEGG pathway annotation of tissue-derived ADP-ribosylation factors compared to annotated genes across the entire human genome.

Supplementary Figure 6

(a) Venn diagram showing the overlap in identified proteins from analyzing Af1521 enrichment samples with HCD versus ETD (comparison of data listed in Supplementary Data 1 and Supplementary Data 5).

(b) Uncropped western blots from Fig. 2d.

Supplementary Note 1 - Estimation of enrichment level

In order to establish a proper lysates:Af1521 level, we incubated a fixed amount of purified Af1521 macrodomain with increasing amounts of a H2O2-treated HeLa lysates (2.5 mg, 5 mg, 10 mg, 15 mg, 20 mg of lysate material, respectively). Following incubation and Af1521 enrichment, we determined the number of identified ADP-ribosylation sites by LC-MS analysis (Figure a). From replicate analyses we observed an increasing amount of identified ADP-ribosylation sites with increasing levels of HeLa lysate. However, a saturation level was observed at levels above 10 mg of cell lysates (Figure a), indicative of saturation of the Af1521 domain. Hence, from these data we determined that the appropriate amount of cell lysate material for our enrichment procedure would be 8-10 mg.

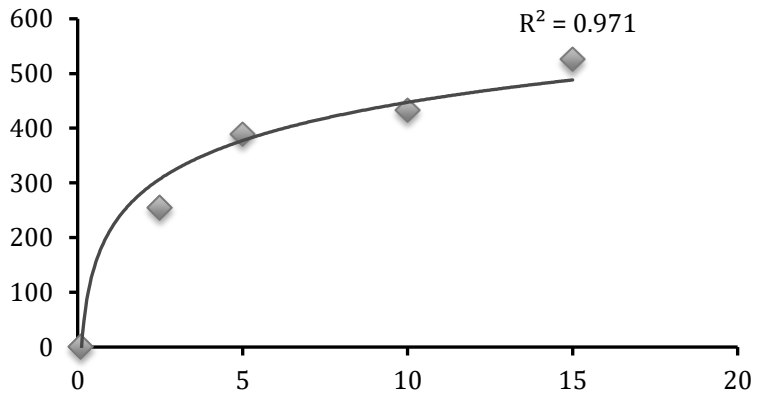

Figure a

To estimate the enrichment level of the developed methodology, we compared the number of identified ADP-ribosylation sites from a non-enriched HeLa cell lysate to the same sample after enrichment with our Af1521 methodology. Both samples were initially treated with 500 µM H_2O_2 to induce formation of ADP-ribosylation, and subsequently both samples were treated with PARG enzyme to convert all PAR into MAR.

However, in the next step, only one lysate sample was used for enrichment of ADP-ribosylation sites using the Af1521 macrodomain while the other whole HeLa cell lysate was left non-enriched. Both samples were subsequently analyzed by LC-MS using identical LC gradient and MS settings, and the obtained data files were processed for identification of ADP-ribosylation sites using the MaxQuant software suite (see method section for further details and settings).

	Total peptides	ADP-ribosylated peptides	Phosphorylated peptides
500 ug whole HeLa cell lysate	~25,000	1	70
Af1521 enrichment – 2.5mg	15,814	244	-
Af1521 enrichment – 5mg	19,122	395	-
Af1521 enrichment – 10mg	19,039	433	-
Af1521 enrichment – 15mg	18,484	526	-

From the LC-MS analysis of the non-enriched whole HeLa lysate (a total of 500 ng lysate was loaded onto the LC column) we identified only a single (1) ADP-ribosylation site, which is in stark contrast to the >500 ADP-ribosylation sites identified using the Af1521 enrichment methodology under identical LC-MS settings (similar LC gradient length and MS acquisition method). To compare this to another PTM, we additionally searched the non-enriched whole HeLa lysate for phosphorylations from which we identified 70 high-confident phosphorylation sites (all with localization score >0.75). From these data we conclude our Af1521 methodology entails an enrichment level of minimum 500.

Supplementary Figure 1

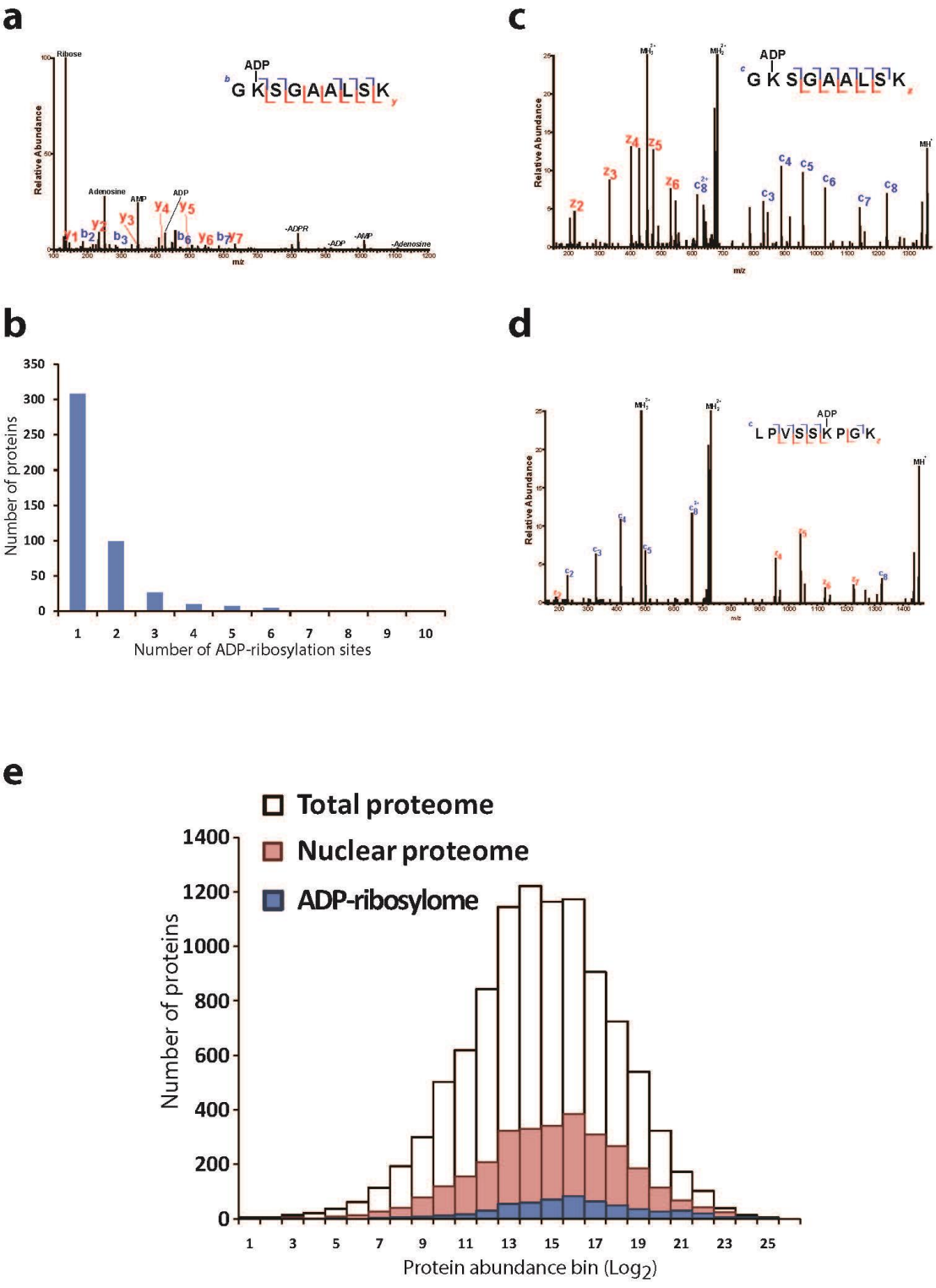

Supplementary Figure 2

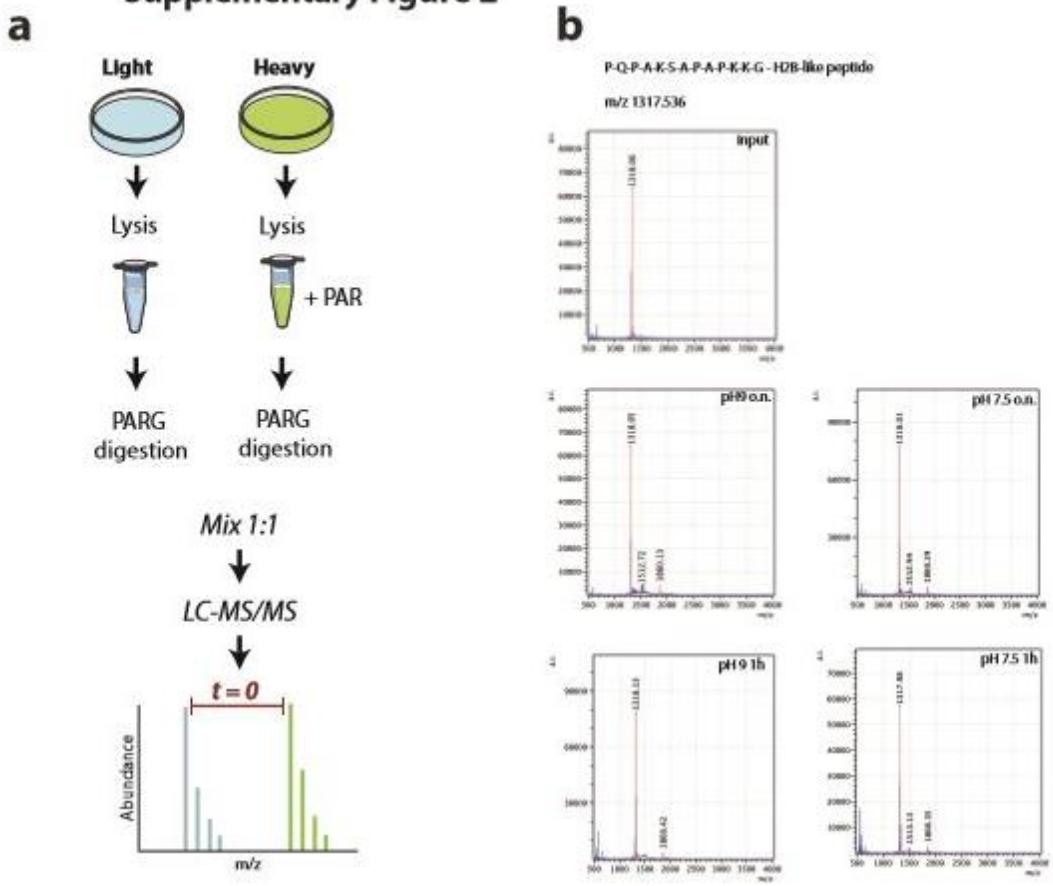

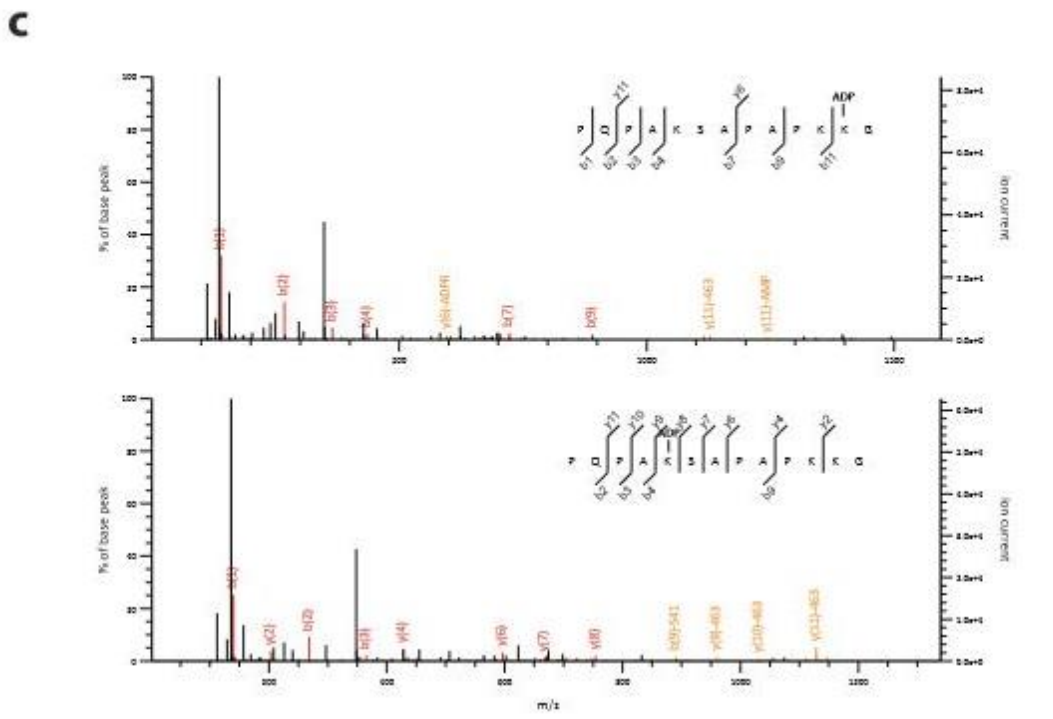

Supplementary Figure 3

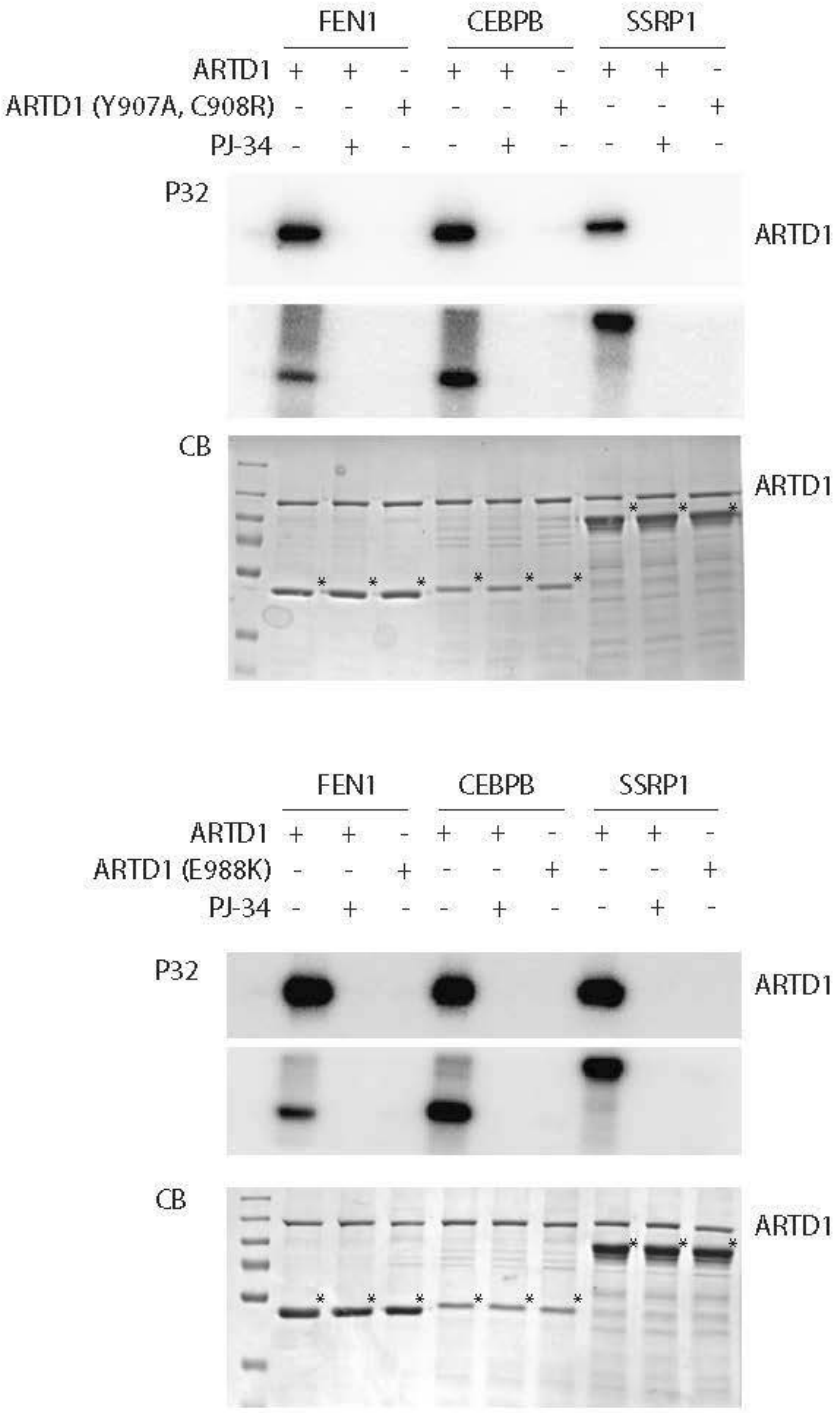

Supplementary Figure 4

a

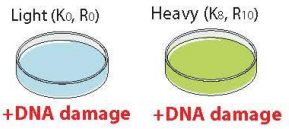

Experiment	Light SILAC	Heavy SILAC
1	0 Min	0 Min
2	0 Min	5 Min
3	0 Min	10 Min
4	0 Min	30 Min
5	0 Min	60 Min
6	0 Min	120 Min

b

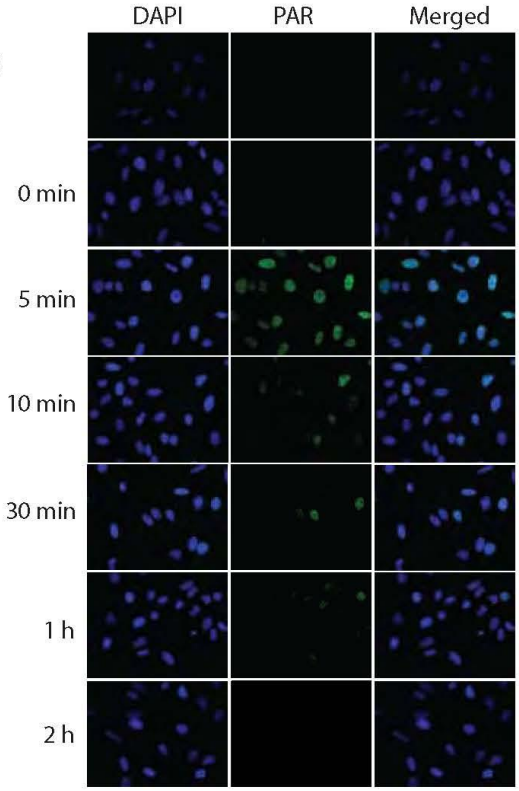

c

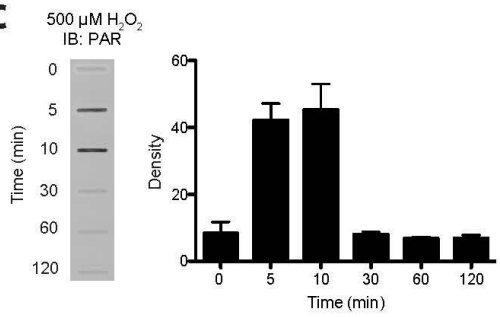

d

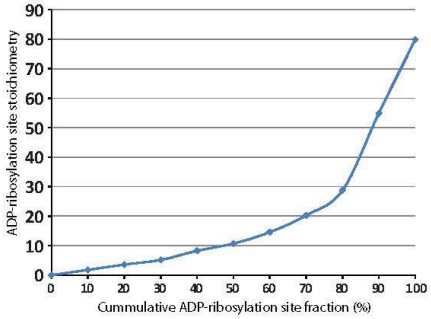

e

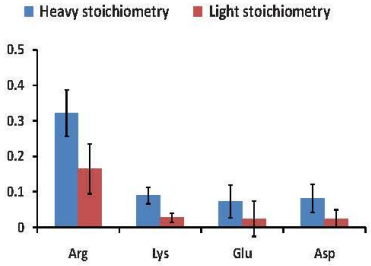

f

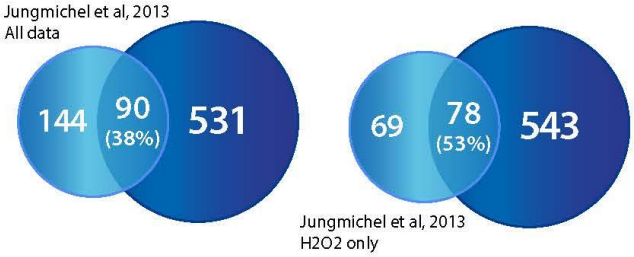

g

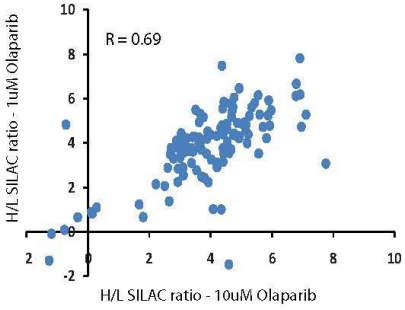

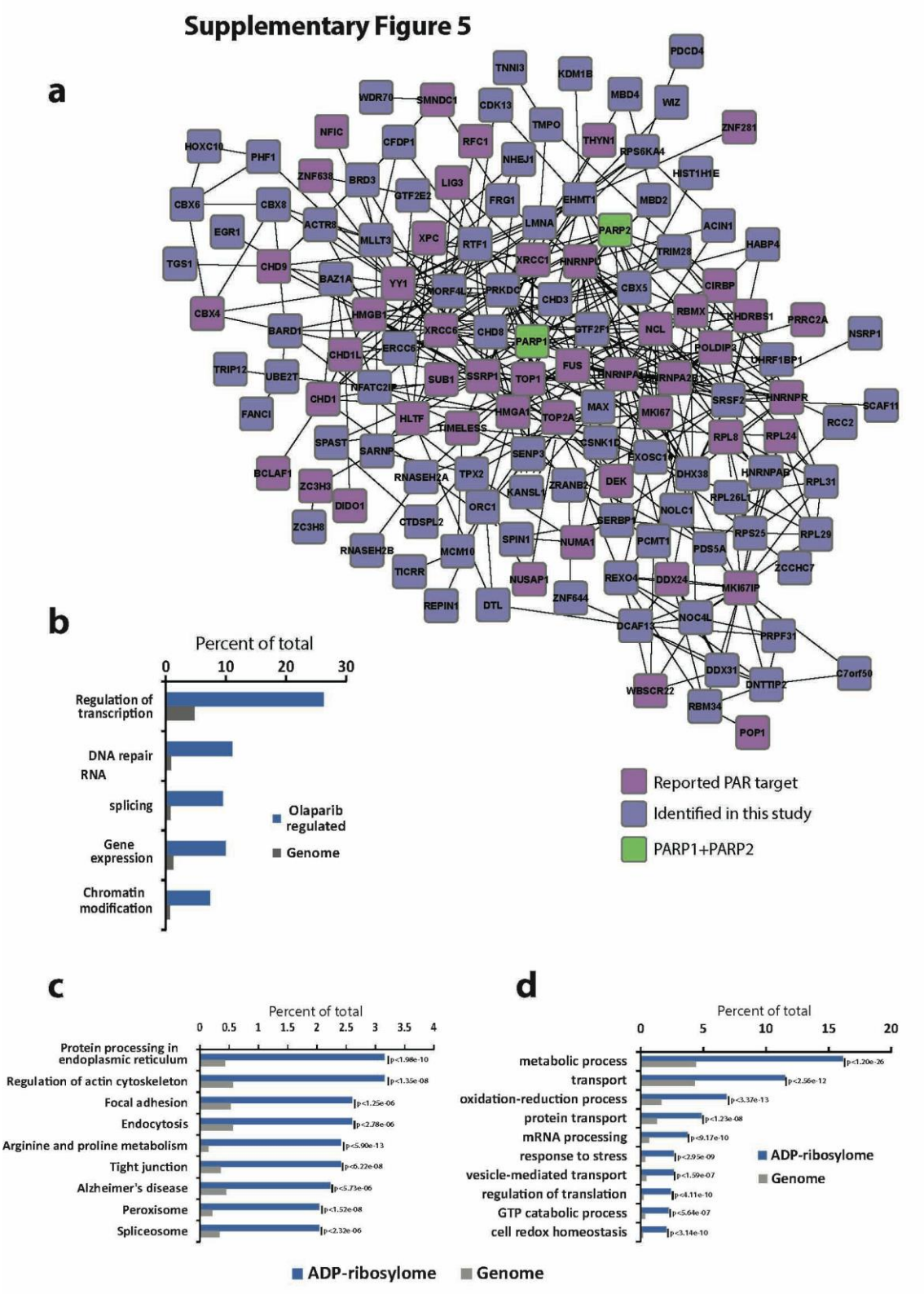
Supplementary Figure 5
a
b
Percent of total
0
10
20
30
Regulation of transcription
DNA repair
RNA
splicing
Gene expression
Chromatin modification
Olaparib regulated
Genome
Reported PAR target
Identified in this study
PARP1+PARP2
c
Percent of total
0
0.5
1
1.5
2
2.5
3
3.5
4
Protein processing in endoplasmic reticulum
Regulation of actin cytoskeleton
Focal adhesion
Endocytosis
Arginine and proline metabolism
Tight junction
Alzheimer's disease
Peroxisome
Spliceosome
ADP-ribosylome
Genome
d
Percent of total
0
5
10
15
20
metabolic process
transport
oxidation-reduction process
protein transport
mRNA processing
response to stress
vesicle-mediated transport
regulation of translation
GTP catabolic process
cell redox homeostasis
ADP-ribosylome
Genome

Supplementary Figure 6

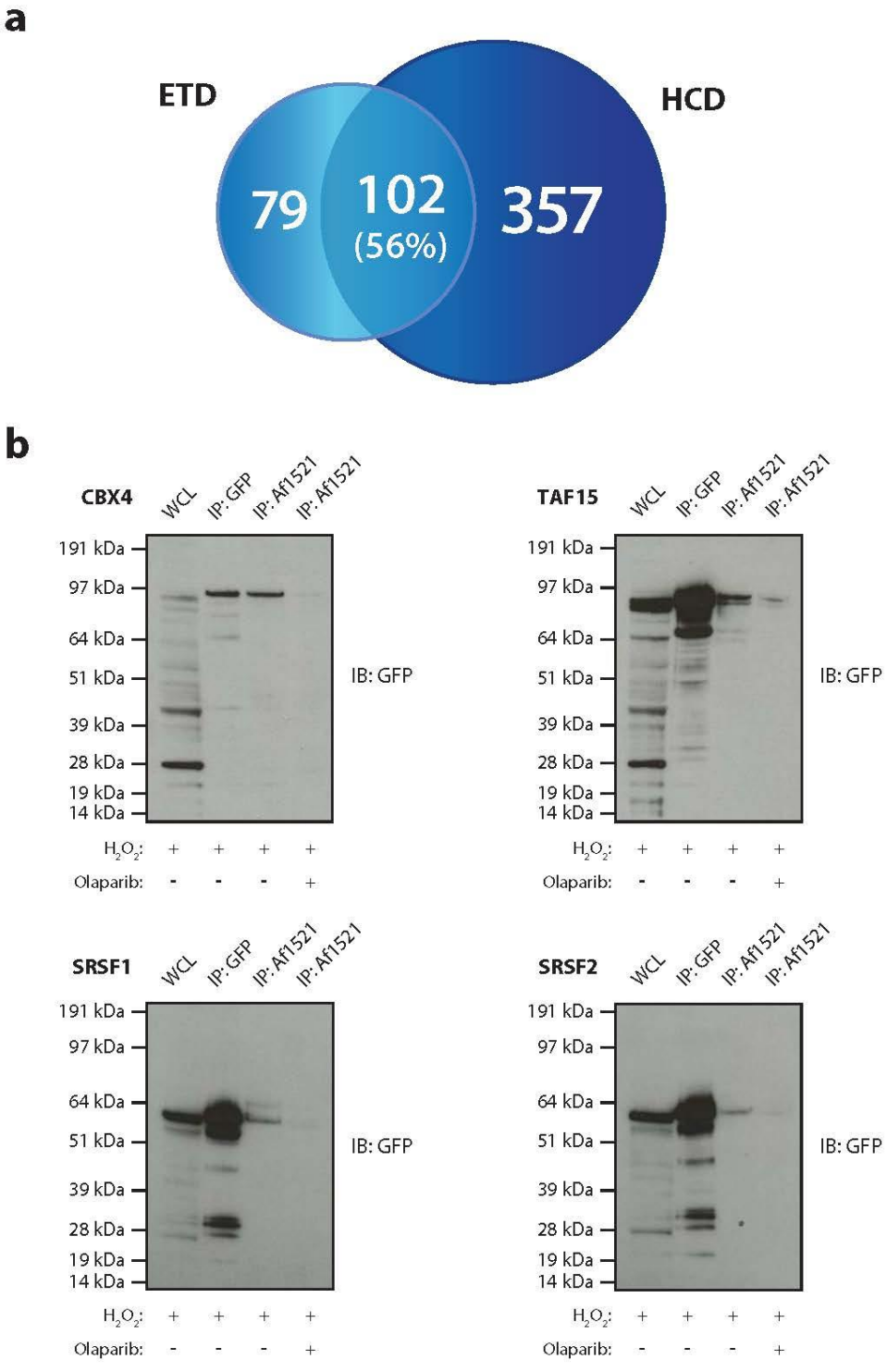

3.2. Overview of submitted manuscripts

3.2.1. Combining HCD and EThcD fragmentations in a product dependent manner provides in-depth characterization of the cellular ADP-ribosylome

Combining HCD and EThcD fragmentations in a product dependent manner provides in-depth characterization of the cellular ADP-ribosylome

Vera Bilan[1,2,] ‡, Mario Leutert[1,2,] ‡, Paolo Nanni[3,] ‡, Christian Panse[3] and Michael O. Hottiger[1]*

[1]Department of Molecular Mechanisms of Disease, 8057 Zurich, Switzerland, [2]Molecular Life Science Ph.D. Program of the Life Science Zurich Graduate School, Switzerland, [3]Functional Genomics Center Zurich, University of Zurich/ETH Zurich, 8057 Zurich, Switzerland

Abstract: Protein ADP-ribosylation is a physiologically and pathologically important post-translational modification. Recent technological advances have improved analysis of this complex modification and led to the discovery of hundreds of ADP-ribosylated proteins in both cultured cells and mouse tissues. Nevertheless, accurate assignment of the ADP-ribose acceptor site(s) within the modified proteins identified remains a challenging task. This is mainly due to poor modified peptides fragmentation. Here, using an Orbitrap Fusion Tribrid mass spectrometer, we present an optimized methodology that not only drastically improves the overall localization scores for the ADP-ribosylation acceptor sites but also boosts ADP-ribosylated peptide identifications. We, first, systematically compared the efficacy of HCD, ETcaD and EThcD fragmentation methods when determining ADP-ribose acceptor sites within complex cellular samples. We, then, further tested the combination of HCD and EThcD fragmentations, where they were employed in a product dependent manner and the unique fragmentation properties of the ADP-ribose moiety were used to trigger targeted fragmentation of only the modified peptides. The best results were obtained using a workflow that included initial fast, high energy HCD (Orbitrap, FT) scans, which produced intense ADP-ribose fragmentation ions. These potentially ADP-ribosylated precursors were then selected and analyzed via subsequent high-resolution HCD and EThcD fragmentation. For the first time, using the resulting high-quality spectra, we were able to identify a lysine-specific modification motif.

Introduction

Protein adenosine diphosphate (ADP)-ribosylation is a reversible post-translational modification that results from NAD^+ hydrolysis and, subsequent, covalent conjugation of a mono-ADP-ribose unit to the acceptor protein (MARylation reaction) or to an ADP-ribose moiety already attached to the protein (PARylation)[1]. The enzyme diphtheria toxin-like ADP-ribosyltransferase 1 (ARTD1), and other ARTD family members (also known as poly ADP-ribosyltransferases (PARPs)) are the major enzymes responsible for catalyzing this reaction in cells[2,3]. Lysine, arginine, aspartic, and glutamic acids are the main acceptors of ADP-ribosylation[2]. Additionally, cysteine, diphthamide, phosphoserine, and asparagine serve as possible ADP-ribosylation acceptor sites[4]. ADP-ribosylation regulates several important cellular functions, including stress responses[5], epigenetic transcriptional regulation[6,7], RNA splicing and transport[8], and cell fate determination[7,9].

For a long time, the tools available to study ADP-ribosylation were limited to radiolabelled NAD^+ and various PAR-detecting antibodies. But, the introduction of mass spectrometry-based (MS) techniques drastically improved the ability to detect ADP-ribosylated proteins and their modification site(s). Due to the low abundance of ADP-ribose modification, enrichment and/or labeling methods prior to MS analysis are crucial to identifying endogenous ADP-ribosylation at the proteomic level. Several MS-based approaches have been described[10-12], unfortunately despite these advances accurate mass spectrometric ADP-ribose acceptor site localization remains challenging. This may be due to the poor ionization capacity and hampered fragmentation properties of the modified peptides, especially PARylated peptides. To tackle this, several strategies have been developed to reduce PAR complexity and to improve identification accuracy. Zhang et al. applied boronic acid enrichment with a chemical elution approach in which the ADP-ribosylated peptides are exposed to hydroxylamine[11]. This converts mono or poly-ADP-ribose modifications to hydroxamic acid derivates that give a 15.01 Da mass shift signature to all modified peptides. Unfortunately, this method is limited to ADP-ribosylated glutamic (D) and aspartic (E) acids. Several acceptor site-independent enzymatic conversion approaches, including the use of phosphodiesterases (i.e. snake

venom phosphodiesterase (SVP)[13]) or ADP-ribosylhydrolases (i.e. poly-ADP-ribose glycohydrolase (PARG)[14]), have also been recently developed. Phosphodiesterase treatment converts PAR and MAR into phosphoribose (212.01 Da), while PARG treatment converts PAR into MAR (541.06 Da). Indeed, these MAR and PAR modification size reductions improve the ionization capacities of all modified peptides.

However, the ADP-ribosyl group and its fragmentation pattern provide interesting features that can be used during MS measurement and downstream bioinformatic analysis. Upon higher energy collisional dissociation (HCD), the ADP-ribose moiety fragments into characteristic marker ions that are mainly represented by: Adenine$^+$ (136.06), Adenosine-H_2O^+ (250.09), AMP$^+$ (348.07) and ADP$^+$ (428.03) (Figure S1A)[15]. The presence of these ADP-ribosylation marker ions can be exploited during the measurement process to trigger product dependent MS events. Moreover, the presence of marker ions in MS/MS spectra validates the presence of ADP-ribosylation on the precursor ion and allows for accurate scoring of its assignment with a search engine. Unfortunately, in some cases, these ions dominate the spectra and obstruct proper precursor fragmentation. Thus, optimization of the applied normalized collision energy (NCE) should be performed to balance precursor fragmentation and marker ions intensity.

Hengel et al. suggested that electron transfer dissociation with supplemental collisional activation (ETcaD) fragmentation could enhance precise ADP-ribose acceptor site localization[16]. When comparing ETcaD to HCD fragmentation, we found that the HCD method identified ADP-ribosylation sites with the same localization probability as ETcaD[15]. Nevertheless, when HCD and ETcaD fragmentation were combined in one run (so called "product dependent method") on an LTQ Orbitrap Velos mass spectrometer the identification of ADP-ribosylation sites in *in vitro* ADP-ribosylated samples increased.

New generation Orbitrap Fusion Tribrid mass spectrometers (Thermo Scientific) introduced an electron-transfer/higher-energy collision dissociation (EThcD) peptide fragmentation methodology that combines HCD and ETcaD into one fragmentation event. This has the advantage that peptide backbone fragmentation is improved and that dual fragmentation generates data-rich MS/MS spectra containing both b/y and c/z ions, which ultimately improves peptide sequence coverage and PTM localization confidence[17]. EThcD fragmentation has already proven beneficial for unambiguous phosphorylation site localization, even on peptides with several possible amino acid acceptors[18].

In this study, we strived to exploit these features of the Orbitrap Fusion Tribrid mass spectrometer for the analysis of ADP-ribosylated peptides. As a model system, we used HeLa cells challenged with oxidative stress in combination with Af1521 peptide enrichment[14]. First, individual HCD, ETcaD, and EThcD fragmentation performances were evaluated by comparing the quality and quantity of identified ADP-ribosylated peptides and ADP-ribosylation site assignment accuracy. Overall, we found that HCD and EThcD fragmentation methods identified complimentary ADP-ribosylated peptide sets and outperformed ETcaD. In a second step, we exploited the ADP-ribose marker ion properties and evaluated how combining HCD and EThcD into one product dependent method performed relative to the individual fragmentation methods. This led to the development of a specialized ADP-ribosylation analysis workflow on the Orbitrap Fusion which significantly augmented our ability to globally characterize the cellular ADP-ribosylome and confidentially assign ADP-ribosylation sites.

Experimental section

ADP-ribosylated peptides enrichment

HeLa cells (Kyoto) were cultured in DMEM (supplemented with 10% FCS and 1% Penicillin/Streptavidin) at 37°C with 5% CO_2. Cells were treated for 10 min with 1 mM H_2O_2 to induce PAR formation, lysed in the lysis buffer (50mM Tris pH 8, 1% NP40, 400 mM NaCl, 1mM EDTA, 0.1% sodium deoxycholate, proteinase inhibitors, 10 μM PJ34, 75 uM tannic acid) and, subsequent, ADP-ribosylated peptide enrichment performed as previously described[14]. Shortly, proteins were precipitated with acetone and solubilized in 6 M urea/2 M thiourea buffer. Disulfide bridges were reduced with 1mM DTT, free -SH groups were alkylated 20 mM CAA and the resulting protein mixture digested with trypsin overnight at room temperature. Peptide clean up, using SepPak C18 columns, was performed and the peptide mix was treated with PARG to convert PAR to MAR. Subsequent ADP-ribosylated peptide enrichment was carried out for 2h at 4°C using the Af1521 macrodomain protein coupled to glutathione-Sepharose beads. Peptides were then eluted with 0.15% TFA and resulting mixture desalted using in-house stage tips packed with C18 filters[19].

Liquid chromatography–mass spectrometry analysis

Mass spectrometry analysis was performed on an Orbitrap Fusion mass spectrometer coupled to a nano EasyLC 1000 (Thermo Fisher Scientific). Solvent compositions in channels A and B were 0.1% formic acid in H_2O and 0.1% formic acid in acetonitrile, respectively. Self-made 75 μm × 150 mm column, packed with reverse-phase C18 material (ReproSil-Pur 120 C18-AQ, 1.9 μm, Dr. Maisch GmbH), were used and 4 μL of peptide solution was loaded onto the columns and eluted over 80 min at a flow rate of 300 nL/min. 2% to 25% B gradient, followed by two steps 35% B for 5 min and 95% B for 5 min elution gradient protocol was used. The mass spectrometer (Tune page v2.0) was set to acquire full-scan MS spectra (300–1500 m/z) at 120000 resolution at 200 m/z after accumulation of automated gain control (AGC) target value of 200000. Charge state screening was enabled, and precursors with +2 to +5 charge states and intensities >50000 selected for MS/MS. Single and unassigned charge states were rejected. Ions were isolated using the quadrupole mass filter with a 2 m/z isolation window. Wide Quadrupole Isolation was used, and injection time was set to 50 ms. For each measurement, the cycle time was set to 3 seconds (top speed mode). In total, 5 different MS/MS acquisition methods were performed and their performances compared. These included: (a) Orbitrap HCD MS/MS (HCD only); (b) Orbitrap ETcaD MS/MS (ETcaD only); (c) Orbitrap EThcD MS/MS (EThcD only); (d) data-dependent HCD followed by EThcD MS/MS when >1

ADP-ribose fragment peaks (136.0623, 250.0940, 348.07091 and 428.0372) was observed in the HCD scan (HCD-PD-EThcD; PD=Product Dependent); (e) low-resolution and high energy data-dependent HCD (named preview HCD), followed by high-quality HCD and EThcD MS/MS when >2 ADP-ribose fragment peaks (136.0623, 250.0940, 348.07091 and 428.0372) were observed in the HCD scan (HCD-PP-HCD-EThcD, PP=Product Preview). The parameters for MS/MS fragmentations changed according to the method applied. The AGC values for MS/MS analysis were set to 500000 and the maximum injection time was 240 ms for all experiments. For the HCD preview scan (method e) only, AGC target was set to 50000 and injection time set to 60 ms. With the exception of the HCD preview scan, whose Normalized Collision Energy (NCE) was set to 38% in order to obtain higher marker ion intensities, all other HCD fragmentations were performed at an NCE of 35%. For ETcaD and EThcD fragmentations, the "use calibrated charge dependent parameter" option was selected. In all cases, precursor masses previously selected for MS/MS measurement were excluded from further selection for 30 seconds, and the exclusion window was set at 10 ppm. All measurements were acquired using internal lock mass calibration on m/z 371.1010 and 445.1200. A complete description of all tandem MS experiments employed in this study can be found in Supplementary Table 1.

Data analysis

MS and MS/MS spectra were converted to Mascot generic format (MGF) using Proteome Discoverer, v2.1 (Thermo Fisher Scientific, Bremen, Germany). When multiple fragmentation techniques (HCD, ETcaD or EThcD) were utilized, a separate MGF files were created from the raw file for each type of fragmentation. All MS/MS spectra were deconvoluted using the MS Spectrum Processor (http://ms.imp.ac.at/?goto=ms2spectrumprocessor). In the ETcaD and EThcD spectra, the precursor, the charge reduced precursor(s), and the neutral loss peaks were removed, within a 0.5 Da window. The MGFs were searched against the UniProtKB human database (taxonomy 9606, version 20140422), which included 35787 Swiss-Prot, 37802 TrEMBL entries, 73589 decoy hits, and 260 common contaminants. Mascot 2.5.1.3 (Matrix Science) was used for peptide sequence identification using previously described search settings[15]. Briefly, a peptide tolerance of 10 ppm and MS/MS tolerance of 0.05 Da were used. For the HCD runs, singly charged b and y ion series, immonium ions, water loss, and ammonia loss ion series were searched. For ETcaD, singly charged c, y, z, z + 1, z + 2 series were considered. For EThcD, singly charged b, c, y, z, z + 1, z + 2 ion series, immonium ions, and water and ammonia loss ion series were used. Enzyme specificity was set to trypsin and up to 4 missed cleavages were allowed. Decoy hits were used to control false discovery rates on the peptide and protein levels. The ADP-ribose variable modification was set differently for HCD, EThcD and ETcaD spectra searches. For HCD and ETcaD MGFs, the modification was set as previously described[15]. For EThcD MGFs, the modification was set to a mass shift of 541.0611 and marker ions at m/z 428.0372, 348.0709, 250.0940, 136.0623 were ignored for scoring. An ADP-ribosylated peptide was considered to be correctly identified when the Mascot score was >20 and the expectation value <0.05. To define ADP-ribosylation site localizations, Mascot site localization analysis, which is based on the work of Savitski et al.[20], was used. Due to the lack of a better estimate, we define correctness as having a site localization confidence of ≧95%.

To screen the spectra for the presence of ADP-ribose marker ions (m/z = 136.0623; 250.0940; 348.0709; and 428.0372), all of the Mascot output.dat files were further analyzed using PTM MarkerFinder[21]. Spectra containing >2 marker ions and marker ion intensity sum ≧3% (for HCD >10%) of the total ion intensities were considered as putative ADP-ribosylated-modified peptide spectra.

Finally, peptide coverage information was obtained using an in-house script. The ".dat" files were screened for the presence of the *in silico* computed m/z peak of fragment ions. Ion intensity was set to 5% of total spectra intensity with a mass tolerance 10 ppm.

Motif discovery using Scaffold PTM

Identification of ADP-ribosylation motifs was carried out using Scaffold PTM software v.2.1.3 (Proteome Software). All files were imported into Scaffold software v.4.2.0 (Proteome Software) and filtered according to a 0.1% FDR peptide threshold and a 3% FDR protein threshold. The resulting files were exported in a mzIdentML format and processed further using Scaffold PTM to search for ADP-ribosylation motifs.

Results and Discussion

EThcD complements HCD identification of ADP-ribosylated peptides

In this study, we analyzed the ADP-ribosylome of HeLa cells during oxidative stress, which was triggered by treating the cells with 1mM H_2O_2 for 10 min Oxidative stress is a well-known and very potent inducer of protein ADP-ribosylation. This is thought to be catalyzed by nuclear ADP-ribosyltransferase (ARTD1, 2 and/or 3) activation[5,22,23] . Following H_2O_2 treatment, cells were lysed in the presence of PARP and PARG inhibitors. The recovered proteins were digested with trypsin, PAR modifications reduced to MARs via PARG treatment and ADP-ribosylated peptides affinity-purified using the Af1521 macrodomain[14]. Initial parameter optimizations on the Orbitrap Fusion Tribrid mass spectrometer, using the HCD fragmentation, revealed that an NCE of 35 was ideal for the fragmentation of ADP-ribosylated peptides (data not shown). In addition, spectra quality increased when higher numbers of ions (AGC 5e5) were accumulated over longer periods of time (240 ms). These optimized acquisition settings were implemented in all further HCD-based MS applications.

The performance of HCD to identify ADP-ribosylated peptides, compared to ETcaD or EThcD fragmentations, was evaluated on these HeLa cell-derived samples (n = 4/MS method). Each fragmentation method was evaluated based on the ADP-ribose fragmentation pattern, and the number and properties of the identified ADP-ribosylated peptides. As previously reported[15], initial spectra analyses revealed that

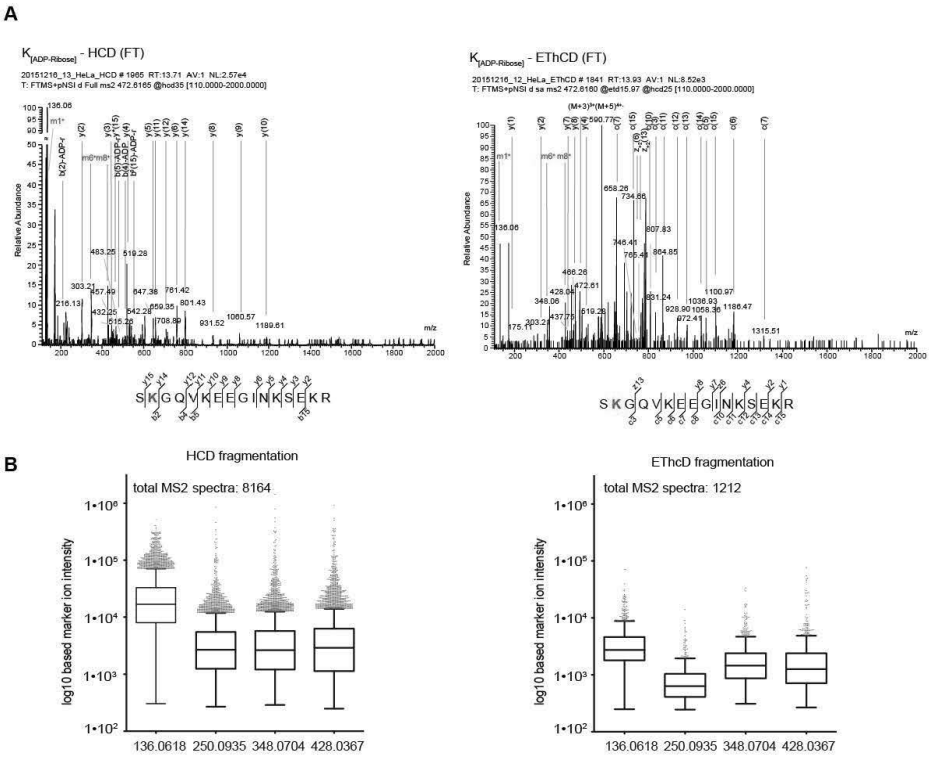

Figure 1: MS/MS Fragmentation of ADP-ribosylated peptides upon HCD and EThcD fragmentation. A) MS/MS spectrum of ADP-ribosylated peptide modified on lysine (K). Spectra of HCD fragmented peptide (left panel), and EThcD fragmented peptide (right panel) are shown. The position of modification is indicated in red. Fragments of ADP-ribose are indicated in the spectra in red according to the ADP-ribose fragmentation nomenclature (Figure S1A). B) The intensity distribution of marker ions in HCD and EThcD fragmentation. Spectra with 3% total intensity and with ≥2 marker ions were analyzed.

primary HCD spectra signals for ADP-ribosylated peptides were generated from ADP-ribose fragmentation (Figure 1A). Applying the PTM Markerfinder tool[21] to the spectra generated by HCD fragmentation we identified 5'313 spectra with ≧2 ADP-ribose marker ions with total intensities >10% (Figure S1B). The Adenine$^+$ (136.0618) marker ion was the most intense ion identified, while all other marker ions were produced with about 10 times lower intensities (Figure 1A and B, Figure S1C). In contrast, ETcaD fragmentation failed to generate any ADP-ribose marker ion containing spectra, even when the total ion intensity threshold was decreased to 3%. The absence of marker ions in ETcaD spectra was expected based on the mild nature of this fragmentation method, as well as the fact that modifications are kept intact during this fragmentation[24]. ADP-ribose marker ions were, however observed in the EThcD analysis, but represented only 3-5% of total ion intensities (Figure 1B, Figure S1C). Decreasing the marker ion intensity threshold to 3% for HCD and EThcD produced spectra significantly reduced the number of spectra containing marker ions for EThcD: 1'212 total MS/MS spectra vs. 8'164 spectra for HCD (Figure 1B). However, out of the total marker ion-containing spectra, around 70% were multiple spectra from the same precursors (i.e. duplicate spectra). After these duplicates had been removed, 380 and 2'291 MS/MS spectra belonging to unique precursors were identified by EThcD and HCD respectively. The Adenosine-H_2O^+ (250.0935) ion had the lowest marker ion intensity in EThcD, while HCD fragmentation generated marker ions (except 136.06 ion) all had similar intensities (Figure 1B). Overall, the relative average abundance of ADP-ribose fragments following EThcD fragmentation was about 5 fold lower than in HCD spectra. Thus, the EThcD and HCD produced marker ion profiles could be used to validate ADP-ribosylated identification.

Table 1 Analysis of ADP-ribosylated peptides identified by HCD, ETcaD, and EThcD fragmentations.

Method	ADP-ribosylated PSM	Unique ADP-ribosylated peptides	Unique ADP-ribosylated sites	
	Total	Total	Total	Localization probability >95% (% of total identifications)
HCD	276	105	92	60 (63.8%)
ETcaD	113	52	40	20 (51.9%)
EThcD	195	71	56	30 (60.5%)

*PSMs - peptide-spectrum matches; unique ADP-ribosylated peptide – unique peptide sequences with localized modification; unique site – unique modification site on protein sequence

Next, we compared the fragmentation by the number of unique identified peptides. A unique peptide was defined as a peptide with a unique modification site. In this case, the two peptides with identical amino acid sequence but with various site localization were considered as two unique peptides. In agreement with our previous findings, ETcaD fragmentation failed to identify large numbers of ADP-ribosylated-modified peptides[15] (Table 1, Figure 2A). In contrast, HCD identified twice as many unique ADP-ribosylated peptides (52 for ETcaCD vs. 105 for HCD) and ETcaD fragmentation required longer acquisition times than HCD, which decreased the overall number of MS/MS spectra generated (total number of MS/MS spectra 45'532 vs. 65'795).

The overall decrease in identified spectra may partially explain why fewer ADP-ribosylated peptides were identified using the ETcaD fragmentation method. EThcD fragmentation, which generated 47'112 spectra, identified 71 unique ADP-ribosylated peptides. This finding highlights the superior performance of this fragmentation method when compared to ETcaD. Comparative analysis of the peptides identified using the different fragmentation methods revealed that EThcD identified 42 unique ADP-ribosylated peptides (gain of 26% total) that were not detected using HCD fragmentation (Figure 2B). 17 of these EThcD unique ADP-ribosylated peptides were also assigned in the ETcaD run. Moreover, ETcaD identified 13 unique ADP-ribosylated peptides (19% gain) that were not present in either the EThcD or HCD runs. Further investigation into the physical properties of the identified ADP-ribosylated peptides (charge, length and chemical composition) revealed that ETcaD demonstrated a clear preference for higher charge-state precursors (3+ and 4+). We did not, however, observe any differences in average ADP-ribosylated peptide length or chemical composition for the tested fragmentation methods (Figure S2).

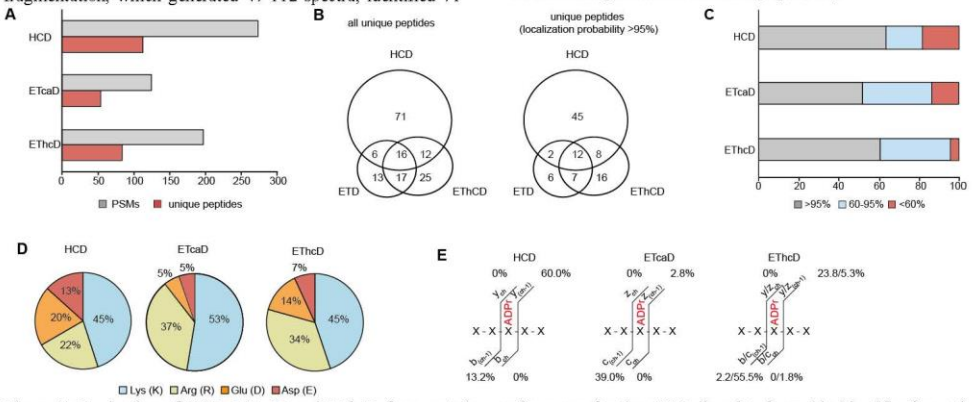

Figure 2: Evaluation of HCD, ETcaD and EThcD fragmentation performance for the ADP-ribosylated peptide identification. A) Number of PSMs and unique peptides (score >20, expectation <0.05) identified by each fragmentation. B) Venn diagram show the overlap in the unique peptide identified by each fragmentation method. C) Distribution of ADP-ribosylated localization probability of unique ADP-ribosylated peptides identified with each fragmentation method. Values were normalized to total numbers of unique ADP-ribosylated peptides. D) Distribution of amino acid acceptor sites from unique ADP-ribosylated peptides. Only peptides with localization probability >95% were considered. E) The presence of modification characteristic ions in the spectra of ADP-ribosylated peptides. Characteristic ions were defined as the first fragment ions carrying the modification. The number close to the ion shows the frequency the ion was observed with the specified fragmentation method.

In conclusion, as judged by the number of PSMs and unique identified ADP-ribosylated peptides, HCD fragmentation performed best. EThcD fragmentation performed less favorably, but identified additional modified peptides. These findings suggested that a combination of HCD and EThcD could be beneficial for in-depth ADP-ribosylome characterization. For HCD around 40% of unique ADP-ribose marker ion containing spectra were also assigned by the mascot search. The unassigned spectra might be partially explained by the poor fragmentation of ADP-ribosylated peptides, peptides which are shorter or longer than the set threshold, peptides which fall under the applied scoring threshold in mascot and/or not fully optimized search algorithm. This suggests the possibility for further improvements in the bioinformatics analysis pipeline.

HCD and EThcD localize ADP-ribose acceptor sites with high confidence

Previous studies reported the benefit of EThcD to accurately localize serine and threonine phosphorylation sites[18]. We, therefore, compared how the different fragmentation methods performed when attempting to confidently assign four described ADP-ribosylation acceptor sites (lysine (K), arginine (R), glutamic acid (D) and aspartic acid (E)). HCD, ETcaD, and EThcD localized all four acceptor amino acids with high confidence. For HCD fragmentation measurements, the modification acceptor sites were assigned with confidences >95% for 63.8% of the identified unique ADP-ribosylated sites. ETcaD assigned 51.9% of the unique ADP-ribosylated sites with similar confidence (Table 1). EThcD performed comparably to HCD, assigning 60.5% of the unique ADP-ribosylated sites with >95% confidence. Moreover, acceptor sites identified with a localization probability of less than 60% represented only 4% of all ADP-ribose acceptor sites identified with EThcD whereas it was 18% of the ADP-ribosylated-sites identified with HCD (Figure 2C). This fact points to the better peptide fragmentation with EThcD in comparison to HCD.

Interestingly, a new peptide species of ARTD1, that simultaneously carries two ADP-ribose moieties, was present and confidently identified using EThcD analysis (Figure S3). Another ARTD1 dual-modified precursor had been previously identified following MS analysis of *in vitro* modified ARTD1[13]. However, this is the first report that K508 and E520 modification sites of ARTD1 are simultaneously present *in vivo*.

The identification of a double modified peptide suggested superior peptide backbone fragmentation using EThcD. This prompted us to compare the peptide coverage information obtained by all fragmentation methods and look for the presence of characteristic ions, which were defined as the first fragment ions carrying the modification. To evaluate peptide sequence coverage, the number of ions used by Mascot for scoring was normalized to the length of the peptide (the presence of a full ion series corresponds to a coverage ratio of 1). In agreement with the localization probability assignments, HCD and EThcD performed comparably, with slightly better fragmentation than ETcaD (Figure S1D). Further, each fragmentation method was compared based on the presence of acceptor site characterizing ions (Figure 2E). For each fragmentation, characteristic y/b or z/c ions were not observed (only in 1.8% c ion series generated by EThcD), but not with other fragmentations. However, HCD and EThcD often produced ions before the modification site, whereas ETcaD did not generate ions close to the assigned modification site. Overall, ETcaD performed significantly worse than HCD and EThcD for ADP-ribosylation site identification and localization. For this reason, ETcaD was excluded from further analysis.

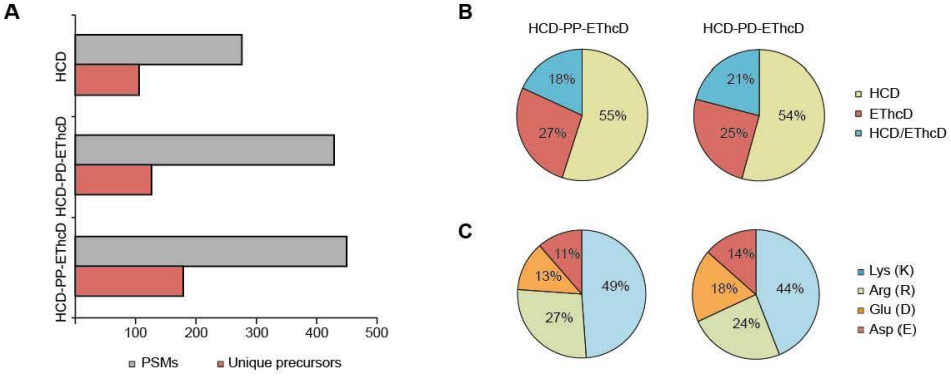

Figure 3: Evaluation of HCD-PD-EThcD and HCD(FT)-PP-EThcD performance for the ADP-ribosylated peptide identification. A) Number of PSMs and unique peptides (score >20, expectation <0.05) identified by each product-dependent method. B) The contribution of HCD and EThcD fragmentations in the product dependent methods for the identification of ADP-ribosylated peptides. C) Distribution of amino acid acceptor sites from unique ADP-ribosylated peptides. Only peptides with localization probability >95% were considered.

In agreement with previous phospho-proteomics studies[18,25], we found that the localization probabilities for ADP-ribosylation showed a general improvement. Together, ADP-ribosylated peptides with localization probabilities >95% represented ~60% of all of the HCD and EThcD identified acceptor sites. EThcD did, however, provide slightly better quality spectra. This workflow represents a significant improvement compared to our previous study performed on an Orbitrap Velos where only 10% of the identified acceptor sites had localization probabilities >95%[15]. Together, these findings suggest that both HCD and EThcD could be used to confidently localize ADP-ribosylated acceptor sites.

ADP-ribose marker ion-dependent combination of HCD and EThcD improves ADP-ribosylation peptide identification

Our previous study[15], together with the findings presented above, suggest that combining different fragmentation methods in an ADP-ribose marker ion product dependent manner could increase the number of ADP-ribosylated peptides identified using the Orbitrap Fusion. The observation that the EThcD fragmentation identified sites were complementary to those identified via HCD, combined with excellent localization scores generated from both fragmentation methods, prompted us to develop a method that would combine HCD and EThcD into a single measurement. Furthermore, to optimize measurement efficiency and focus specifically on ADP-ribosylated peptides, we integrated a precursor selection criteria that is based on the detection of ADP-ribose marker ions, whose presence triggers subsequent product-dependent EThcD and/or HCD. For this product dependent method (HCD-PD-EThcD), HCD MS/MS spectra were generated as described for the single HCD method. When at least one ADP-ribose marker ion was observed during the HCD MS/MS scan, the same precursor was selected again and fragmented using EThcD. The HCD-PD-EThcD methodology significantly increased ADP-ribosylated PSMs (429 vs. 276 for HCD alone; Figure 3A, Table 1 and 2). Despite this increase, 20% increase in unique ADP-ribosylated peptides identifications was observed (126 unique ADP-ribosylated peptides vs. 105 for HCD alone).

This could, potentially, result from mass spectrometer speed capacity saturation. To fully exploit the advantages of this dual fragmentation method we aimed to optimize the instrument's cycle time and implement a new method called HCD-PP-HCD/EThcD. In this workflow, every MS1 spectrum acquisition was followed by a Product Preview (PP) HCD MS/MS scan, performed in the Orbitrap (FT acquisition) at low resolution (30k) with high NCE (38). These settings resulted in fast MS/MS lower quality spectra acquisitions that gave very intense ADP-ribose marker ion signals. Given that PP FT-HCD injection times are four times shorter than FT-HCD injection times, these alterations generated four times more scans per duty cycle. After initial PP-FT-HCD scan, the instrument was then programmed to select precursors with >2 ADP-ribose marker ions to record additional MS/MS spectra via high quality HCD and EThcD fragmentation. When compared to the HCD-PD-EThcD method described above, this new HCD-PP-HCD/EThcD strategy identified additional 42% unique ADP-ribosylated peptides (Figure 3 A), and 70% more when compared to HCD alone. The contribution of EThcD fragmentation to the identification of ADP-ribosylated peptides in these product dependent methods was similar to the EThcD method performance alone, and contributed to at least 22% of all identifications (Figure 3B, Table 2). Given these positive results, we also attempted to implement an HCD (IT)-PP-HCD/EThcD method. Unfortunately, we found that the preview scan in the ion trap led to a high proportion of false positives and the overall performance of this method was worse than other product dependent methods (data not shown). Product dependent methods, which combine HCD and ETcaD fragmentations, have been previously reported for the analysis of complex post-translational modifications i.e.

Table 2 Identification of ADP-ribosylated peptides using the product dependent methods including contribution of HCD and EThcD to the total assignment

Method	ADP-ribosylated PSMs*	Unique ADP-ribosylated precursors		Unique ADP-ribosylated sites	
	Total	Total	%	Total	%
HCD-PD-EThcD	429	126		99	
Including: HCD	265	69	55	58	59
EThcD	164	30	24	22	22
overlap	-	27	21	19	19
HCD-PP-EThcD:	450	179		141	
Including: HCD	349	97	54	86	61
EThcD	196	49	27	31	22
overlap	-	33	19	24	17

*PSMs - peptide-spectrum matches; unique ADP-ribosylated peptide – unique peptide sequences with modifications; unique site – unique modification site on protein sequence.

glycoproteins[26,27]. We, therefore, optimize machine duty time and tested whether use of ADP-ribose marker ions triggered product-dependent MS/MS measurements would promote efficient ADP-ribosylation acceptor site identification. To this end, we found that the fast, high energy, low-resolution preview HCD MS/MS scans, which triggered subsequent MS/MS (>2 ADP-ribose fragmentation ions), optimized machine capacity and efficiently selected the appropriate ADP-ribosylated precursors. Moreover, when combined with subsequent HCD and EThcD, this strategy significantly enhanced ADP-ribosylated peptide identifications compared to HCD or EThcD alone.

Improved ADP-ribosylation site assignments identified a lysine ADP-ribosylation motif

Next, we assessed the distribution of known ADP-ribose acceptor sites (K, R, D, E) that were identified with high localization confidence (localization probability >95%) using the different fragmentation methods. Interestingly, K was the most abundant acceptor amino acid identified in our study and represented 45% of total unique sites for both HCD and EThcD, and 52% for ETcaD. We also found that R was more often observed as acceptor site using ETcaD or EThcD fragmentation methods and that the identification of E and D acceptor sites was under-represented in the ETcaD fragmentations datasets (Figure 2D and 3C)

These high-quality ADP-ribosylated peptide spectra and their corresponding acceptor site identifications prompted us to further analyze the peptide sequences for potential ADP-ribosylation motifs. When the lysine acceptor sites were studied, 48% of the modification sites (44 out of 90) contained a xxxxxxKSxxxxx motif (Figure 4). Interestingly, all of the identified proteins that contain this K motif localize in the nucleus, indicating that these proteins may be nuclear ARTDs targets. We were not able to detect any consensus modification sequences for D, E or R acceptor sites in our dataset. We then determined whether ADP-ribosylated peptides that were identified here contain known/published ADP-ribosylated modification motifs. To this end, we first searched for the three E acceptor site motifs reported by Gibson et al.[12] (xxExPxx, xxxEPxxx and xxEExxxx) and found that out of the 44 assigned E acceptor sites only three peptides, six peptides or seven peptides (5 of which cover the same sequence in ARTD1 protein) contained each of the respective motifs. Together, these 16 peptides represent 10 proteins. We then analyzed if the peptides we identified contained any of the E ADP-ribosylation motifs reported by Zhang et al.[11]. Here, only four additional peptides (two covering the same protein sequence) were found in our dataset. So far the determinants of ARTDs enzyme specificity are not well understood. Moreover, ARTD enzymes have potential substrate redundancy that was not extensively studied up to date and can obstruct the motif identification.

Conclusions

Several techniques to enrich, process and analyze ADP-ribosylated peptides from complex samples have been published. These techniques, however, usually employ standard mass spectrometric methods. The analysis of complex PTMs like ADP-ribosylation, however, requires an optimized methodology that specifically tackles the specific features of the PTM and resulting modified peptides. Here, we harnessed the full MS potential of the Orbitrap Fusion Tribrid and exploited the unique properties of ADP-ribose fragmentation to establish an ADP-ribosylome customized MS workflow.

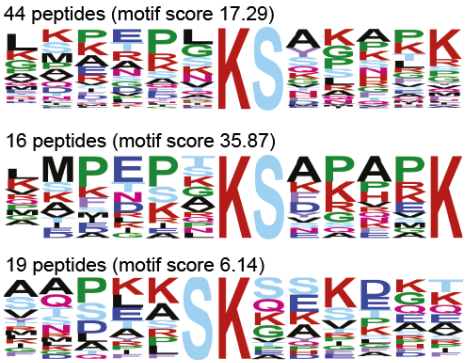

Figure 4: Putative ADP-ribosylation motif for Lysine acceptor sites. ADP-ribosylated modification motif for K sites identified with Scaffold PTM.

Parameter optimization and systematic performance comparisons of HCD, ETcaD and EThcD fragmentation of endogenous ADP-ribosylated peptides revealed that HCD alone identified the most of modified peptides. Importantly, we also discovered that EThcD fragmentation identified 42 unique ADP-ribosylated-modified peptides that were not present in the HCD dataset. These findings suggested that a combination of HCD and EThcD fragmentation would allow in-depth characterization of the cellular ADP-ribosylome. To this end, we established a HCD-PP-HCD/EThcD method that supported robust ADP-ribosylome discovery studies. The method consists of several important implementations: 1. initial fast, high energetic HCD scans that promote generation of ADP-ribose marker ions and allows preselection of potential ADP-ribosylated-peptide precursors; and 2. two high-quality MS/MS spectra are acquired for these preselected precursors using a high-resolution HCD and EThcD measurements. This method significantly improved the efficient identification of ADP-ribosylated peptides and accurately localized ADP-ribose acceptor sites within the peptide. To our knowledge, this HCD-PP-HCD/EThcD workflow is the most optimized and efficient method for ADP-ribosylation site identification in complex samples.

Importantly, the improvements described here generated a unique and highly accurate dataset that allowed us to define the first modification motif for K as ADP-ribose acceptor site. Identification of ADP-ribosylation motifs would greatly benefit the effort to identify potentially ADP-ribosylation targets, as it was seen in the phosphorylation field. It remains to be clarified if and what the biological relevance of the identified motif is since this might help to determine the target

specificity of the ARTD enzymes. Furthermore, the techniques for proteome-wide ADP-ribosylation site mapping are only started to develop.

SUPPORTING INFORMATION

Table S1: Overview of the evaluated MS/MS methods.
Table S2: Identified ADP-ribosylated peptides with K motif and corresponding protein IDs.
Figure S1: MS/MS fragmentation of ADP-ribosylated peptides.
Figure S2: Physicochemical characteristics of identified ADP-ribosylated peptides identified with HCD, ETcaD and EThcD fragmentations.
Figure S3: EThcD Fragmentation of a dual-modified peptide.

The raw file, peak list files (MGFs), and result files (mzIdent) from the presented study were uploaded into Proteome Xchange and can be accessed within PXD004676 dataset number.

Corresponding Author

* (Give contact information for the author(s) to whom correspondence should be addressed.

Author Contributions

‡These authors contributed equally.

ACKNOWLEDGMENT

We thank Ms. Monika Fey for the expression and purification of recombinant human PARG. Stephan Christen and Deena Leslie Pedrioli (University of Zurich) provided editorial assistance and critical input during the writing. ADP-ribosylation research in the laboratory of MOH is funded by the Swiss National Science Foundation (SNF 310030B_138667) and SystemX grant (2012/145).

REFERENCES

(1) Sung, V. M. *Biochimie* **2015**, *113*, 35-46.
(2) Hottiger, M. O.; Hassa, P. O.; Luscher, B.; Schuler, H.; Koch-Nolte, F. *Trends Biochem Sci* **2010**, *35*, 208-219.
(3) Barkauskaite, E.; Jankevicius, G.; Ahel, I. *Mol Cell* **2015**, *58*, 935-946.
(4) Rosenthal, F.; Hottiger, M. O. *Front Biosci (Landmark Ed)* **2014**, *19*, 1041-1056.
(5) Luo, X.; Kraus, W. L. *Genes Dev* **2012**, *26*, 417-432.
(6) Guetg, C.; Santoro, R. *Epigenetics* **2012**, *7*, 811-814.
(7) Hottiger, M. O. *Annu Rev Biochem* **2015**, *84*, 227-263.
(8) Bock, F. J.; Todorova, T. T.; Chang, P. *Mol Cell* **2015**, *58*, 959-969.
(9) Erener, S.; Hesse, M.; Kostadinova, R.; Hottiger, M. O. *Mol Endocrinol* **2012**, *26*, 79-86.
(10) Jungmichel, S.; Rosenthal, F.; Altmeyer, M.; Lukas, J.; Hottiger, M. O.; Nielsen, M. L. *Mol Cell* **2013**, *52*, 272-285.
(11) Zhang, Y.; Wang, J.; Ding, M.; Yu, Y. *Nat Methods* **2013**, *10*, 981-984.
(12) Gibson, B. A.; Zhang, Y.; Jiang, H.; Hussey, K. M.; Shrimp, J. H.; Lin, H.; Schwede, F.; Yu, Y.; Kraus, W. L. *Science* **2016**.
(13) Daniels, C. M.; Ong, S. E.; Leung, A. K. *J Proteome Res* **2014**, *13*, 3510-3522.
(14) Martello, R.; Leutert, M.; Jungmichel, S.; Bilan, V.; Larsen, S.; Young, C.; Hottiger, M. O.; Nielsen, M. *Nature Communications, in press* **2016**.
(15) Rosenthal, F.; Nanni, P.; Barkow-Oesterreicher, S.; Hottiger, M. O. *J Proteome Res* **2015**, *14*, 4072-4079.
(16) Hengel, S. M.; Shaffer, S. A.; Nunn, B. L.; Goodlett, D. R. *J Am Soc Mass Spectrom* **2009**, *20*, 477-483.
(17) Senko, M. W.; Remes, P. M.; Canterbury, J. D.; Mathur, R.; Song, Q.; Eliuk, S. M.; Mullen, C.; Earley, L.; Hardman, M.; Blethrow, J. D.; Bui, H.; Specht, A.; Lange, O.; Denisov, E.; Makarov, A.; Horning, S.; Zabrouskov, V. *Anal Chem* **2013**, *85*, 11710-11714.
(18) Frese, C. K.; Zhou, H.; Taus, T.; Altelaar, A. F.; Mechtler, K.; Heck, A. J.; Mohammed, S. *J Proteome Res* **2013**, *12*, 1520-1525.
(19) Rappsilber, J.; Mann, M.; Ishihama, Y. *Nat Protoc* **2007**, *2*, 1896-1906.
(20) Savitski, M. M.; Lemeer, S.; Boesche, M.; Lang, M.; Mathieson, T.; Bantscheff, M.; Kuster, B. *Mol Cell Proteomics* **2011**, *10*, M110 003830.
(21) Nanni, P.; Panse, C.; Gehrig, P.; Mueller, S.; Grossmann, J.; Schlapbach, R. *Proteomics* **2013**, *13*, 2251-2255.
(22) Boehler, C.; Gauthier, L. R.; Mortusewicz, O.; Biard, D. S.; Saliou, J. M.; Bresson, A.; Sanglier-Cianferani, S.; Smith, S.; Schreiber, V.; Boussin, F.; Dantzer, F. *Proc Natl Acad Sci U S A* **2011**, *108*, 2783-2788.
(23) Andersson, A.; Bluwstein, A.; Kumar, N.; Teloni, F.; Traenkle, J.; Baudis, M.; Altmeyer, M.; Hottiger, M. O. *Nucleic Acids Res* **2016**.
(24) Mikesh, L. M.; Ueberheide, B.; Chi, A.; Coon, J. J.; Syka, J. E.; Shabanowitz, J.; Hunt, D. F. *Biochim Biophys Acta* **2006**, *1764*, 1811-1822.
(25) Frese, C. K.; Altelaar, A. F.; van den Toorn, H.; Nolting, D.; Griep-Raming, J.; Heck, A. J.; Mohammed, S. *Anal Chem* **2012**, *84*, 9668-9673.
(26) Wu, S. W.; Pu, T. H.; Viner, R.; Khoo, K. H. *Anal Chem* **2014**, *86*, 5478-5486.
(27) Saba, J.; Dutta, S.; Hemenway, E.; Viner, R. *Int J Proteomics* **2012**, *2012*, 560391.

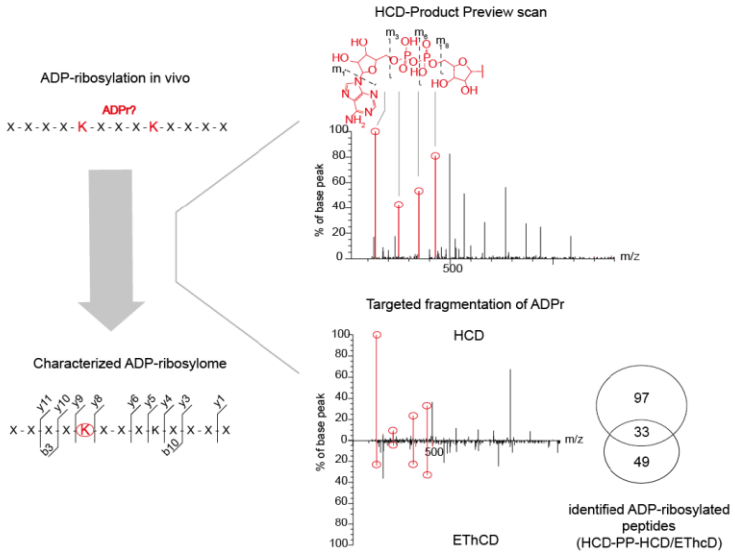

Graphical abstract

Combining HCD and EThcD fragmentations in a product dependent manner provides in-depth characterization of the cellular ADP-ribosylome

Vera Bilan[1,2,] ‡, Mario Leutert[1,2,] ‡, Paolo Nanni[3,] ‡, Christian Panse[3] and Michael O. Hottiger[1]*

[1]Department of Molecular Mechanisms of Disease, 8057 Zurich, Switzerland, [2]Molecular Life Science Ph.D. Program of the Life Science Zurich Graduate School, Switzerland, [3]Functional Genomics Center Zurich, University of Zurich/ETH Zurich, 8057 Zurich, Switzerland

SUPPORTING INFORMATION

MS Method		Description	Fragmentation events			Cycle Time (sec)	Data collection (MS1/ MS/MS)	MS/MS scans									m/z product ions (n≥1)
								FT preview			FT			Reagent			
			HCD	ETcaD	EThcD			AGC Target	injection time (ms)	NCE (%)	AGC Target	injection time (ms)	NCE (%)	AGC Target	injection time (ms)	NCE (%)	
a	HCD	only HCD MS/MS	X	-	-	3	FT, p	-	-	-	500000	240	35	-	-		-
b	ETcaD	only ETcaD MS/MS	-	X	-	3	FT, p	-	-	-	500000	240	-	calibrated ETD parameters, with sa* (NCE 20)			-
c	EThcD	only EThcD MS/MS	-	-	X	3	FT, p	-	-	-	500000	240	-	calibrated ETD parameters, with sa* (NCE 25)			-
d	HCD-PD-EThcD	HCD product dependent EThcD	X	-	X	3	FT, p	-	-	-	500000	240	35	calibrated ETD parameters, with sa* (NCE 25)			1 36.0623; 250.094; 348.0709; 428.037
e	HCD-PP-HCD/EThcD	HCD product preview HCD-EThcD	X, X	-	X	3	FT, p	50000	60	38	500000	240	35	calibrated ETD parameters, with sa* (NCE 25)			1 36.0623; 250.094; 348.0709; 428.037

Table S1: Overview of the evaluated tandem mass spectrometry methods.

NCE: Normalized Collision Energy; sa*: supplementary activation; HCD: Higher Energy Collision induced dissociation; ETcaD electron transfer dissociation with supplemental collisional activation; EThcD . electron-transfer/higher-energy collision dissociation; FT: Fourier Transformation; p: profile

Table S2 Protein lists with a presence of K modification motifs

Motif 1 -----KS---- (motif score 17.29)

Surrounding Sequence	Accession	Site	Best Ascore	Localization Probability
AAKGKLKSQNTKP	sp|Q8IYA6|CKP2L_HUMAN	K30	117.14	100.00%
NLRSSLKSSLHTL	sp|Q13415|ORC1_HUMAN	K448	112.68	100.00%
VVAPRGKSGAALS	sp|P09874|PARP1_HUMAN	K498	179.49	100.00%
MPEPAKSAPAPK	sp|P06899|H2B1J_HUMAN	K6	54.94	100.00%
AKEAAGKSSGPTS	sp|Q00839|HNRPU_HUMAN	K186	125.73	100.00%
QVSDERKSYSPRK	sp|P35251-2|RFC1_HUMAN	K280	52.22	100.00%
VDMNSPKSKKAKK	sp|Q9NR30|DDX21_HUMAN	K73	30.66	100.00%
MIKKKTKSSKPSK	sp|P35251-2|RFC1_HUMAN	K1124	85.19	100.00%
LVIGDHKSTSHFR	sp|O00193|SMAP_HUMAN	K62	145.84	100.00%
LKQRLGKSNIQAR	sp|Q9Y3Y2-3|CHTOP_HUMAN	K82	121.78	100.00%
KSDEPKKSVAFKK	sp|P07305-2|H10_HUMAN	K86	42.69	100.00%
STRDPVKSQSKSN	sp|P46013-2|KI67_HUMAN	K2622	54.47	100.00%
GAATPKKSAKKTP	sp|P10412|H14_HUMAN	K149	52.22	100.00%
LSDEFSKSHKSRR	sp|Q9BQ39|DDX50_HUMAN	K87	39.43	100.00%
DQEQQLKSAQSPS	sp|Q14669-2|TRIPC_HUMAN	K123	60.43	100.00%
LQRAPLKSVGPDF	sp|P78527|PRKDC_HUMAN	K2694	87.44	100.00%
GAALSKKSKGQVK	sp|P09874|PARP1_HUMAN	K506	41.83	100.00%
MPEAAVKSTANKY	sp|P51858|HDGF_HUMAN	K39	66.24	100.00%

GSTNYGKSQRRGG	sp|Q99729-3|ROAA_HUMAN	K271	46.99	100.00%
LDAAPGKSQKRKY	sp|Q9NVU7-2|SDA1_HUMAN	K477	36.58	100.00%
PAKNAQKSNQNGK	sp|P06748|NPM_HUMAN	K206	67.18	100.00%
KDVADYKSKGKFD	sp|O15347|HMGB3_HUMAN	K161	21.56	100.00%
PPKTFEKSMMNLQ	sp|P11387|TOP1_HUMAN	K642	65.93	100.00%
KPKVPLKSAPPPM	sp|Q68D10-2|SPT2_HUMAN	K161	146.11	100.00%
LWERNIKSHLGNV	sp|Q8WW12|PCNP_HUMAN	K167	1,000.00	100.00%
QSVSQNKSYLAVR	sp|Q9UMY1|NOL7_HUMAN	K170	74.94	100.00%
MPEPTKSAPAPK	sp|P58876|H2B1D_HUMAN	K6	58.97	100.00%
MPEPSKSAPAPK	sp|P33778|H2B1B_HUMAN	K6	51.08	100.00%
PPKPRLKSGGGFG	sp|Q9H4L4|SENP3_HUMAN	K43	125.55	100.00%
ASIISLKSDKKRK	sp|Q9H0A0|NAT10_HUMAN	K989	43.02	100.00%
GKKSGKKSYLSGG	sp|P25490|TYY1_HUMAN	K183	165.44	100.00%
KKSNKNKSGKNQF	sp|Q00839|HNRPU_HUMAN	K694	57.6	100.00%
YSPERSKSYSFHQ	sp|Q8NEY8-2|PPHLN_HUMAN	K167	144.15	100.00%
KEEGINKSEKRMK	sp|P09874|PARP1_HUMAN	K518	39.54	100.00%
INLLPSKSSVTKI	sp|Q9ULW0|TPX2_HUMAN	K357	37.15	100.00%
MPEPVKSAPVPK	sp|Q99879|H2B1M_HUMAN	K6	70.69	100.00%
LKFTKGKSFRHEK	sp|Q14978-2|NOLC1_HUMAN	K678	81.07	100.00%
MPDPAKSAPAPK	sp|P23527|H2B1O_HUMAN	K6	41.7	100.00%
LKFTKGKSFRHEK	sp|Q14978-3|NOLC1_HUMAN	K669	81.07	100.00%
RTPRRSKSDGEAK	sp|P26358|DNMT1_HUMAN	K142	53.57	100.00%
LKAVTQKSSNSLV	sp|Q99575|POP1_HUMAN	K125	194.76	100.00%
EQRRELKSAGGLM	sp|Q9UNQ2|DIM1_HUMAN	K23	69.08	100.00%
GGATPKKSAKKTP	sp|P16403|H12_HUMAN	K149	52.22	100.00%
ENYRRNKSYSFIA	sp|Q8IWX8|CHERP_HUMAN	K901	141.33	100.00%

Motif 2 ----KS----K (motif score 35.87)

Surrounding Sequence	Accession	Site	Best Ascore	Localization Probability
MPEPAKSAPAPK	sp|P06899|H2B1J_HUMAN	K6	54.94	100.00%
QVSDERKSYSPRK	sp|P35251-2|RFC1_HUMAN	K280	52.22	100.00%
VDMNSPKSKKAKK	sp|Q9NR30|DDX21_HUMAN	K73	30.66	100.00%
MIKKKTKSSKPSK	sp|P35251-2|RFC1_HUMAN	K1124	85.19	100.00%
KSDEPKKSVAFKK	sp|P07305-2|H10_HUMAN	K86	42.69	100.00%
GAALSKKSKGQVK	sp|P09874|PARP1_HUMAN	K506	41.83	100.00%
PAKNAQKSNQNGK	sp|P06748|NPM_HUMAN	K206	67.18	100.00%
MPEPTKSAPAPK	sp|P58876|H2B1D_HUMAN	K6	58.97	100.00%
MPEPSKSAPAPK	sp|P33778|H2B1B_HUMAN	K6	51.08	100.00%
ASIISLKSDKKRK	sp|Q9H0A0|NAT10_HUMAN	K989	43.02	100.00%
KEEGINKSEKRMK	sp|P09874|PARP1_HUMAN	K518	39.54	100.00%
MPEPVKSAPVPK	sp|Q99879|H2B1M_HUMAN	K6	70.69	100.00%
LKFTKGKSFRHEK	sp|Q14978-2|NOLC1_HUMAN	K678	81.07	100.00%
MPDPAKSAPAPK	sp|P23527|H2B1O_HUMAN	K6	41.7	100.00%
LKFTKGKSFRHEK	sp|Q14978-3|NOLC1_HUMAN	K669	81.07	100.00%
RTPRRSKSDGEAK	sp|P26358|DNMT1_HUMAN	K142	53.57	100.00%

Motif 3 ----SK----- (motif score 6.14)

Surrounding Sequence	Accession	Site	Best Ascore	Localization Probability
FQLFLSKVEETFQ	sp|Q96T88-2|UHRF1_HUMAN	K730	65.84	100.00%
VADYKSKGKFDGA	sp|O15347|HMGB3_HUMAN	K163	39.54	100.00%
AAQAKSKQAILAA	sp|O60869|EDF1_HUMAN	K25	127.41	100.00%
TASKASKEKTPSP	sp|Q9H1E3|NUCKS_HUMAN	K199	64.45	100.00%
LSDEFSKSHKSRR	sp|Q9BQ39|DDX50_HUMAN	K87	39.43	100.00%
SGAALSKKSKGQV	sp|P09874|PARP1_HUMAN	K505	25.23	100.00%
ADDIKSKKKREQS	sp|P45973|CBX5_HUMAN	K104	25.23	100.00%
GRPTASKASKEKT	sp|Q9H1E3|NUCKS_HUMAN	K196	53.06	100.00%
SQPLASKQEKDGT	sp|P17096-2|HMGA1_HUMAN	K15	69.08	100.00%
AAATSSKTPS	sp|Q9UNZ5|L10K_HUMAN	K96	129.75	100.00%
SQPLASKQEKDGT	sp|P17096-3|HMGA1_HUMAN	K15	69.08	100.00%
MNSPKSKKAKKKE	sp|Q9NR30|DDX21_HUMAN	K75	20.98	99.90%
ALSKKSKGQVKEE	sp|P09874|PARP1_HUMAN	K508	174.88	100.00%
KKTKSSKPSKPEK	sp|P35251-2|RFC1_HUMAN	K1127	61.26	100.00%
MPEPSKSAPAPK	sp|P33778|H2B1B_HUMAN	K6	51.08	100.00%
YSPERSKSYSFHQ	sp|Q8NEY8-2|PPHLN_HUMAN	K167	144.15	100.00%
INLLPSKSSVTKI	sp|Q9ULW0|TPX2_HUMAN	K357	37.15	100.00%
RTPRRSKSDGEAK	sp|P26358|DNMT1_HUMAN	K142	53.57	100.00%
VTSKKSKGESDDF	sp|P11388-2|TOP2A_HUMAN	K1518	39.54	100.00%

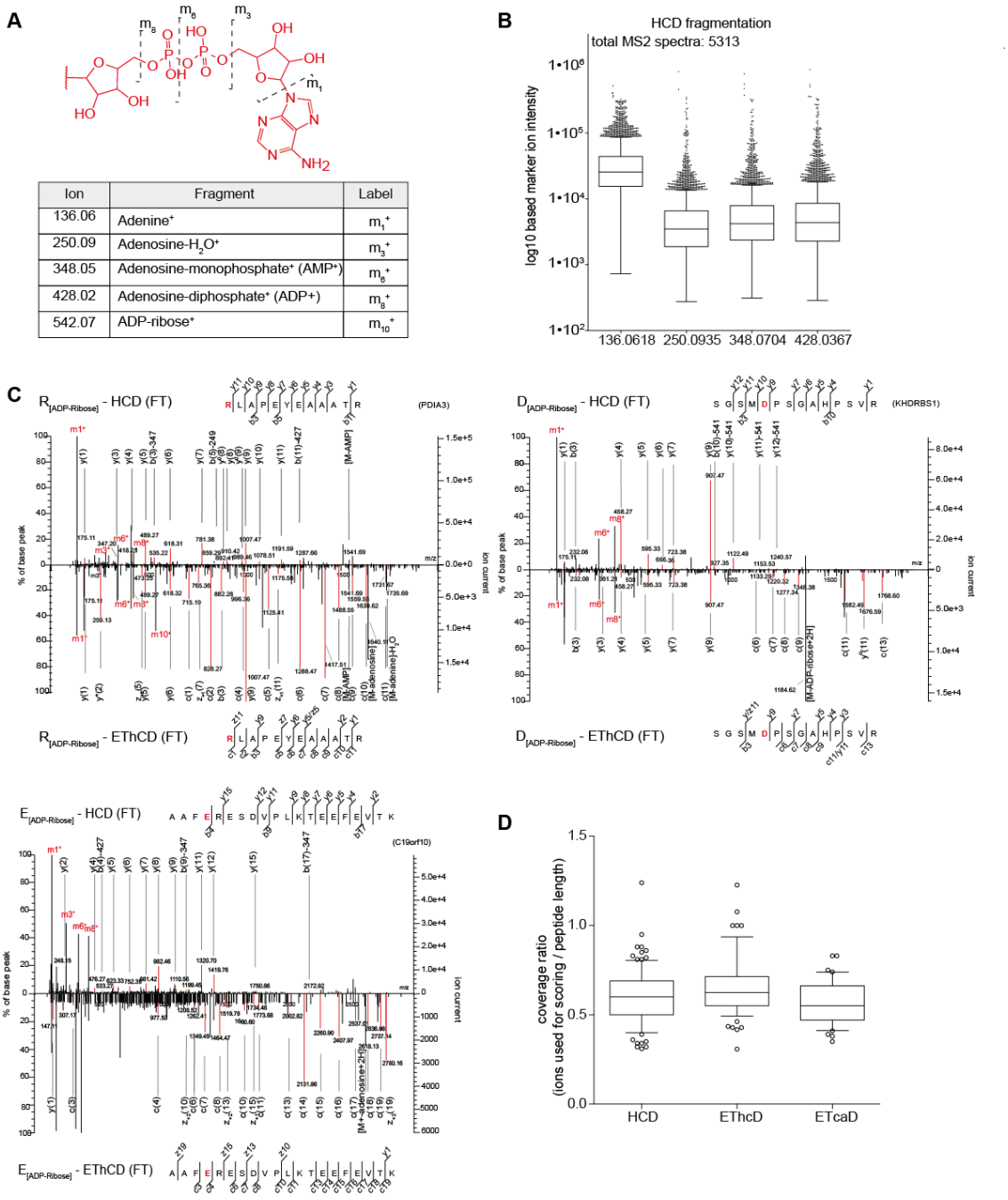

Ion	Fragment	Label
136.06	Adenine$^+$	m_1^+
250.09	Adenosine-H_2O^+	m_3^+
348.05	Adenosine-monophosphate$^+$ (AMP$^+$)	m_6^+
428.02	Adenosine-diphosphate$^+$ (ADP+)	m_8^+
542.07	ADP-ribose$^+$	m_{10}^+

Figure S1: MS/MS fragmentation of ADP-ribosylated peptides.
A) Fragmentation pattern of ADP-ribose upon HCD fragmentation. B) Distribution of ADP fragment ions in MS/MS spectra from HCD fragmentation. Only spectra containing at least two indicative ions with relative intensity of at least 10% of total spectra intensity were considered. C) Fragmentation of ADP-ribosylated peptides in HCD (upper panel) and EThcD (lower panel). Spectra for D, E, and R sites are shown. The position of modification is indicated in red. Presented spectra were deconvoluted, and precursor peak was excluded from the analysis. D) The coverage ratio of the fragmented precursors in each fragmentation method. The ratio was calculated as the number of assigned fragment ions normalized to the length of the peptide.

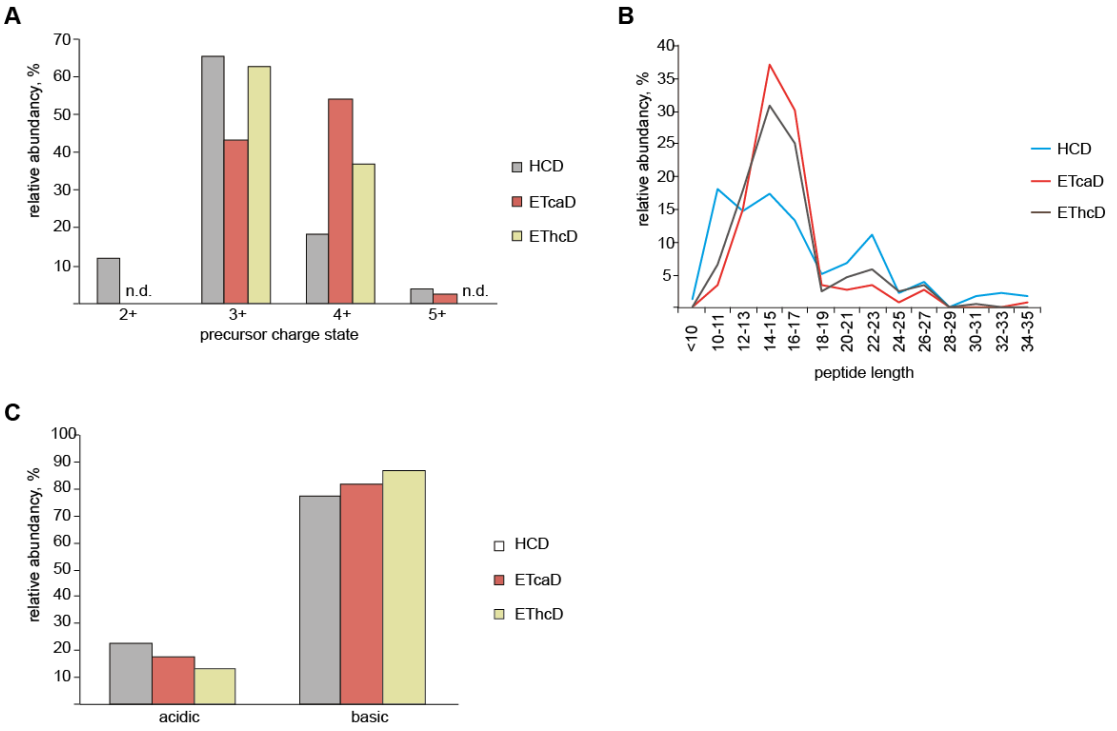

Figure S2: Physicochemical characteristics of identified ADP-ribosylated peptides identified with HCD, ETcaD and EThcD fragmentations. PSMs containing ADP-ribosylation were used for the analysis. The values are normalized over total ADP-ribosylated PSMs count for each fragmentation method. A) Distribution of charge states for ADP-ribosylated precursors identified with HCD, ETcaD, and EThcD. B) Peptide length distribution for ADP-ribosylated precursors identified with HCD, ETcaD, and EThcD. C) Basic/acidic properties of peptides were evaluated by the presence of acidic (D, E) and basic amino acids (K, R, H) in the sequence.

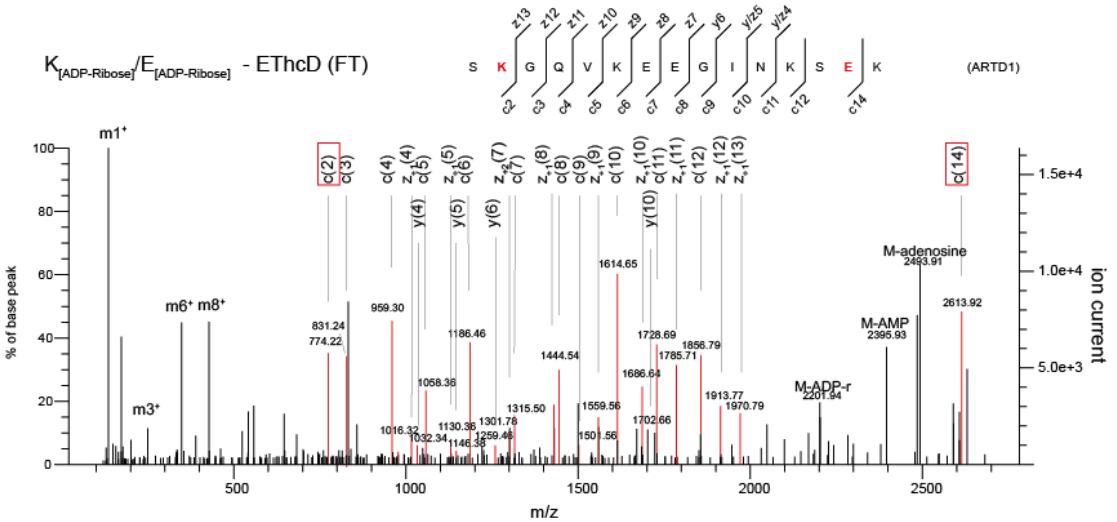

Figure S3: EThcD Fragmentation of a dual-modified peptide. Characteristic ion carrying both modification sites (c(14)) and c2 ion characteristic for the K site are indicated in red square. The position of modification is indicated in red. Presented spectra were deconvoluted, and precursor peak was excluded from the analysis.

3.2.3. Identification of ADP-ribose acceptor sites on in vitro modified Proteins by Liquid Chromatography – Tandem Mass Spectrometry

Identification of ADP-ribose acceptor sites on *in vitro* modified Proteins by Liquid Chromatography – Tandem Mass Spectrometry

Mario Leutert[1,2,4], Vera Bilan[1,2,4], Peter Gehrig[3], and Michael O. Hottiger[1]

[1] Department of Molecular Mechanisms of Disease

[2] Molecular Life Science PhD Program of the Life Science Zurich Graduate School

[3] Functional Genomics Center Zurich, University of Zurich/ETH Zurich, Switzerland, Winterthurerstrasse 190, 8057 Zurich, Switzerland

[4] These authors contributed equally

Summary/Abstract

Protein ADP-ribosylation is a covalent, reversible post-translational modification (PTM) catalyzed by ADP-ribosyltransferases (ARTs). Proteins can be either mono- or poly-ADP-ribosylated under a variety of physiological and pathological conditions. To understand the functional contribution of protein ADP-ribosylation to normal and disease/stress states, modified protein and corresponding ADP-ribose acceptor site identification is crucial. Since ADP-ribosylation is a transient and relatively low abundant PTM, systematic and accurate identification of ADP-ribose acceptor sites has only recently become feasible. This is due to the development of specific ADP-ribosylated protein/peptide enrichment methodologies, as well as technical advances in high accuracy liquid chromatography - tandem mass spectrometry (LC-MS/MS). The standardized protocol described here allows the identification of ADP-ribose acceptor sites in *in vitro* ADP-ribosylated proteins and will, thus, contribute to the functional characterization of this important PTM.

ii. Key Words

ADP-Ribosylation, ADP-ribosylome, ARTD, PARP, PARG, Mass Spectrometry, Ti^{4+}-IMAC enrichment, phosphoenrichment

1. Introduction

Protein ADP-ribosylation is a covalent post-translational modification (PTM) catalyzed by different ADP-ribosyltransferases (ARTs). These enzymes use nicotinamide adenine dinucleotide (NAD+) as a substrate to transfer the ADP-ribose (ADPr) moiety onto specific amino acid side chains, a process termed protein mono-ADP-ribosylation (MARylation). ARTs can also mediate poly-ADP-ribosylation (PARylation) by transferring the ADPr moiety onto an existing protein-bound ADP-ribose unit. Currently, 22 cellular human ARTs are known. They are subdivided into ARTCs (C for C2/C3 toxin-like) and ARTDs (D for diphtheria toxin-like, also called PARPs). While ARTCs are membrane-associated or secreted ARTs, human ARTDs form a family of 18 intracellular enzymes with confirmed or putative mono- or poly-ADP-ribosyltransferase activity (***1-3***).

Several enzymes that remove ADP-ribose from mono- and poly-ADP-ribosylated substrates have also been identified, rendering ADP-ribosylation a fully reversible PTM. Several mammalian ADP-ribosylhydrolases have been characterized so far, including poly-ADP-ribose glycohydrolase (PARG), ADP-ribosylhydrolase 3 (ARH3), both of which are able to hydrolyze poly-ADP-ribose, and the mono-ADP-ribosylarginine hydrolase 1 (ARH1). In addition, the macrodomain-containing proteins MacroD1, MacroD2 and C6orf130 have recently also been shown to exhibit mono-ADP-ribosylhydrolase activity (***4-6***).

To elucidate the functional role of protein ADP-ribosylation, systematical analysis of all ADP-ribosylated proteins and identification of their ADP-ribose acceptor sites is necessary. Comparable to many other PTMs, the fraction of ADP-ribosylated cellular proteins is very low. Thus, studying this group of modified proteins requires specific

ADP-ribosylated protein/peptide enrichment methodologies. Mass spectrometry (MS)-based proteomics is probably the most powerful tool for the analysis of PTMs. However, the analysis of this PTM has proven to be very challenging for several reasons, including the highly transient nature and the low abundance of ADP-ribosylated proteins, the special physicochemical properties of the PTM (bulky, highly charged, heterogeneous structure, labile) and the number of different amino acids that were reported to be modified (acidic and basic amino acids with a primary amino group on the side chain) (***7***). Characterization of ADP-ribose acceptor sites by MS has significantly improved following the development of high-resolution mass spectrometers and novel fragmentation techniques.

In the past few years, several methods for the identification of ADP-ribose acceptor sites on *in vitro* and *in vivo* ADP-ribosylated proteins have been published. Zhang et al. (***8***) established an enrichment protocol based on the isolation of ADP-ribosylated peptides by boronate affinity chromatography and subsequent modified peptide elution using hydroxylamine (NH_2OH). This methodology leaves a characteristic mass signature of 15.01 Da at the ADP-ribose acceptor site (***8***). A major drawback of this protocol is that the chemical reaction employed here limits the detection of ADP-ribosylated amino acids to glutamates and aspartates only. Other groups have also used boronate affinity enrichment, but in combination with acidic elution, which leaves the ADP-ribose moiety intact and leads to a release of all bound peptides. This, unfortunately, resulted in high background of unmodified peptides. Additionally, hydroxylamine treatment has also been used as a stand-alone procedure without any enrichment but this method only seems useful for strongly ADP-ribosylated targets (***9,10***).

Phosphoproteomic approaches were also found to co-enrich ADP-ribosylated peptides, and protocols have been optimized for the specific enrichment of ADP-ribosylated or phosphoribosylated peptides (***11-14***). Chapman et al. (***13***) and Daniels et al. (***14***) used phosphodiesterases to reduce the mono- and poly-ADP-ribosylation

modification (MAR or PAR, respectively) to a protein-bound phosphoribose. The resulting phosphoribosylated peptides are subsequently enriched using either Fe(III)-immobilized metal ion affinity chromatography (IMAC) or TiO_2 microspheres. The conversion of protein bound MAR or PAR to phosphoribose leads to a detectable mass signature of 212.01 Da.

The most recent enrichment approach published by Martello et al. (***15***) makes use of PARG enzymatic treatment to convert *in vivo* PARylated peptides into MARylated peptides, which are subsequently enriched by the ADP-ribose binding protein AF1521 and described in chapter XX of this book. This technique allows the accurate and reproducible identification of ADP-ribose acceptor sites *in vivo*. However, this enrichment strategy has so far not been tested or optimized for *in vitro* modified proteins.

Here, we thus describe an updated protocol using a Ti^{4+}-IMAC enrichment based on the work done by Chapman et al (***13***) and Daniels et al (***14***) to map ADP-ribose acceptor sites on *in vitro* ADP-ribosylated proteins. This protocol is more readily applicable to a variety of different samples than the boronate affinity chromatography based protocol described by our group in the previous edition of this book for *in vitro* modified proteins (***9***). More importantly, this new methodology is not biased against specific ADP-ribose acceptor sites. The problem that phosphorylated peptides might co-enrich with phosphoribosylated/ADP-ribosylated peptides and interfere with the sensitivity of the detection is not an obstacle due to the low complexity of *in vitro* modified samples.

2. Materials

2.1 ADP-ribosylation assay and PARG treatment

1. hARTD1 is expressed and purified from insect cells as carboxyl-terminal His-tagged protein and stored in liquid nitrogen.

2. hPARG is expressed and purified from insect cells as carboxyl-terminal His-tagged protein and stored in liquid nitrogen (see note 1).

3. 10 mM β-Nicotinamide adenine dinucleotide (NAD^+) hydrate >99% (Sigma–Aldrich) in Milli-Q water is stored at −20°C.

4. 10 mM PJ-34 hydrochloride hydrate ≥98% (Sigma-Aldrich) in Milli-Q water is stored at -20°C.

5.ADP-ribosylation buffer (always prepare freshly): 50 mM Tris–HCl pH 8.0, 4 mM $MgCl_2$, 250 µM DTT, cOmplete™ EDTA-free Protease Inhibitor Cocktail.

2.2 FASP Trypsin Digestion

1. 5x disulfide bond reduction buffer: 250 mM DTT, 250 mM Tris-HCl pH 8.2, 5 M urea.

2. 0.5 ml Microcon 30kDa centrifugal filter units with Ultracel-30 membranes (Millipore, MRCF0R030).

3. Urea buffer: 8 M urea in 50 mM Tris-HCl pH 8.2.

4. Iodoacetamide solution: 0.05 M iodoacetamide in urea buffer (kept protected from light).

5. 0.5 M NaCl.

6. 0.05 M ammonium bicarbonate (prepare freshly).

7. Sequencing grade modified trypsin (Promega).

2.3 ADP-ribosylated Peptide Enrichment

1. MagReSyn® Ti4+-IMAC from ReSyn Biosciences.

2. 70% ethanol.

3. Loading Buffer: 1 M glycolic acid in 80% acetonitrile.

4. Wash buffer: 80% acetonitrile and 0.1% acetic acid in H_2O.

5. Elution buffer: 50 mM Tris-HCl pH 8, 10 mM diammonium hydrogen phosphate, 5% acetonitrile.

2.4 Stage Tip Desalting

1. C18 Empore High performance extraction disks (3M).

2. 100% methanol.

3. Stage Tip Solution A: 0.5% acetic acid in H_2O.

4. Stage Tip Solution B: 80% acetonitrile and 0.5% acetic acid in H_2O.

5. Stage Tip Elution Solution: 60% acetonitrile and 0.5% acetic acid in H_2O.

2.5 Mass Spectrometry

1. HPLC solvent A: H_2O containing 0.1% formic acid.

2. HPLC solvent B: Acetonitrile containing 0.1% formic acid.

3. Frit column (inner diameter 75 µm, length 15 cm) packed with reversed phase material (C18-AQ, particle size 1.9 µm, pore size 120 Å, Dr. Maisch GmbH, Germany).

4. Instrumentation: Orbitrap Fusion Tribrid mass spectrometer (Thermo Scientific, San Jose, CA), connected to an Easy-nLC 1000 HPLC system (Thermo Scientific). See (see note 2).

3. Methods

3.1 Overview of the protocol

In vitro auto- and especially trans-ADP-ribosylation reactions are often not efficient and lead to a low abundance of ADP-ribosylated proteins. We, therefore, recommend *in vitro* ADP-ribosylated peptide enrichment following a previously described phosphoenrichment technique that is based on immobilized titanium ion affinity chromatography (***16***). This protocol facilitates modified peptide enrichment and increases the possibilities of a successful analysis, including ADP-ribosylation site determination. *In vitro* reactions should be carried out according to the optimized protocols for the different ADP-ribosyltransferases. The original protocol used phosphodiesterases to reduce mono- and poly-ADP-ribosylation modifications (MAR or PAR, respectively) to a protein-bound phosphoribose and to enrich subsequently phosphoribosylated peptides. We have, however, found that treatment of ADP-ribosylated proteins with poly(ADP-ribose) glycohydrolase (PARG), which reduces the complexity of PAR to protein bound mono-ADP-ribose, works very reliable and allows

efficient ADP-ribose enrichment. PARG-treated proteins are further digested with trypsin using filter-aided sample preparation (FASP) protocol (***17***). The ADP-ribosylated peptides are finally enriched with magnetic microspheres with chelated Ti^{4+} ions. This protocol is optimized to use only very mild buffers for the binding, washing and peptide elution steps in order to preserve the ADP-ribose and its linkage to the modified amino acid residue. Samples are desalted using a C18 Stage Tip protocol (***18***) and analyzed on an Orbitrap Fusion Tribrid mass spectrometer. HCD fragmentation has previously been shown to lead to reproducible identification of ADP-ribosylated peptides and this method allows the accurate identification of the modified amino acid (***19***). Mascot searches are performed to identify ADP-ribose acceptor sites by setting ADP-riboslyation as a variable modification for lysine, arginine, glutamate and aspartate. A representative, annotated spectrum of an identified ADP-ribosylated ARTD1 peptide after the Ti^{4+} IMAC enrichment and the HCD ADP-ribose fragmentation pattern are shown in Figure 1.

3.2 ADP-ribosylation assay and PARG treatment

1. For *in vitro* auto ADP-ribosylation of ARTD1, incubate 20 pmol hARTD1 in the presence of 10 pmol annealed double-stranded oligomer (5-GGAATTCC-3) and 100 nM NAD^+ in ADP-ribosylation buffer (see note 3). Reaction volume: 50 µl, reaction conditions: 15 min, 30°C. Terminate the reactions by adding PJ-34 (ADP-ribosylation inhibitor) to a final concentration of 10 µM. To generate larger amounts of modified target protein, several reactions can be run in parallel (see note 4).

2. To reduce the complexity of PAR and generate MARylated proteins, samples are incubated with 5 pmol hPARG. Adjust the $MgCl_2$ and NaCl buffer concentrations to 10 mM and 50 mM, respectively, and incubate for 1 h at 37°C.

3. For the identification of ADP-ribose acceptor sites in peptides proceed immediately with the FASP trypsin digestion or, alternatively, freeze the proteins at -20°C.

3.3 FASP Trypsin Digestion

1. Add 5x reduction buffer to the protein sample to achieve 1x and incubate at 37°C for 30 min to reduce the disulfide bonds.

2. Load up to 250 µl of reduced sample onto the Microcon-30kDa centrifugal filter unit. Centrifuge at 14'000xg for ~15-20 min at room temperature (RT). Repeat until the sample is completely loaded onto the filter.

3. Add 200 µl of urea buffer to the filter unit. Centrifuge at 14'000xg for ~20 min at RT.

4. Add 100 µl iodoacetamide solution to the filter unit. Gently shake for 5 min and centrifuge at 14'000xg for ~15-20 min at RT.

5. Add 100 µl of 0.5 M NaCl to the filter unit. Centrifuge at 14'000xg for ~15-20 min at RT. Repeat step once.

6. Add 100 µl of ammonium bicarbonate solution to the filter unit. Centrifuge at 14'000xg for ~15-20 min at RT. Repeat step twice.

7. Transfer the filter units to new collection tubes.

8. Add 120 µl of trypsin (1:25 trypsin to protein), dissolved in ammonium bicarbonate solution, to the filter unit and gently shake for 1 min.

9. Incubate the filter units at RT overnight in a humidity chamber.

10. The next day, centrifuge the filter units at 14'000xg for ~15-20 min. The flow-through contains the digested proteins.

11. Re-elute the column with 80 µl of ammonium bicarbonate solution.

12. Dry the eluted peptides in a vacuum concentrator (see note 5).

3.4 Enrichment of ADP-ribosylated Peptides

1. Thoroughly resuspend MagReSyn® Ti^{4+}-IMAC microspheres to ensure homogeneous suspension.

2. Transfer 25 µl (0.5 mg) MagReSyn® Ti^{4+}-IMAC to a 2 ml microcentrifuge tube.

3. Place the tube on a magnetic separator, allow 10 s for the microspheres to clear, and discard the storage solution.

4. Wash the microspheres, with gentle agitation, in 200 µl of 70% ethanol for 5 min.

5. Place the tube on the magnetic separator and allow the microspheres to clear. Discard the ethanol solution.

6. Repeat steps 4 & 5.

7. Add 50 µl loading buffer to microspheres, and let stand for 60 s to equilibrate.

8. Place the tube on the magnetic separator and allow the microspheres to clear. Remove the loading buffer. Important: The microspheres equilibration step should be performed immediately before sample loading.

9. Repeat the equilibration process two additional times.

10. Mix dried protein digests with 100 µl of loading buffer and add mixture to the equilibrated microsphere pellet (see note 6).

11. Incubate at room temperature for 30 min with continuously shaking to ensure adequate sample and microsphere interaction.

12. Place the tube on the magnetic separator and allow the microspheres to clear. Discard the coupling supernatant.

13. Remove unbound sample by washing microspheres with 100 µl loading buffer for 30 s with gentle agitation.

14. Place the tube on a magnetic separator and allow 10 s for the microspheres to clear. Remove the supernatant.

15. Remove non-specifically bound peptides by resuspending the microspheres in 100 µl wash buffer for 2 min with gentle agitation.

16. Place the tube on a magnetic separator and allow 10 s for the microspheres to clear and remove the supernatant.

17. Repeat steps 15&16 twice for a total of three washes.

18. Elute the bound peptides from the microspheres by adding 60 µl elution buffer and letting stand for 15 min. Ensure that the microspheres remain in suspension by gently agitating the tube.

19. Place the tube on the magnetic separator and allow the microspheres to clear. Remove the eluate and transfer it to a new tube.

20. Repeat the elution steps 18&19 twice for a final elution volume of 180 µl.

3.5 Stage Tip Desalting

1. Prepare StageTips by plugging 2 C18 disks in a 200 µl pipette tip (see note 7).

2. Make a hole in the lid of a 1.5 ml Eppendorf tube and fit stage tip in. The tip should be tightly attached to the lid and the tip should not touch the bottom of the tube.

3. Activate the Stage Tip by adding 200 µl 100% methanol to the stage tip, centrifuge at 1,000 x g for approx. 3 min.

4. Add 200 µl Stage Tip Solution B to the stage tip, centrifuge at 1,000 x g for approx. 3 min.

5. Add 200 µl Stage Tip Solution A to the stage tip, centrifuge at 1,000 x g for approx. 3 min.

6. Add 200 µl of your peptide sample, centrifuge at 1,000 x g for approx. 3 min. Repeat step until the whole sample is loaded.

7. Wash Stage Tip by adding 50 µl of Stage Tip Solution A, centrifuge at 1,000 x g for approx. 3 min until Stage Tip is completely dry.

8. Elute Stage Tip by adding 20 µl of Stage Tip Elution solution, centrifuge at 1000 x g for approx. 1 min. Repeat elution step once more and combine elutions.

9. Partially dry the eluted samples in a vacuum concentrator (see note 5). The samples can be stored at -20°C or directly proceed by LC-MS/MS.

3.6 LC-MS/MS

All data are acquired on an Orbitrap Fusion Tribrid mass spectrometer connected to an Easy-nLC 1000 HPLC system (see note 2). 4 µl of peptide sample in 0.1 % formic acid are loaded and separated at a flow rate of 300 nl per min. The following LC gradient was applied: 0 min: 2% HPLC solvent B, 60 min: 30% B, 70 min: 97% B, 80 min: 97% B.

Survey scans were recorded in the Orbitrap mass analyzer in the range of m/z 350-1800, with a resolution of 120'000 and a maximum injection time of 50 ms. Higher energy collisional dissociation (HCD) spectra were acquired in the Orbitrap mass analyzer. A maximum injection time of 240 ms, an AGC target value of 5e5, and a resolution of 120'000 were used. The precursor ion isolation width was set to m/z 2.0, and the normalized collision energy was 35%. Charge state screening was enabled, and charge states 2-5 were included. The threshold for signal intensities was 5e4, and precursor masses already selected for MS/MS acquisition were excluded for further selection during 30 s.

3.7 Database Analysis and Configuration of Mascot Modifications

MS data are analyzed as previously described (***19***). MS and MS/MS spectra are converted into Mascot generic format (mgf) using Proteome Discoverer, v2.1 (Thermo Fisher Scientific, Bremen, Germany). All high-resolution HCD MS/MS spectra are deconvoluted using MS Spectrum Processor, v0.9 (***20***). Searches were performed against the UniProtKB human database (taxonomy 9606, version 20140422), which includes 35'787 Swiss-Prot, 37'02 TrEMBL entries, 73'589 reversed sequences, and 260 common contaminants. Mascot 2.5.1 (Matrix Science) is used for peptide identification using the following search settings: singly charged b and y ion series, immonium ions, and water and ammonia loss ion series are searched. Enzyme specificity is set to trypsin, allowing up to 4 missed cleavages. The ADP-ribose variable modification is set to a mass shift of 541.0611, with scoring of the neutral

losses equal to 347.0631 and 249.0862. The marker ions at m/z 428.0372, 348.0709, 250.0940, 136.0623 are ignored for scoring. Lysine, arginine, glutamic- and aspartic acid are set as variable ADP-ribose acceptor sites. Peptides are considered correctly identified when a Mascot score >20 and an expectation value <0.05 are obtained. To assess the location of the ADP-ribose acceptor sites, we use the site localization analysis provided by Mascot, which is based on the work by Savitski et al. (***20***) and was developed especially for phosphorylation. Due to the lack of a better estimate, we define correctness as having a confidence of ≧95% in the Mascot site localization analysis (see note 8).

Notes

1. As an alternative to PARG treatment, enzymes converting ADP-ribose to phosphoribose (e.g. nudix hydrolases, snake venom phosphodiesterase I) can be used, but these require individually optimized reaction conditions and are expensive in the case of snake venom phosphodiesterase I (***21,14***). None of the available methods to date are capable of distinguishing between mono and poly-ADP-ribose acceptor sites. We envision that a specific set of binding proteins with affinities for either PAR or MAR, or conversion of PAR in to a specific moiety could solve this problem in the near future.

2. We measured all our samples on an Orbitrap Fusion Tribrid mass spectrometer, but it is also possible to conduct a similar analysis on other mass spectrometers with optimized machine settings.

3. Higher NAD^+ concentrations can trigger the generation of very long ADP-ribose polymers that might interfere with trans-ADP-ribosylation or subsequent analysis.

4. We started our analysis with 50 µg ARTD1 and ended up with enough material for 9 mass spectrometry injections. The amount of initial starting protein and the peptide solution that is injected into the mass spectrometer need to be optimized depending on the efficiency of the ADP-ribosylation reaction, the HPLC and the mass

spectrometer used for the analysis.

5. Partial drying of the peptides (leave 1-2 µl) increases the overall yield.

6. To control for the enrichment and MS analysis, standard phosphopeptides can be added into the sample prior to sample preparation.

7. Video tutorial describing how to build and use the stage tips (***18***): https://www.biochem.mpg.de/226863/Tutorials.

8. This method is not optimized for ADP-ribosyl modifications due to the lack of standard peptides with known modification sites. For this reason, even if Mascot states a correctness of 95% for the site localization, this value is arbitrary and cannot be validated experimentally.

Acknowledgement

The authors would like to thank Paolo Nanni (member of the Functional Genomics Center Zurich, University of Zurich, Zurich, Switzerland) for advice and technical assistance. We also thank Felix R. Althaus (Institute of Pharmacology and Toxicology, University of Zurich-Vetsuisse) for providing hPARG expressing baculo virus. Stephan Christen and Deena Leslie Pedrioli (both University of Zurich) provided editorial assistance and critical input during the writing. Work on ADP-ribosyltransferases in the laboratory of M.O.H is supported by the Swiss National Science Foundation (SNF 310030B_138667, 310030_157019).

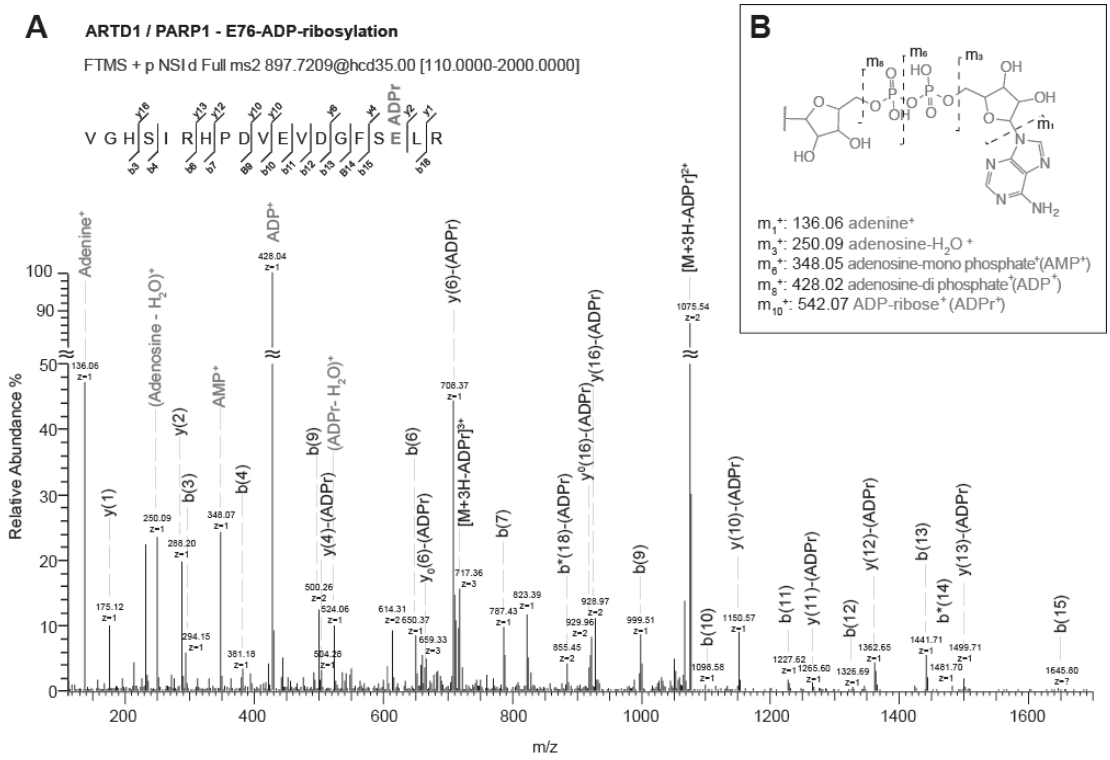

Figure 1

HCD Fragmentation of an ADP-ribosylated peptide. (A) Representative annotated spectrum for the ARTD1 peptide VGHSIRHPDVEVDGFSELR that was found to be ADP-ribosylated on E76. ADP-ribose fragmentation ions are shown in red. (B) Nomenclature of ADP-ribose fragments as described by Hengel *et al.* (***22***). The ADP-ribose fragment ions with strong signals in the HCD MS/MS spectra are shown.

5. References

1. Hassa PO, Haenni SS, Elser M, Hottiger MO (2006) Nuclear ADP-ribosylation reactions in mammalian cells: where are we today and where are we going? Microbiology and molecular biology reviews : MMBR 70 (3):789-829. doi:10.1128/MMBR.00040-05

2. Hottiger MO, Hassa PO, Luscher B, Schuler H, Koch-Nolte F (2010) Toward a unified nomenclature for mammalian ADP-ribosyltransferases. Trends in biochemical sciences 35 (4):208-219. doi:10.1016/j.tibs.2009.12.003

3. Vyas S, Matic I, Uchima L, Rood J, Zaja R, Hay RT, Ahel I, Chang P (2014) Family-wide analysis of poly(ADP-ribose) polymerase activity. Nature communications 5:4426. doi:10.1038/ncomms5426

4. Slade D, Dunstan MS, Barkauskaite E, Weston R, Lafite P, Dixon N, Ahel M, Leys D, Ahel I (2011) The structure and catalytic mechanism of a poly(ADP-ribose) glycohydrolase. Nature 477 (7366):616-620. doi:10.1038/nature10404

5. Rosenthal F, Feijs KL, Frugier E, Bonalli M, Forst AH, Imhof R, Winkler HC, Fischer D, Caflisch A, Hassa PO, Luscher B, Hottiger MO (2013) Macrodomain-containing proteins are new mono-ADP-ribosylhydrolases. Nature structural & molecular biology 20 (4):502-507. doi:10.1038/nsmb.2521

6. Jankevicius G, Hassler M, Golia B, Rybin V, Zacharias M, Timinszky G, Ladurner AG (2013) A family of macrodomain proteins reverses cellular mono-ADP-ribosylation. Nature structural & molecular biology 20 (4):508-514. doi:10.1038/nsmb.2523

7. Daniels CM, Ong SE, Leung AK (2015) The Promise of Proteomics for the Study of ADP-Ribosylation. Molecular cell 58 (6):911-924. doi:10.1016/j.molcel.2015.06.012

8. Zhang Y, Wang J, Ding M, Yu Y (2013) Site-specific characterization of the Asp- and Glu-ADP-ribosylated proteome. Nature methods 10 (10):981-984. doi:10.1038/nmeth.2603

9. Rosenthal F, Messner S, Roschitzki B, Gehrig P, Nanni P, Hottiger MO (2011) Identification of distinct amino acids as ADP-ribose acceptor sites by mass spectrometry. Methods in molecular biology 780:57-66. doi:10.1007/978-1-61779-270-0_4

10. Gagne JP, Ethier C, Defoy D, Bourassa S, Langelier MF, Riccio AA, Pascal JM, Moon KM, Foster LJ, Ning Z, Figeys D, Droit A, Poirier GG (2015) Quantitative site-specific ADP-ribosylation profiling of DNA-dependent PARPs. DNA repair 30:68-79. doi:10.1016/j.dnarep.2015.02.004

11. Matic I, Ahel I, Hay RT (2012) Reanalysis of phosphoproteomics data uncovers ADP-ribosylation sites. Nature methods 9 (8):771-772. doi:10.1038/nmeth.2106

12. Lang AE, Schmidt G, Schlosser A, Hey TD, Larrinua IM, Sheets JJ, Mannherz HG, Aktories K (2010) Photorhabdus luminescens toxins ADP-ribosylate actin and RhoA to force actin clustering. Science 327 (5969):1139-1142. doi:10.1126/science.1184557

13. Chapman JD, Gagne JP, Poirier GG, Goodlett DR (2013) Mapping PARP-1 auto-ADP-ribosylation sites by liquid chromatography-tandem mass spectrometry. Journal of proteome research 12 (4):1868-1880. doi:10.1021/pr301219h

14. Daniels CM, Ong SE, Leung AK (2014) Phosphoproteomic Approach to Characterize Protein Mono- and Poly(ADP-ribosyl)ation Sites from Cells. Journal of proteome research 13 (8):3510-3522. doi:10.1021/pr401032q

15. Martello R, Leutert M, Jungmichel S, Bilan V, Larsen SC, Young C, Hottiger MO, Nielsen ML (2016) Proteome-wide identification of the endogenous ADP-ribosylome of mammalian cells and tissue. Nature communications in press

16. Zhou H, Ye M, Dong J, Han G, Jiang X, Wu R, Zou H (2008) Specific phosphopeptide enrichment with immobilized titanium ion affinity chromatography adsorbent for phosphoproteome analysis. Journal of proteome research 7 (9):3957-3967. doi:10.1021/pr800223m

17. Wisniewski JR, Zougman A, Nagaraj N, Mann M (2009) Universal sample preparation method for proteome analysis. Nature methods 6 (5):359-362. doi:10.1038/nmeth.1322

18. Rappsilber J, Mann M, Ishihama Y (2007) Protocol for micro-purification, enrichment, pre-fractionation and storage of peptides for proteomics using StageTips. Nature protocols 2 (8):1896-1906. doi:10.1038/nprot.2007.261

19. Rosenthal F, Nanni P, Barkow-Oesterreicher S, Hottiger MO (2015) Optimization of LTQ-Orbitrap Mass Spectrometer Parameters for the Identification of ADP-Ribosylation Sites. Journal of proteome research 14 (9):4072-4079. doi:10.1021/acs.jproteome.5b00432

20. Savitski MM, Mathieson T, Becher I, Bantscheff M (2010) H-score, a mass accuracy driven rescoring approach for improved peptide identification in modification rich samples. Journal of proteome research 9 (11):5511-5516. doi:10.1021/pr1006813

21. Daniels CM, Thirawatananond P, Ong SE, Gabelli SB, Leung AK (2015) Nudix hydrolases degrade protein-conjugated ADP-ribose. Scientific reports 5:18271. doi:10.1038/srep18271

22. Hengel SM, Shaffer SA, Nunn BL, Goodlett DR (2009) Tandem mass spectrometry investigation of ADP-ribosylated kemptide. Journal of the American Society for Mass Spectrometry 20 (3):477-483. doi:10.1016/j.jasms.2008.10.025

3.2.4. Proteome-wide identification of endogenous ADP-ribose acceptor sites by Liquid Chromatography–Tandem Mass Spectrometry

Proteome-wide identification of endogenous ADP-ribose acceptor sites by Liquid Chromatography–Tandem Mass Spectrometry

Sara C. Larsen[1,4], Mario Leutert[2,3,4], Vera Bilan[2,3], Rita Martello[1], Stephanie Jungmichel[1], Clifford Young[1], Michael O. Hottiger[2] and Michael L. Nielsen[1*]

[1] Department of Proteomics, Novo Nordisk Foundation Center for Protein Research, University of Copenhagen, Faculty of Health and Medical Sciences, DK-2200 Copenhagen, Denmark

[2] Department of Molecular Mechanisms of Disease, University of Zurich, CH-8057 Zurich, Switzerland

[3] Molecular Life Science Program of the Life Science Graduate School, University of Zurich, Switzerland

[4] These authors contributed equally

* To whom correspondence should be addressed: michael.lund.nielsen@cpr.ku.dk

Abstract

ADP-ribosylation is a post-translational modification (PTM) affecting a variety of cellular processes. In recent years, mass spectrometry (MS)-based proteomics has become a valuable tool for studying ADP-ribosylation. However, it has remained a challenge to study this PTM *in vivo* in an unprejudiced and sensitive manner under physiological conditions. Here, we describe a detailed protocol for unbiased analysis of endogenous ADP-ribosylated proteins and their ADP-ribose acceptor sites under physiological conditions. The method relies on the enrichment of mono-ADP-ribosylated peptides using the macrodomain Af1521, combined with high resolution liquid chromatography-tandem MS (LC-MS/MS). The 5-day protocol explains the enrichment of ADP-ribosylated peptides step-by-step from cell culture and all the way to data processing using the MaxQuant software suite [1].

Key words: ADP-ribosylation, ADP-ribosylome, mass spectrometry, proteomics, Af1521 macrodomain enrichment, affinity purification, PARG

1. Introduction

Protein ADP-ribosylation is a post-translational modification (PTM) where an ADP-ribose moiety is transferred from NAD^+ to the amino acid side-chains of target proteins (i.e. mono-ADP-ribosylation, MARylation). This protein bound ADP-ribose can subsequently serve as attachment points for the linkage of additional ADP-ribose units to form poly-ADP-ribosylation (PARylation). These chemical reactions are primarily catalyzed by ADP-ribosyltransferases (ARTs) and certain Sirtuin deacetylases [2,3]. A detailed understanding of the molecular mechanisms and functions affected by ADP-ribosylation remains elusive, since the amino acid residues modified by ADP-ribosylation *in vivo* remains unclear. Current experimental evidence suggests that ADP-ribosylation in eukaryotes primarily occurs on four different amino acids; Lys [4], Arg [5], Asp and Glu residues [6]. In addition, Cys residues were reported to be MARylated by certain ARTDs or bacterial toxins [7,8].

Protein ADP-ribosylation is a low abundant PTM that is rapidly degraded. To overcome this challenge cellular poly(ADP-ribosyl) glycohydrolase (PARG) levels are often knocked down by siRNA or its expression completely abolished by genetic deletion (i.e. using PARG knockout cells) [9,6]. Unfortunately, cellular absence of PARG affects the PAR homeostasis leading to physiological alterations in cells and mice [10-12]. Consequently, strategies requiring knockdown or omission of PARG constitute an unphysiological setting for analyzing cellular ADP-ribosylation and its associated mechanisms [13].

High-resolution mass spectrometry (MS) has become a valuable tool for comprehensive identification of PTMs [14]. The two most current published MS-based approaches for mapping ADP-ribose acceptor sites *in vivo* are either biased towards modifications of only Glu and Asp [6], or lack sensitivity due to co-enrichment of several other PTMs (i.e. phosphorylated peptides) [9]. Moreover, a chemical genetic discovery method for ARTD targets was recently reported [15]. However, this approach renders the identification of ARTD-specific substrates under different cellular conditions, and at physiological NAD+ levels unattainable. Hence, to address these limitations we have developed a protocol for the unbiased mapping of endogenous ADP-ribose acceptor sites in proteins under genetically unperturbed physiological conditions [16]. Collectively, the protocol described herein represents a non-incremental advance in the detection of ADP-ribose acceptor sites and the identification of cellular processes regulated by ADP-ribosylation.

Together, the application of the described protocol allows the detection of the cellular ADP-ribosylome under defined conditions and will promote our understanding

of ADP-ribosylation as a regulatory mechanism of complex physiological and pathological processes.

2. Materials and equipment

All buffers are made using sequencing grade chemicals and Milli-Q water.

2.1. Cell culture and lysis

1. Cells of interest.
2. Dulbeccos Modified Eagle Medium (D-MEM) supplemented with 10% fetal bovine serum (FBS) and penicillin/streptomycin (100 U/mL).
3. Phosphate Buffered Saline (PBS).
4. Hydrogen peroxide or alternative ADP-ribosylation-inducing agents of interest.
5. Modified RIPA buffer (high salt): 50 mM Tris-HCl, pH 7.5, 400 mM NaCl, 1 mM EDTA, 1% NP-40, 0.1% Na-deoxycholate, 40 µM PJ-34, 1 µM ADP-HPD (Note 1), Protease inhibitor cocktail.
6. Modified RIPA buffer (no salt): 50 mM Tris-HCl, pH 7.5, 1 mM EDTA, 1% NP-40, Protease inhibitor cocktail.
7. Acetone.
8. Equipment: Cell lifters.
9. Equipment: Centrifuge (with cooling) including a swinging bucket rotor.

2.2. In-solution digestion

1. Denaturation buffer: 6 M urea, 2 M thiourea, 10 mM HEPES, pH 8.0.
2. Bradford reagent or alternative assay for measuring protein concentration.
3. Reduction buffer: 1 M Dithiothreitol (DTT).
4. Alkylation buffer: 550 mM Chloracetamide (CAA).
5. Lys-C protease.
6. Digestion buffer: 25 mM Ammonium Bicarbonate (ABC).
7. Sequencing grade modified trypsin.
8. 10% trifluoroacetic acid (TFA)
9. Equipment: Centrifuge (with cooling) including a swinging bucket rotor.
10. Equipment: Thermomixer.

2.3 Concentration of peptides on Sep-Pak

1. 100% acetonitrile.
2. 0.1% TFA.
3. Equipment: Centrifuge including a swinging bucket rotor.

4. Equipment: Sep-Paks.

2.4 GST-protein expression and purification of Af1521

1. Bacterial expression plasmid for N-terminal GST fused macrodomain Af1521 [17].
2. BL21 competent E. coli cells.
3. Super Optimal broth with Catabolite repression (SOC).
4. Agar plates containing ampicillin (Amp-plates).
5. Luria-Bertani (LB) medium.
6. Terrific Broth (TB) medium.
7. Isopropyl-beta-D-thiogalactopyranoside (IPTG)
8. Lysis buffer: 50 mM Tris-HCl, pH 7.5, 150 mM NaCl, 1 mM $MgCl_2$, 1 mM DTT, 1 x Bug Buster, 1 µL/mL Benzonase, 200 µg/mL Lysozyme, Protease inhibitor cocktail.
9. Glass beads.
10. Glutathione Sepharose 4B.
11. Wash buffer: 50 mM Tris-HCl, pH 7.5, 150 mM NaCl, 1 mM DTT.
12. Equipment: Centrifuge (with cooling) including a fixed angle rotor for eppendorf tubes.
13. Equipment: Centrifuge (with cooling) including a swinging bucket rotor

2.5 Enrichment of ADP-ribosylated peptides

1. 50% acetonitrile.
2. 80% acetonitrile.
3. 5 x Affinity precipitation (AP) buffer: 250 mM Tris-HCl, pH 8.0, 50 mM $MgCl_2$, 1.25 mM DTT, 250 mM NaCl. (For 1 x AP buffer dilute 5 x AP buffer in Milli-Q).
4. hPARG is expressed and purified from insect cells as carboxyl-terminal His-tagged protein and stored in liquid nitrogen.
5. Purified Af1521.
6. 0.15% TFA.
7. Equipment: Vacuum concentrator (SpeedVac).
8. Equipment: NanoDrop or alternative assay for measurement of peptide concentration.
9. Equipment: Centrifuge (with cooling) including a fixed angle rotor for eppendorf tubes.
10. Tabletop centrifuge.

2.6 Purification and desalting of peptides for mass spectrometric analysis

1. C18 material.
2. Methanol.
3. Buffer B: 80% acetonitrile, 0.5% acetic acid.
4. Buffer A: 0.5% acetic acid.
5. Equipment: StageTip adapters for microcentrifuge tubes.
6. Equipment: Centrifuge including a fixed angle rotor for eppendorf tubes.

2.7 LC-MS/MS analysis of ADP-ribosylated peptides

1. StageTip elution buffer 1: 40% acetonitrile, 0.5% acetic acid.
2. StageTip elution buffer 2: 60% acetonitrile, 0.5% acetic acid.
3. Buffer A*: 5% acetonitrile, 0.1% TFA.
4. C18-packed nanospray column. We use 15 cm analytical columns (75 µm inner diameter) pulled and packed in-house with 1.9 µm C18 beads (Reprosil Pur-AQ, Dr. Maisch, Germany).
5. Equipment: Liquid chromatography (LC) system e.g. nanoscale UHPLC system EASY-nLC1200.
6. Equipment: Nanospray column heater (Sonation GmbH).
7. Equipment: Mass spectrometer e.g. a Q Exactive HF.
8. Data analysis software such as the freely available MaxQuant software suite (www.maxquant.org).

3. Methods

Here, we describe a sensitive and unbiased method for the identification of *in vivo* ADP-ribosylated sites using high resolution LC-MS/MS. The described protocol allows the study of basal ADP-ribosylation levels as well as their changes upon specific stimulations. In principle the protocol is applicable to any cell line of interest as long as enough material can be collected. The basal *in vivo* ADP-ribosylation activity has been described as low, but it is greatly increased by genotoxic stress in particular through the activation of ARTD1, and regulated by the opposing actions of PARG [18]. Thus, DNA shearing during cell lysis was shown to cause unphysiological PAR formation despite fast and gentle sample handling [19]. It is therefore crucial to complement the lysis buffer with PARP and PARG inhibitors in order to preserve the physiological ADP-ribosylome and avoid lysis-induced artifacts. In order to enhance

identification of ADP-ribosylation sites, the isolated proteins are digested to peptides and treated with PARG converting all PARylated amino acids to their MARylated counterparts. Although the PARG treatment prevents discriminating whether the modification was originally PARylation or MARylation, the conversion is crucial for feasible MS analysis. MARylated peptides can be unbiasedly enriched using ADP-ribose-specific binders such as the Af1521 macrodomain, which has an affinity to ADP-ribose in the range of Kd ~ 0.13 µM [20,17,19]. Subsequently the modified peptides and their ADP-ribose acceptor sites are identified by high resolution LC-MS/MS.

The presented method can be divided into seven parts: cell culture and lysis, protein digestion, concentration of peptides, expression and purification of the Af1521 macrodomain, enrichment of ADP-ribosylated peptides, purification of samples for MS analysis and analysis of the peptide mixture using LC-MS/MS.

While the below described instructions are optimized for identification of ADP-ribose acceptor sites on *in vivo* modified proteins from cell cultures, the method is also suitable for the identification of the ADP-ribosylome from tissues. However, starting with tissues requires an optimization of different steps in particular the extraction conditions and will be discussed elsewhere.

3.1 Cell culture and lysis

1. Seed cells into eight 150 mm cell culture dishes per condition and grow them to approximately 80% confluency. This will yield approximately 30-40 mg of total protein.
2. Wash cells once with warm PBS. Add H_2O_2 (0.5-1 mM) in PBS and incubate for 5-10 min at 37°C. (Note 2)
3. Wash the cells carefully and briefly with ice-cold PBS and make sure to remove all PBS.
4. Place the washed 150 mm cell culture dishes on ice and add 0.2 mL ice-cold modified RIPA (high salt) per plate. Incubate on ice for 5 min, scrape the cells off into the buffer, tilt the plate and transfer the lysis buffer and cells to a 15 mL falcon tube placed on ice.
5. Centrifuge for 20 min, 4°C at 5000 x G to clear the lysate. Transfer supernatant to a 50 mL falcon tube for acetone precipitation.
6. Dilute sample in salt-free RIPA (final concentration of NaCl of 133 mM) in order to make pellet easier to dissolve in urea. (Note 3)

7. Acetone precipitate the proteins overnight by adding five-fold volume of ice-cold acetone to reach a concentration of 80% acetone. Samples can be stored in acetone for several weeks.

3.2 In-solution digestion

1. Centrifuge the acetone precipitated proteins for 5 min, 4°C at 1000 x G and carefully discard the acetone completely by suction.
2. At room temperature, add denaturation buffer (urea) to the 50 mL falcon tubes to dissolve the protein pellets. The added volume depends on pellet size. An ideal protein concentration is approximately 5 mg/mL. (Note 4)
3. Determine protein concentration e.g. by Bradford reagent.
4. Reduce disulfide bridges and unwind proteins by adding 1/1000 volume of reduction buffer (DTT), mix well and incubate for 60 min at room temperature shaking.
5. Alkylate the free –SH groups by adding 1/100 volume of alkylation buffer (CAA) and incubate for 60 min at room temperature in the dark shaking.
6. Cleave the proteins to peptides by adding proteases. Add 1 µg Lys-C for every 100 µg protein to pre-digest the proteins. Lys-C will cleave at the carboxyl site of lysine residues. Incubate at room temperature for 3-4 hrs shaking.
7. Dilute the sample 1:4 with 25 mM ABC to reduce urea concentration to <2 M. Make sure pH is 8.0-8.5, if pH is too high add water.
8. Add 1 µg Trypsin for every 100 µg protein. Trypsin will cleave on the carboxyl site of lysine and arginine residues. Digest overnight at room temperature shaking.
9. Carefully add 10% TFA dropwise until peptide solution has reached pH 2 in order to terminate trypsin digestion. The digested proteins can be stored at 4°C until further processing.

3.3 Concentration of peptides on Sep-Pak

1. Clarify the peptide mixture by centrifugation for 5 min, room temperature at 1800 x G. Retain supernatant.
2. Insert the Sep-Pak C18 column into a 10 mL syringe (use gravity flow and clamps). The capacity of the Sep-Pak is approximately 5% wt/wt of packing material weight.
3. Add 5 mL of 100% acetonitrile to pre-wet the Sep-Pak cartridge.
4. Wash the column by adding 2 x 4 mL 0.1% TFA. Remove bubbles in the top of the Sep-Pak by using a P-200 pipette to ensure flow through the material.

5. Load approximately 5 mL of the peptide mixture unto the Sep-Pak column at a time (the column might turn yellow) and remove any bubbles forming at the top of the Sep-Pak. Load the rest of the peptides.

6. Wash the column by adding 3 x 5 mL Milli-Q water. Measure the pH of the flow-through. It must be >6, otherwise add more Milli-Q water. Store the Sep-Pak at 4°C until further use. The Sep-Pak can be stored at 4°C for several months.

3.4 GST-protein expression and purification of Af1521

1. Add 1 µL of cooled Af1521 plasmid to freshly thawn BL21, stir carefully and leave on ice for 15 min.
2. Heat shock for 45 sec at 42°C.
3. Incubate for 1 min on ice.
4. Add 900 µL SOC and shake vigorously for 40 min at 37°C.
5. Centrifuge for 2 min, room temperature at 2000 x G and discard approximately 600 µL of the supernatant.
6. Resuspend the bacteria in the remaining media, streak everything on to Amp-plates and grow them overnight at 37°C.
7. Inoculate a single colony in 5 mL of LB media containing ampicillin (1:1000) and grow them overnight at 37°C.
8. Dilute the starter culture 1:500 in 200 mL pre-warmed TB media containing ampicillin (1:1000) in a 0.5 mL flask. (Note 5)
9. Grow them at 37°C and measure OD_{600} continuously.
10. Induce protein expression by adding freshly thawn IPTG (0.5 mM) when the OD_{600} is approximately 0.55-0.65.
11. Express proteins for 5-6 hrs at 30°C.
12. Pour 50 mL of the bacteria suspension into a 50 mL falcon tube and centrifuge for 15 min, room temperature at 3000 x G.
13. Discard the supernatant and pour 50 mL of the bacteria suspension into the same 50 mL falcon tube.
14. Centrifuge for 15 min, room temperature at 3000 x G, remove supernatant and freeze pellets at -80°C. Pellets can be stored at -80°C for several months.
15. Thaw bacterial pellet and resuspend it in 4 mL freshly prepared lysis buffer. Incubate for 20 min at room temperature rotating.
16. Break cells by adding glass beads and vortex for approximately 30 sec.
17. Transfer liquid to microcentrifuge tubes and pellet cell debris by centrifugation for 5 min, 4°C at 14,500 x G.
18. Transfer 2 mL of Glutathione Sepharose 4B slurry to a 15 mL falcon tube.

19. Add 8 mL of wash buffer and centrifuge for 2 min, 4°C at 2000 x G.

20. Discard supernatant, add 9 mL of wash buffer and centrifuge for 2 min, 4°C at 2000 x G.

21. Discard supernatant, transfer the cleared lysate to the 15 mL falcon tube containing the equilibrated beads and incubate for 4 hrs at 4°C head-over-tail rotating.

22. Centrifuge the slurry for 2 min, 4°C at 2000 x G and remove supernatant.

23. Wash the beads four times with freshly prepared wash buffer. Mix by inverting the tube 5 times. Centrifuge for 2 min, 4°C at 2000 x G.

24. Remove the supernatant and resuspend the beads in wash buffer for a total volume of 10 mL. Proteins can be stored at 4°C coupled to beads for a few weeks. (Note 6)

3.5 Enrichment of ADP-ribosylated peptides

1. Elute the peptides off the Sep-Pak with 3 mL 50% acetonitrile followed by 1.5 mL 80% acetonitrile.

2. Aliquot the 4.5 mL elution-mix into four 1.5 mL microcentrifuge tubes. Add 40 µL of 5 x AP buffer per tube, mix by pipetting up and down.

3. Reduce the volumes to 200 µL per tube by vacuum centrifugation at 45°C. This will take approximately 60 min.

4. Combine volumes of the four vials into one to attain a final volume of 800 µL.

5. Clear peptide solution by centrifugation for 5 min, 4°C at 1800 x G. Cool on ice.

6. Determine peptide concentration, e.g., at 280 nm using a NanoDrop. Use approximately 10 mg of peptides for enrichment of ADP-ribosylated peptides and save some for proteome analysis.

7. Add 4.2 µg PARG enzyme per sample to reduce PAR complexity. Incubate for 3 hrs at 37°C shaking.

8. Cool down peptide mixture on ice.

9. Add 500 µL of purified Af1521 macrodomain and incubate for 2 hrs at 4°C head-over-tail rotating.

10. Centrifuge the peptides and slurry for 1 min, 4°C at 1000 x G and remove supernatant.

11. Wash the beads three times with 1 mL of ice-cold 1 x AP buffer. Mix by inverting tubes 5 times. Avoid longer incubation. Centrifuge for 1 min, 4°C at 1000 x G and remove supernatant.

12. Wash the beads three times with 1 mL of ice-cold Milli-Q water. Mix by inverting tubes 5 times. Avoid longer incubation. Centrifuge for 1 min, 4°C at 1000 x G and remove supernatant.

13. Elute the ADP-ribosylated peptides by addition of 100 µL 0.15% TFA to the beads, tap the bottom of the tube several times (do not vortex) and let stand at room temperature for 10 min.

14. Tap the bottom of the tube again, centrifuge in a tabletop centrifuge for a few seconds, remove the supernatant using a gel-loading tip and transfer it to a new labeled microcentrifuge tube.

15. Repeat elution step with additional 100 µL of 0.15% TFA for 10 min, combine the eluates and load onto C18 stage tips.

3.6 Purification and desalting of peptides for mass spectrometric analysis

1. Prepare one C18 StageTip for each sample. Making of StageTips are described in Rappsilber et al. [21]. We recommend stacking two C18 discs on top of each other for each StageTip.

2. Activate the discs by adding 100 µL 100% methanol to the StageTips and let it pass through the C18 material by centrifuging for approximately 2 min, room temperature at 600 x G. It is important never to let the material run dry.

3. Condition the discs by adding 100 µL Buffer B and centrifuge for approximately 2 min, room temperature at 600 x G.

4. Equilibrate the discs by adding 100 µL Buffer A and centrifuge for approximately 2 min, room temperature at 600 x G.

5. Load the eluted peptides onto the activated StageTip and centrifuge for approximately 4 min, room temperature at 600 x G.

6. Wash the StageTips by adding 50 µL Buffer A and centrifuge for approximately 3 min, room temperature at 600 x G. Centrifuge until dryness. The StageTips can be stored at 4°C for several months.

3.7 LC-MS/MS analysis of ADP-ribosylated peptides

1. Elute StageTips by addition of 20 µL of StageTip elution buffer 1 followed by 20 µL of StageTip elution buffer 2 into a 96 well plate suitable for the LC autosampler.

2. Remove acetonitrile from the elutions by vacuum centrifugation until volume is approximately 7 µL. This will take approximately 25 min at 30°C. If less than 7 µL is left, fill up to 7 µL with Buffer A.

3. Add 1 µL of Buffer A* to all wells.

4. Design a LC gradient of 60 min or more. We recommend analyzing each sample using a 180 min gradient ranging from 5% to 64% acetonitrile in 0.5% formic acid at a flow rate of 250 nL/min. (Note 7)

5. Injection volume should be kept to 5 µL or below for each sample. (Note 8)

6. For separation of peptides we typically use an in-house packed analytical LC column made from a 20 cm long fused silica with 75 µm inner diameter and packed with 1.9 µm C 18 beads.

7. To facilitate identification of ADP-ribosylated peptides it is recommended to operate the Q-Exactive mass spectrometer using the previously described 'sensitive settings' [22] (Note 8). Briefly, the sensitive settings correspond to a top 10 method on the Q-Exactive with 60,000 MS resolution and 60,000 MS/MS resolution

8. The scan range for the MS should be set to 400–1600 m/z, for MS/MS fixed first mass should be set to 100 m/z.

9. Automatic gain control AGC target for MS should be set to 1e6 or higher, for MS/MS it should be 10× lower (100,000 in this case).

10. Keep maximum injection at 45 ms for MS and 110 ms for MS/MS.

11. Normalized collisional energy should be set to a value between 25 and 30, we recommend 28 as safe median.

12. Dynamic exclusion should be set to 30 s.

13. Process raw files using the MaxQuant software suite supported by the Andromeda search engine. We use the following settings:

Fixed modifications: Carbamidomethyl (C)

Variable modifications: Oxidation (M), Acetyl (Protein N-term), mono-ADP-ribosylation ($C_{10}H_{13}N_5O_9P_2$) on lysine, arginine, glutamic acid and aspartic acid.

To increase confidence in identified ADP-ribosylated peptide identifications, we typically add neutral losses and diagnostic ion masses in the MaxQuant search parameters (Note 9).

Max. missed cleavages: 3

Min. peptide length: 7

Protein FDR: 0.01; Peptide FDR: 0.01; Site FDR: 0.01.

4. Notes

1. The stability of ADP-HPD in solution is critical. Following reconstitution of the powder, aliquots are only stable for up to 1 week at -20°C.

2. We do recommend treating the cells in some way to induce ADP-ribosylation. In our hands, treatment with H_2O_2 for 5-10 min increases the number of ADP-ribosylated targets significantly. Several other DNA damage-inducing agents can be used.

3. Protein concentration can be determined after lysis (e.g. by Bradford) and an aliquot of the protein lysate can be kept for western blotting. If stable isotope labeling by amino acids in cell culture (SILAC) is applied, we recommend mixing of SILAC samples before acetone precipitation. Alternatively, samples can be mixed when dissolved in urea.

4. It is important to add urea to the protein pellets at room temperature. At low temperatures, urea will crystalize while it will induce artifacts at higher temperatures [23].

5. If possible, we recommend making several starting cultures for preparation of a large batch of Af1521.

6. For western blot analysis, we recommend crosslinking the macrodomain to the sepharose beads. In brief, wash resin three times with 10 mL 0.2 M borate-NaOH, pH 9.0. Centrifuge for 2 min, room temperature at 2000 x G. Add 10 mL freshly prepared DMP solution (20 mM) and incubate for 60 min, room temperature head-over-tail rotating. Centrifuge for 2 min, room temperature at 2000 x G. Stop crosslinking reaction by adding 10 mL 0.1 M glycine-HCl, pH 2.5 to remove non-covalently linked molecules that may be present due to reduced coupling efficiencies. Crosslinking can be verified by SDS-PAGE. GST-protein should only elute from the resin prior to addition of DMP.

7. Described LC settings are applied for the analysis of enriched ADP-ribosylome from treated cells. The gradient have to be adapted based on the complexity of the sample and used instrumentation.

8. An injection volume of 5 µL will take approximately 20 min to load onto the column at a constant pressure of 500 bars. An injection volume of more than 5 µL will result in longer loading times. By using a nanoscale UHPLC system e.g. EASY-nLC1200 (Thermo Fisher Scientific) the loading pressure can be increased and the loading time thereby shortened.

9. To help assign ADP-ribosylated peptides in MaxQuant, the following parameters can be added to the Andromeda search engine:

Monoisotopic mass: 541.0611088074

Composition: H(21)C(15)N(5)O(13)P(2)

Position: notCterm

NeutralLoss: H(21)C(15)N(5)O(13)P(2) for lysine, arginine, aspartic acid and glutamic acid.

Diagnostic peak: H(5)C(5)N(5), H(11)C(10)N(5)O(3), H(14)C(10)N(5)O(7)P, H(15)C(10)N(5)O(10)P(2), H(21)C(15)N(5)O(13)P(2) for lysine, arginine, aspartic acid and glutamic acid.

Acknowledgements

Ms. Monika Fey is acknowledged for the expression and purification of recombinant human PARG (University of Zurich) and Paolo Nanni for technical support for the MS measurements (FGCZ, University of Zurich). We also thank Felix R. Althaus (Institute of Pharmacology and Toxicology, University of Zurich-Vetsuisse) for providing hPARG expressing baculo virus. Stephan Christen and Deena Leslie Petrioli provided editorial assistance and critical input during the writing (University of Zurich). The work carried out in the laboratory of MLN was in part supported by the Novo Nordisk Foundation Center for Protein Research; the Novo Nordisk Foundation (grant number NNF14CC0001 and NNF13OC0006477); the Lundbeck Foundation (Grant number R171-2014-1496); The Danish Council of Independent Research, grant agreement number DFF 4002-00051 (Sapere Aude) and grant agreement number DFF 4183-00322A. ADP-ribosylation research in the laboratory of MOH is funded by the Kanton of Zurich, the University Research Priority Program (URPP) in Translational Cancer Biology at the University of Zurich, and the Swiss National Science Foundation (grant 310030B_138667).

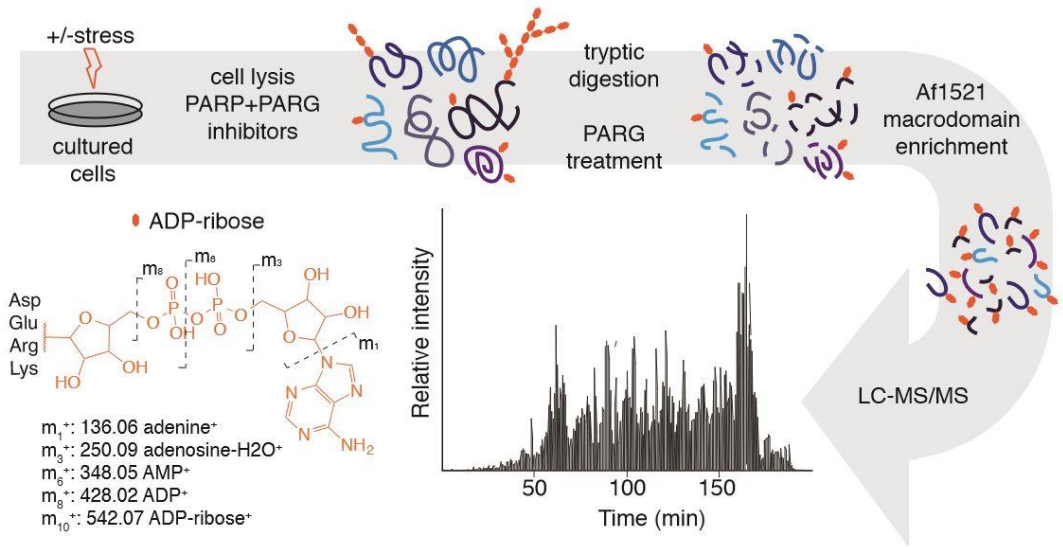

Figure 1. Graphical abstract

References

Cox J, Mann M (2008) MaxQuant enables high peptide identification rates, individualized p.p.b.-range mass accuracies and proteome-wide protein quantification. Nature biotechnology 26 (12):1367-1372

2. Haigis MC, Mostoslavsky R, Haigis KM, Fahie K, Christodoulou DC, Murphy AJ, Valenzuela DM, Yancopoulos GD, Karow M, Blander G, Wolberger C, Prolla TA, Weindruch R, Alt FW, Guarente L (2006) SIRT4 inhibits glutamate dehydrogenase and opposes the effects of calorie restriction in pancreatic beta cells. Cell 126 (5):941-954. doi:10.1016/j.cell.2006.06.057

3. Rack JG, Morra R, Barkauskaite E, Kraehenbuehl R, Ariza A, Qu Y, Ortmayer M, Leidecker O, Cameron DR, Matic I, Peleg AY, Leys D, Traven A, Ahel I (2015) Identification of a Class of Protein ADP-Ribosylating Sirtuins in Microbial Pathogens. Mol Cell 59 (2):309-320. doi:10.1016/j.molcel.2015.06.013

4. Altmeyer M, Messner S, Hassa PO, Fey M, Hottiger MO (2009) Molecular mechanism of poly(ADP-ribosyl)ation by PARP1 and identification of lysine residues as ADP-ribose acceptor sites. Nucleic Acids Res 37 (11):3723-3738. doi:10.1093/nar/gkp229

5. Vandekerckhove J, Schering B, Barmann M, Aktories K (1987) Clostridium perfringens iota toxin ADP-ribosylates skeletal muscle actin in Arg-177. FEBS Lett 225 (1-2):48-52

6. Zhang Y, Wang J, Ding M, Yu Y (2013) Site-specific characterization of the Asp- and Glu-ADP-ribosylated proteome. Nat Meth 10 (10):981-984. doi:10.1038/nmeth.2603

7. Vyas S, Matic I, Uchima L, Rood J, Zaja R, Hay RT, Ahel I, Chang P (2014) Family-wide analysis of poly(ADP-ribose) polymerase activity. Nature communications 5:4426. doi:10.1038/ncomms5426

8. McDonald LJ, Moss J (1994) Enzymatic and nonenzymatic ADP-ribosylation of cysteine. Molecular and cellular biochemistry 138 (1-2):221-226

9. Daniels CM, Ong SE, Leung AK (2014) Phosphoproteomic Approach to Characterize Protein Mono- and Poly(ADP-ribosyl)ation Sites from Cells. Journal of proteome research 13 (8):3510-3522. doi:10.1021/pr401032q

10. Min W, Cortes U, Herceg Z, Tong WM, Wang ZQ (2010) Deletion of the nuclear isoform of poly(ADP-ribose) glycohydrolase (PARG) reveals its function in DNA repair, genomic stability and tumorigenesis. Carcinogenesis 31 (12):2058-2065. doi:10.1093/carcin/bgq205

11. Hanai S, Kanai M, Ohashi S, Okamoto K, Yamada M, Takahashi H, Miwa M (2004) Loss of poly(ADP-ribose) glycohydrolase causes progressive

neurodegeneration in Drosophila melanogaster. Proc Natl Acad Sci U S A 101 (1):82-86. doi:10.1073/pnas.2237114100

12. Yu SW, Andrabi SA, Wang H, Kim NS, Poirier GG, Dawson TM, Dawson VL (2006) Apoptosis-inducing factor mediates poly(ADP-ribose) (PAR) polymer-induced cell death. Proceedings of the National Academy of Sciences of the United States of America 103 (48):18314-18319. doi:10.1073/pnas.0606528103

13. Cuzzocrea S, Mazzon E, Genovese T, Crisafulli C, Min WK, Di Paola R, Muia C, Li JH, Malleo G, Xu W, Massuda E, Esposito E, Zhang J, Wang ZQ (2007) Role of poly(ADP-ribose) glycohydrolase in the development of inflammatory bowel disease in mice. Free radical biology & medicine 42 (1):90-105. doi:10.1016/j.freeradbiomed.2006.09.025

14. Olsen JV, Mann M (2013) Status of large-scale analysis of post-translational modifications by mass spectrometry. Mol Cell Proteomics 12 (12):3444-3452. doi:10.1074/mcp.O113.034181

15. Gibson BA, Zhang Y, Jiang H, Hussey KM, Shrimp JH, Lin H, Schwede F, Yu Y, Kraus WL (2016) Chemical genetic discovery of PARP targets reveals a role for PARP-1 in transcription elongation. Science. doi:10.1126/science.aaf7865

16. Martello R, Leutert M, Jungmichel S, Bilan V, Larsen SC, Young C, Hottiger MO, Nielsen ML (2016) Proteome-wide identification of the endogenous ADP-ribosylome of mammalian cells and tissue. Nature communications. doi:10.1038/ncomms12917

17. Dani N, Stilla A, Marchegiani A, Tamburro A, Till S, Ladurner AG, Corda D, Di Girolamo M (2009) Combining affinity purification by ADP-ribose-binding macro domains with mass spectrometry to define the mammalian ADP-ribosyl proteome. Proc Natl Acad Sci U S A 106 (11):4243-4248. doi:0900066106 [pii]
10.1073/pnas.0900066106

18. Bonicalzi ME, Haince JF, Droit A, Poirier GG (2005) Regulation of poly(ADP-ribose) metabolism by poly(ADP-ribose) glycohydrolase: where and when? Cellular and molecular life sciences : CMLS 62 (7-8):739-750. doi:10.1007/s00018-004-4505-1

19. Jungmichel S, Rosenthal F, Altmeyer M, Lukas J, Hottiger MO, Nielsen ML (2013) Proteome-wide identification of poly(ADP-Ribosyl)ation targets in different genotoxic stress responses. Molecular cell 52 (2):272-285. doi:10.1016/j.molcel.2013.08.026

20. Karras GI, Kustatscher G, Buhecha HR, Allen MD, Pugieux C, Sait F, Bycroft M, Ladurner AG (2005) The macro domain is an ADP-ribose binding module. Embo J 24 (11):1911-1920. doi:DOI 10.1038/sj.emboj.7600664

21. Rappsilber J, Mann M, Ishihama Y (2007) Protocol for micro-purification, enrichment, pre-fractionation and storage of peptides for proteomics using StageTips. Nature protocols 2 (8):1896-1906. doi:10.1038/nprot.2007.261
22. Kelstrup CD, Young C, Lavallee R, Nielsen ML, Olsen JV (2012) Optimized fast and sensitive acquisition methods for shotgun proteomics on a quadrupole orbitrap mass spectrometer. J Proteome Res 11 (6):3487-3497. doi:10.1021/pr3000249
23. Poulsen JW, Madsen CT, Young C, Poulsen FM, Nielsen ML (2013) Using guanidine-hydrochloride for fast and efficient protein digestion and single-step affinity-purification mass spectrometry. J Proteome Res 12 (2):1020-1030. doi:10.1021/pr300883y

3.2. Unpublished results

3.3.1. Identification of ADP-ribosylation sites on in vitro ARTD1, ARTD2 and ARTD10 using m-aminophenylboronic enrichment

The exact mechanism how ARTD enzymes catalyse ADP-ribosylation at all four known acceptor sites (lysine, arginine, glutamic, and aspartic acid) is not studied. To gain insight into the enzyme specificity, we evaluated auto-modification sites present on ARTD1, ARTD2, and ARTD10. To increase the amount of modified peptides for downstream MS/MS analysis, we performed m-aminophenylboronic beads enrichment following the protocol published by Zhang et al. [117]. Indeed, we were able to localize E and D modification sites on all three enzymes. Only two ADP-ribose acceptor sites were assigned on ARTD10, which can be associated with the low activity of the recombinant full-length protein. The application of this procedure to *in vitro* modified ARTD2 led to the identification of previously unknown acceptor sites. Previously published ARTD1 acceptor sites [152] were confirmed by this method (Figure 8). In conclusion, all four enzymes were able to perform auto-modification reaction targeting E and D acceptor sites.

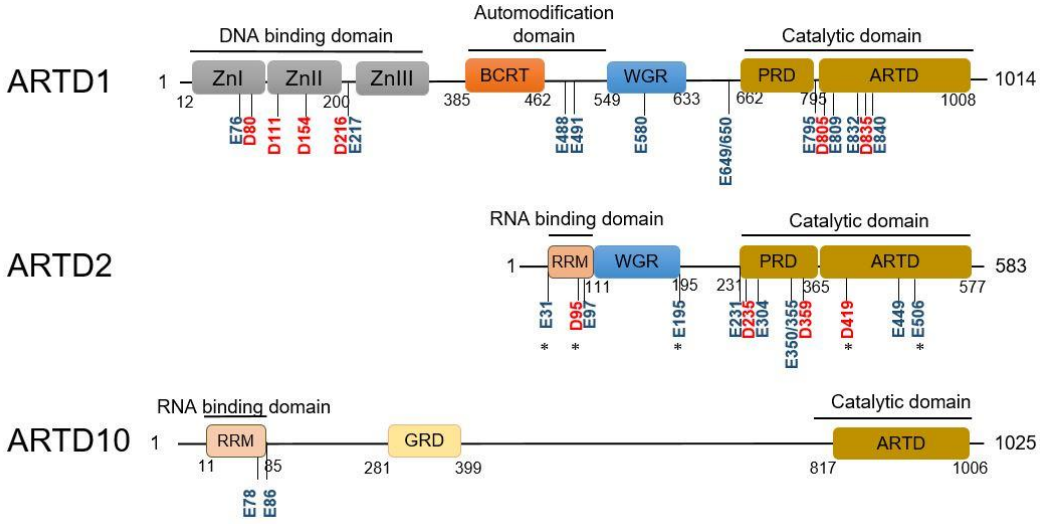

Figure 8. Identified acceptor sites of *in vitro* modified ARTD1 and ARTD2 using m-aminophenylboronic beads. The position and site of the identified ADP-ribosylation are marked with vertical labels. Red marks D sites, blue marks E sites. ZnI-III – Zn-finger domains, PRD – PARP regulatory domain, GRD - glycine-rich domain. * indicates new ADP-ribosylated acceptor sites.

3.3.2. Potential oxidative stress-induced ADP-ribosylome identified with the m-aminophenylboronic beads enrichment

Considering the successful application of m-aminophenylboronic beads to *in vitro* proteins, analysis of *in vivo* ADP-ribosylated samples was the next step to understand the function of ADP-ribosylation. Next, we evaluated the application of m-aminophenylboronic enrichment method to complex samples like cell lysates. First, the ability of m-aminophenylboronic beads to pull down *in vitro* modified ARTD1 spiked into HeLa lysate was tested. Indeed, ARTD1 was efficiently bound to the beads and enriched from this complex background. Unspecific binding of GAPDH was removed by four consequent washes (Figure 9A). Second, the efficiency of HA elution

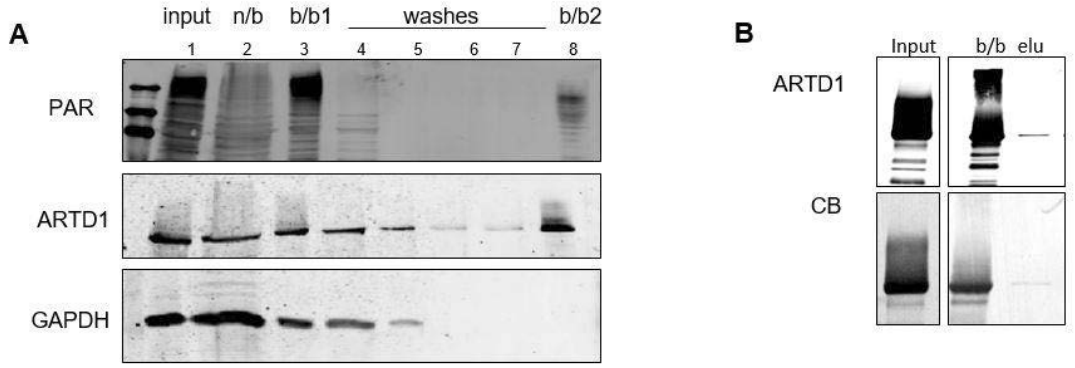

Figure 9. Binding of ADP-ribosylated ARTD1 to m-aminophenylboronic beads. A). Recovery of *in vitro* ADP-ribosylated ARTD1 from a complex background. *in vitro* ADP-ribosylated ARTD1 was spiked into 30 µg of HEK lysate. B). *in vitro* modified ARTD1 is eluted inefficiently from m-aminophenylboronic beads. Input represent 100% of used material. b/b – bound beads, where b/b1 – beads before washes and b/b2 – beads after washes. Elution (marked as elu) was performed with 0,5 M HA overnight.

was evaluated with *in vitro* modified PARylated ARTD1. The binding of ARTD1 to the beads was strong, and HA elution released barely detectable amounts of modified protein from the beads (Figure 9B). Although the elution efficiency was low for ARTD1 bound to m-aminophenylboronic beads and eluted with HA, it was enough for MS/MS analysis (as shown in Figure 8).

However, the efficient elution is critical for an analysis of a cell lysate as the HA elution of cell lysate pull-down was empty. To overcome the inefficient elution, we decided to perform on-beads digest of the bound proteins. To preserve the modification from degradation during the lysis procedure, MEFs PARG -/- cells were selected for the experiment. The cells were either treated with 1mM H_2O_2 or with PBS as a control. The lysates were then incubated with m-aminophenylboronic beads and bound proteins were digested with trypsin. Released proteins were analysed by

MS/MS to identify the proteins that bind to m-aminophenylboronic beads. Since the lysis was performed under denaturing conditions (1% SDS), all interactions between the proteins were disturbed. Thus, only potentially modified proteins are bound to the beads (Figure 10).

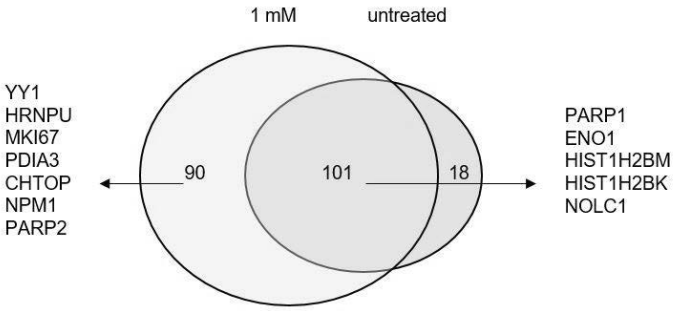

Figure 10. Identified proteins pulled down with m-aminophenylboronic beads. Venn diagram represents the overlay between 1mM and untreated samples (n=3). Some of the known ADP-ribosylation targets are indicated by an arrow in the unique 1mM and common protein groups.

The proteins identified in 1mM treated sample showed GO enrichment for DNA repair proteins and nuclear proteins. Moreover, the proteins were enriched for functional GO terms associated with DNA and RNA binding. Interestingly, ARTD2 was identified as one of the hits. The proteins shared between the samples were not enriched for nuclear proteins, although some of the nuclear proteins like Histones and ARTD1 were present in this category.

Moreover, some of the proteins in both groups e.g. Zink transporter ZIP6 and Sodium- and chloride-dependent taurine transporter localized to the membrane. Due to the chemical mechanism of m-aminophenylboronic enrichment, the beads enrich any ribose-containing substrate, e.g. membrane localized glycosylated proteins. Since the ADP-ribose acceptor site assignment was not possible with this method, validation of the potential candidates has to be carried out to confirm the presence of ADP-ribosylation and identify the sites.

3.3.3. Oxidative stress-induced ADP-ribosylome is significantly overlapping in HeLa and U2OS cells

After the development of Af1521 pull down, the identification of ADP-ribosylated proteins and site assignment became feasible in single MS/MS measurement [153]. Af1521 enrichment method was applied to HeLa and U2OS cells, commonly used in genotoxic stress response studies, to understand cell type variability of ADP-ribosylome in oxidative stress. For that, the cell lines were treated with 1mM of H_2O_2 for 10 min to trigger PARylation. Both cell lines showed overlap for the identified ADP-ribosylome (Figure 11A), indicating that the oxidative stress-induced ADP-

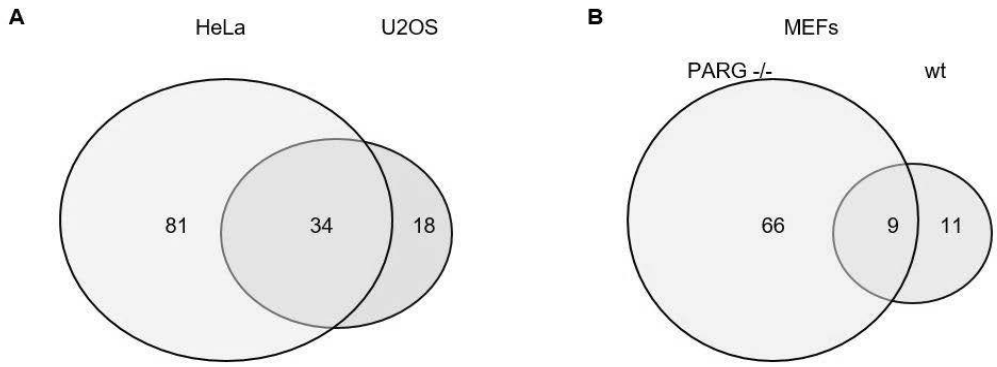

Figure 11. Oxidative stress induced ADP-ribosylome of different cell lines identified with Af1521 pull-down. The cells were treated with 1mM H_2O_2 A). Venn diagram showing the overlap between oxidative stress-induced ADP-ribosylome in HeLa and U2OS cells. B). Venn diagram showing the overlap in ADP-ribosylome of MEFs cells WT or PARG -/-. Upon knockout of PARG, the increased number of identification is observed. U2OS n=1, MEFs n=1, HeLa n=7

ribosylome is not cell type specific, but rather a constant set of oxidative stress-responsive proteins. However, we detected the fewer number of ADP-ribosylated proteins in U2OS cells. The low number of identifications points on faster catabolism of the modification or different dynamic of ADP-ribosylation in these cells.

Since m-aminophenylboronic beads enrichment was performed in MEFs and showed promising results, we applied the Af1521 method to the same cells (Figure 11B). PARG -/- showed the significantly larger number of identified proteins compared to wildtype cells. The increased number of ADP-ribosylated proteins in PARG -/- clearly points that PARG plays a key role in the dynamic of the modification in cells. Moreover, as was shown by Jungmichel *et al.* [121] PARG -/- leads to increased level of PARylation in cells. Whether the proteins gain the modification under physiological conditions remains to be confirmed.

3.3.4. Increased ADP-ribosylome size in ARTD2 -/- and ARTD3 -/- U2OS cells

To understand the target specificity of ARTDs in oxidative stress, we performed Af1521 pull-down on U2OS cells, which were CRISP-Cas9 recombined to remove ARTD1, ARTD2, and ARTD3 (kindly provided by K.W.Caldecott). First, to gain insight into qualitative changes of ADP-ribosylome, we analysed the enriched sample with shotgun MS/MS (Figure 12, Table 3).

Only three modified proteins were identified in ARTD1 -/- sample independent of the treatment. Among these proteins, we detected most abundant nuclear proteins: H2B histone and HNRNPU and ER-localized protein PDIA3. In other cell lines, we

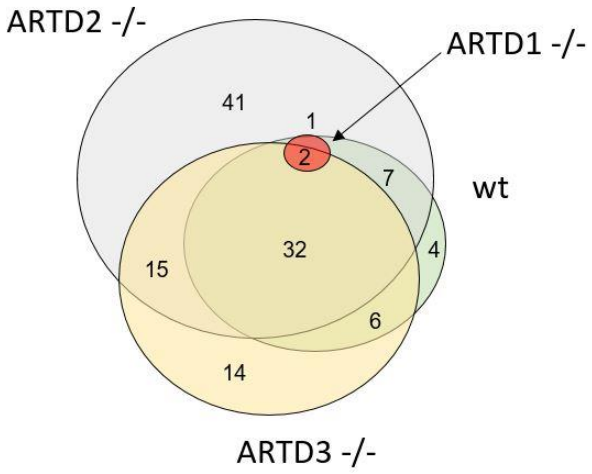

Figure 12. Oxidative stress induced ADP-ribosylome of U2OS ARTDs KO cells. Venn diagram shows the overlap in the identified modified proteins identified after 1mM H_2O_2 treatment in U2OS cells WT, ARTD1-/-, ARTD2-/- and ARTD3 -/-. Three proteins identified in ARTD1 -/- are indicated in Table 3.

observed oxidative stress-dependent induction of the ADP-ribosylation level. Surprisingly, ARTD2 -/- and ARTD3 -/- cells had a larger number of assigned modified proteins when compared to WT. This qualitative increase of ADP-ribosylome indicates the possible regulation of ARTD1 activity by either/both enzymes. Nevertheless, ARTD2 or ARTD3 auto-modification was not observed.

Protein name	Peptide sequence	Score	Expectation value
HNRNPU	EAAG(K)SSGPTSLFAVTVAPPGAR	46.85	4.60E-05
PDIA3	(R)LAPEYEAAATR	33	0.0082
HIST1H2BJ	P(E)PAKSAPAPK	27.51	0.033

Table 3. Proteins ADP-ribosylated in ARTD1 -/- U2OS cells. ADP-ribosylation site is indicated in brackets.

3.3.5. H2B ADP-ribosylation at the position 2 is neither a target of ARTD1, ARTD2 nor ARTD3 in vitro

Histone H2B ADP-ribosylation at position 2 (depending on the isoform either E or D site) is a highly abundant modification that is present also in basal conditions. Previous *in vitro* experiments showed that ARTD1 is not the writer of the site [154]. However, the study was performed with truncated short peptides fused to GST at N-terminal that potentially can interfere with the enzymatic reaction. To find the writer of the modification, we repeated the modification assay with all three DNA-dependent ARTDs i.e. ARTD1, ARTD2 and ARTD3 (Figure 13B) using H2B tail. ARTD1 and ARTD3 modified GST-H2B tail, while ARTD2 did not show any trans-modification. Further to elucidate the potential modification site we performed the reaction with GST-H2B mutants: E2 to A (m1), first 4Ks to 4A (m2), and 3Rs to A (m3) (Figure 13A). The other K sites present on H2B tail since they were not identified

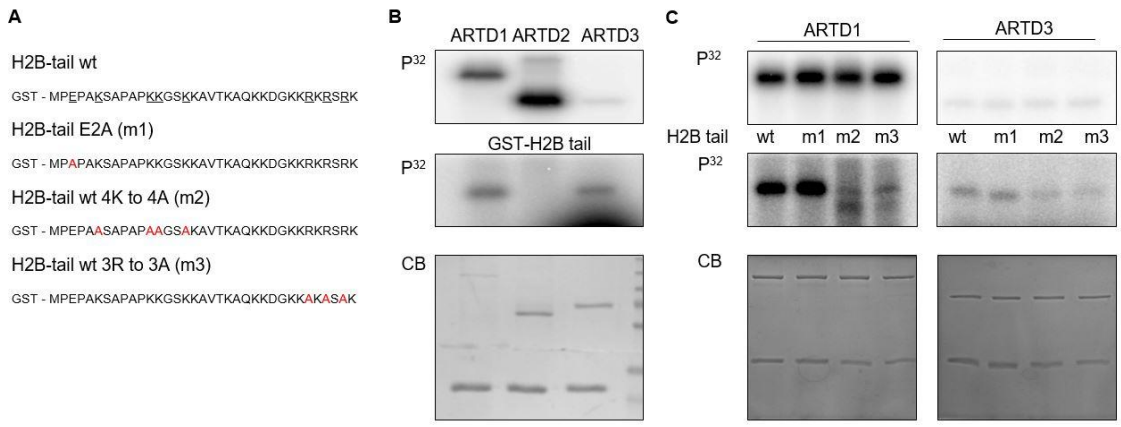

Figure 13. *in vitro* modification of H2B tail. A). Sequences of H2B tails used in the *in vitro* reactions. The mutated sites are underscored on WT sequence and shown in red on the mutant tails (named as m1-3) B).Trans-modification of H2B tail with ARTD1, ARTD2, and ARTD3. C). Trans-modification of H2B tail carrying mutations at potential modification sites with ARTD1 and ARTD3. Oxidative stress-induced H2B ADP-ribosylation at the position 2 is not a target of ARTD1 or ARTD3 *in vivo*

as acceptor sites of modification by a previous study [154]. Surprisingly for us, neither of the enzymes showed the specificity towards E2 site, since E2 to A mutant was still modified to the same extent as WT protein. The assay indicated that both enzymes potentially modify Ks and Rs present on the tail as for both K and R mutants the modification level dropped almost 100%. However, 3-4 point mutations introduced into the H2B tail changed the electrical charge of the protein that might interfere with the biochemical reaction. In this case, the tail was not recognized by ARTDs as potential substrate. Moreover, H2B tail used in this experiment has N-terminal GST tag that potentially can cover the modification site from the enzyme.

3.3.6. H2B ADP-ribosylation at the position 2 is neither a target of ARTD1 nor ARTD3 in vivo

To obtain information about quantitative changes in ADP-ribosylation upon ARTDs KO, we performed PRM measurement with ARTD1-/- and ARTD3-/- cells. WT cells were used as a control. In consistency with shotgun measurement (see section 3.3.4), only a few sites were modified in ARTD1 -/- cells. Moreover, no ADP-ribosylation induction was observed upon 1mM H_2O_2 treatment (Figure 14). This result indicates that ARTD1 mainly catalyse an oxidative stress-induced ADP-ribosylome. Interestingly, ADP-ribosylation of PDIA3 and P4HB (also known as PDIA1) was downregulated in ARTD3 -/- cells in untreated as well as in H_2O_2 treated sample. Considering the different localization of ARTD3 and downregulated proteins, the

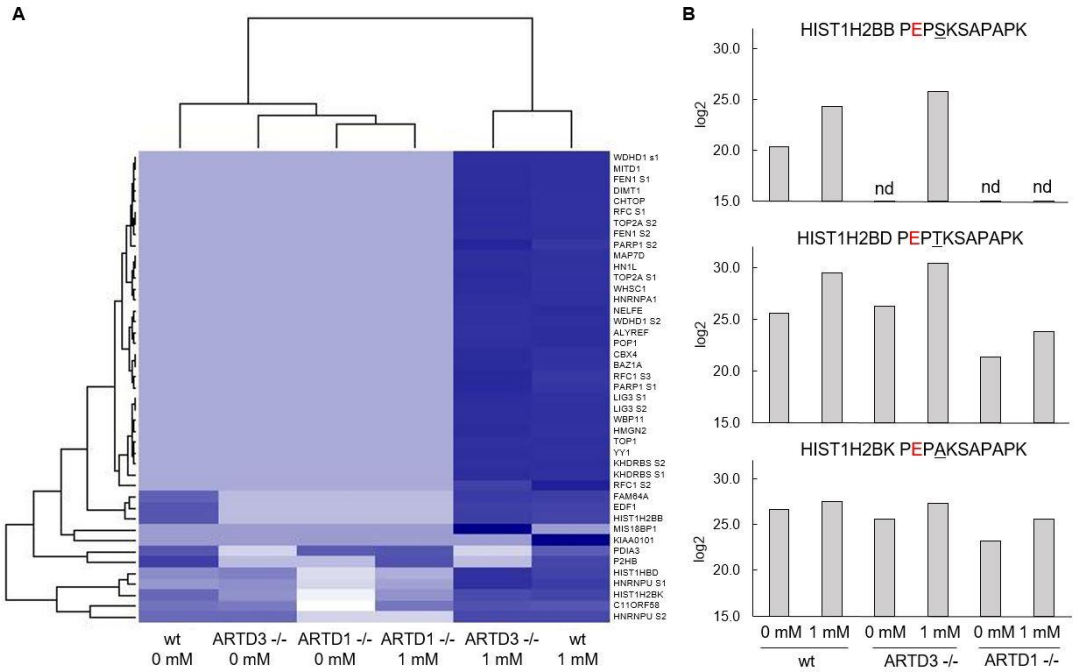

Figure 14. Quantification of ADP-ribosylation in U2OS ARTDs KO cells. A). Heatmap represents the quantitative differences between the samples. The total fragment intensity for each peptide was log2 transformed. The blue intensity correlates with the abundance of the ADP-ribosylated peptide. B). Quantitative differences in H2B E2 ADP-ribosylation is shown. The amino acid that is different for each isoform is underscored. ADP-ribosylation site is labelled in red.

signaling pathway connecting ER and nucleus is potentially involved in this downregulation.

One of the few proteins that was still modified in ARTD1 -/- cells was histone H2B. Three isoforms (with a difference at the position 4) of H2B histone were detected in the samples. Although the measurement was performed only once, several preliminary conclusions can be made. First, ADP-ribosylation levels changed differently in different histone isoforms. For example, H2B isoform K did not show induction upon H_2O_2 treatment in WT cells (induction 1.8 fold), whereas other isoforms were upregulated around 15 fold. Second, ARTD3 does not contribute to the modification level of H2B tail at the monitored site for D and K isoforms. However, ARTD3 potentially can modify B isoform since the basal modification level was downregulated in ARTD3 -/- cells. Third, ARTD1 is not the only enzyme that writes the modification. The level of H2B E2 modification was decreased in ARTD1 -/- cells but was clearly detectable (except isoform B). ARTD1 -/- H2B modification level increased upon oxidative stress indicating that other ARTD carried out the reaction in these cells.

3.3.7. Methods for unpublished results

m-aminophenylboronic beads enrichment. The protocol was adapted from [117]. For *in vitro* reaction, elution was performed with 0.5 M NH_2OH overnight at room temperature on an end-to-end rotator. Cell lysate enrichment performed on protein level with m-aminophenylboronic acid–agarose (Sigma). Loaded with protein beads were washed with 50 mM ammonium bicarbonate pH8. The beads were then incubated with 5 mM dithiothreitol for 1h at 37^{o}C, followed by 5 mM chloroacetamide for 1h in the dark. The trypsin digest was performed overnight at 37^{o}C with gentle shaking. 0.15% trifluoroacetic acid was added to the reaction to stop the digest, and the supernatant containing peptides was collected. GO analysis was performed with Panther database (http://pantherdb.org).

***In vitro* modification assay with ARTDs.** The reactions were performed as described in method paper with following modifications. 5 pmol DNA template was added to the reaction to activate the enzymes. 40 mer was used to activate ARTD1 and 40 mer with a nick (5' phosphate) for ARTD3. For trans-modification reaction, 50 pmol target protein was added into the reaction. The reaction was carried out at 30^{o}C for 15 min. For pull-down experiments, a total of 50 µg of modified enzyme was used. To generate this amount of modified protein, several reactions were performed in parallel and pulled together before the enrichment step.

Enrichment of ADP-ribosylated peptides with Af1521. The enrichment is performed as described [153].

MS/MS analysis of U2OS ARTDs -/- cells. The ADP-ribosylated peptides were analysed on Orbitrap FUSION Tribrid with HCD(FT)-PP-HCD/EThcD method [155]. PRM method was adapted from [156] and new targets were included based on shotgun measurements. The data analysis was performed using Skyline-daily (v3.5.1.999). mProphet second best peak model was trained on WT sample and used to perform automatic peak peaking. FDR was set to 0.05. Unsupervised clustering heatmap was generated with R using "R for Proteomics" package.

4. DISCUSSION AND PROSPECTIVE

4.1. Summary of the results

Despite over 50 years of ADP-ribosylation research, in-depth knowledge about the cellular function of this modification is still missing. The difficulties are mainly associated with the lack of appropriate tools used to study this complex protein modification. Thus, this thesis was aimed at defining the oxidative stress-induced ADP-ribosylome in various normal and cancer cell lines and to analyze its changes at the quantitative and qualitative levels using mass spectrometry-based assays.

The first objective was to identify the ADP-ribosylome specifically during oxidative stress. To enrich low abundant protein ADP-ribosylation from cell lysates, we established an enrichment method using the Af1521 macrodomain, which binds MAR and PAR with strong affinity. The developed enrichment step in combination with MS/MS analysis enabled the identification of ADP-ribosylated proteins and their acceptor sites both in stressed cells and in mouse organs [153]. To further improve the identification of ADP-ribosylated proteins and the assignment of the modified site (i.e. ADP-ribose acceptor site), we have developed an optimized shotgun HCD(FT)-PP-HCD/EThcD method employing special features of ADP-ribose fragmentation. This method allows an in-depth characterization of the cellular ADP-ribosylome with high confidence of the acceptor site assignment. The obtained high-quality dataset enabled us to identify a K modification site motif [155].

The second aim of the project was to understand the qualitative and quantitative changes of protein ADP-ribosylation under various degrees of oxidative stress. Using a shotgun quantification approach, we observed that for high levels of oxidative stress (64 µM-1 mM of H_2O_2), the ADP-ribosylome remains qualitatively and quantitatively stable. To detect changes under low oxidative stress (0-16 µM of H_2O_2), we improved the reproducibility of the quantification measurements by developing a parallel reaction monitoring (PRM) method targeting defined ADP-ribosylated peptides. Application of the PRM method enabled us to monitor changes in ADP-ribosylation. While the ADP-ribosylation levels increased for many tested proteins, surprisingly we also detected a decrease of ADP-ribosylation for some targeted proteins at a low degree of oxidative stress in HeLa cells [156]. Finally, we applied the developed PRM method to a set of ovarian cancer cell lines challenged with oxidative stress. The

obtained results indicate a lower abundance of ARTD1 and a tighter regulation of its activity in PARPi resistant cell line.

4.2. Unbiased enrichment method for ADP-ribosylation

A significant improvement of ADP-ribosylation enrichment methods has been achieved during the last five years. Several approaches were developed, and their combination with shotgun MS analysis identified the ADP-ribosylome under basal (i.e. untreated) and stress conditions [117, 121, 124]. We identified the ADP-ribosylome of HeLa cells upon oxidative stress [153]. The overlap of identified ADP-ribosylated proteins between the different studies is rather modest (not more than 40%) [153, 157]. However, since the studies were performed using different enrichment methods and cell types, a careful interpretation of the published results is necessary to define a common cellular ADP-ribosylome. Gibson *et al*. identified ADP-ribosylated targets using a chemical genetic discovery approach with NAD^+ analogues and analogue-sensitive ARTD enzymes [124]. The overlap of ADP-ribosylated proteins identified in this study was 30% with our Af1521 enrichment results [153]. Considering the generally modest reproducibility of shotgun measurements [158], such an overlap can be considered as good. Moreover, Gibson *et al.* identified targets of ARTD1, 2 and 3, whereas the ADP-ribosylome upon oxidative stress identified by our Af1521 pull-down is mainly ARTD1 dependent (Figure 12). The enzymes analyzed in the Gibson *et al*. study were activated by sperm DNA, a strong inducer of DNA-dependent ARTD activity. Moreover, since the experiments were performed after cell lysis, the cellular localization of the proteins was disturbed. Two questions arise: (1) whether these proteins are indeed ADP-ribosylated under physiological conditions and (2) which stimulus triggers their modification. The results reported by Zhang *et al*., where oxidative stress was used as an inducer for ADP-ribosylation *in vivo*, are more comparable to our dataset. [117]. The overlap between the reported ADP-ribosylomes is 40%. However, several factors should be considered. First, the $PARG^{-/-}$ background used by Zhang *et al*. potentially causes perturbations in the regulation of ADP-ribosylation. Increased PAR formation in $PARG^{-/-}$ cells was detected by western blot [121] and by immunofluorescence [159] in oxidative stress-induced as well as under basal (untreated) conditions. Second, the acceptor site bias introduced by HA elution from m-aminophenylboronic beads (allowing identification of E and D sites only) is a limiting factor for the identification of a comprehensive ADP-ribosylome.

To date, Af1521 is the most unbiased approach to characterize ADP-ribosylation under physiological conditions since it enables the identification of all four acceptor sites without the need to knockout PARG. Nevertheless, we cannot exclude the possibility of specific substrate recognition by the Af1521 domain. Since the domain has particular functions in cells, the domain might bind a preferential protein sequence and/or preferential acceptor sites. E.g. in oxidative stress-induced HeLa cells, K was identified as the dominant ADP-ribose acceptor [153]. This preference can be explained either by the specificity of ARTD1 to modify Ks upon oxidative stress or by the specificity of Af1521 to bind K-linked ADP-ribosylation. The fact that Rs in mouse organs were identified as major ADP-ribose acceptor sites [160] rather points to the first explanation. Nevertheless, the linkage specificity of Af1521 can still not be completely ruled out (i.e. specificity towards basic acceptor sites). Indeed, studies to biochemically characterize the properties of ADP-ribose binding domains are usually performed with free ADP-ribose or its derivatives [44]. Thus, it is not clear if the studied domains have substrate specificity, and if so, which factors would define it. Along this line, MacroD1 and TARG showed different affinities for ADP-ribosylated peptides *in vitro* [161]. If this specificity would also be confirmed *in vivo*, the quality of domains could be used to better characterize cellular ADP-ribosylation in various conditions by performing a combination of pull downs with different macrodomains. E.g., domains with a potential specificity for R sites would allow identifying ADP-ribosylated proteins with these acceptor sites. Moreover, knowledge about the macrodomains in combination with bioinformatics analysis (GO analysis, motif search) and cell culture techniques (e.g. siRNA screening), might help to define the writer and potentially the eraser of certain modification sites as well as novel functions of ADP-ribosylation.

4.3. Protein ADP-ribosylation as a marker of stressed cells

Oxidative stress is a pathological cellular condition involved in the development of many diseases such as age-related metabolic diseases, acute neurological disorders, as well as chronic neurodegenerative diseases and cancer [162, 163]. Here, we show that oxidative stress-induced ADP-ribosylation is mainly mediated by ARTD1. Indeed, the involvement of ARTD1 activity has been reported for many of these oxidative stress-induced diseases [163, 164]. Moreover, most proposed theories of PARPi action are based on the inhibition of the enzymatic activity of ARTD1 [165], although many

PARPi are not specific [88]. Thus, the activity of ARTD1 could potentially be used to predict the efficacy of PARPi treatment and/or to define the stage of a certain disease. Therefore, a more detailed understanding of protein ADP-ribosylation dynamics in response to oxidative stress may be a useful tool to detect pathological conditions.

The National Institute of Health (USA) defines a biomarker as "a characteristic that is objectively measured and evaluated as an indicator of normal biological processes, pathogenic processes, or pharmacologic responses to a therapeutic intervention" [166]. Due to their core function in cellular events and their relatively easy accessibility through body fluids, proteins are the best candidates for use as biomarkers compared to other cellular components. MS-based proteomics is a powerful tool that boosted the search and validation of biomarkers for cancers and other pathological conditions. At an early stage, shotgun discovery methods are used to identify potential biomarkers, which are further validated by targeted MS proteomic analysis [167]. The profiling of cancer cells using SRM allowed measurements of over 1000 cancer-associated proteins [168]. Thus, the ADP-ribosylation field has all the necessary tools to test and validate ADP-ribosylated proteins for their predictive properties. Here, we showed that cancer cells have a variability regarding ARTD1 abundance. Additionally, the basal and H_2O_2-induced ADP-ribosylomes also vary [156]. However, this is just a first step to understand if these differences could be used as predictive biomarkers.

In our studies, we concentrated our efforts on the oxidative stress-induced ADP-ribosylome. Interestingly, ovarian cancer cells had different basal and H_2O_2-induced ADP-ribosylomes. This observation raises the question if there are other pathways able to induce ADP-ribosylation in cancer cells. These pathways might drive PARPi sensitivity. Indeed, PARPi might function via disturbance of cellular energy metabolism [107]. Thus, to understand PARPi sensitivity, quantitative ADP-ribosylation studies should be performed under different stimuli.

It would be interesting to test if oxidative stress-induced ADP-ribosylated targets are also detected in blood samples. Blood is a convenient patient sample since its collection is a standard routine procedure in clinics. Although MS measurements of blood plasma are well established, they remain a challenging task. Half the blood protein content consists of albumin, the most abundant protein in plasma [169]. However, the level of albumin is constant and has not been reported to change under any conditions, [170]. Thus, established MS protocols suggest depleting albumin to

uncover interesting candidates that otherwise would be shielded by highly abundant proteins. Optimization of enrichment protocols will be necessary to evaluate the amount of required material and adaptation for blood samples. Since ARTC enzymes are localized on cellular membranes, their interference with detection of ARTD ADP-ribosylated targets should be considered.

4.4. Perspective of MS-based quantification of ADP-ribosylation

Quantitative MS measurements are a valuable tool to study the dynamics and functions of PTMs in cells. Here, we developed a PRM method to study ADP-ribosylation in stressed cells [156]. PRM measurements are ideal comparing different experimental conditions in a reproducible manner. They help to quantify the modification level of cells as well as studying the function of ADP-ribosylation writers and erasers in detail. Upon knockout of a respective ARTD enzyme, changes at the level of specific ADP-ribosylation sites can be monitored using a PRM method. Here, we applied the PRM method to study ARTD specificity by monitoring the E2 ADP-ribosylation site identified on various H2B isoforms under basal and oxidative stress-induced conditions. Our *in vitro* modification assays revealed that ARTD1 and ARTD3 can modify the H2B tail (Figure 13B). Performing PRM measurements of U2OS cells indicate that mainly ARTD1, not ARTD3, is the writer of the H2B E2 modification site (Figure 13). One possible explanation for this contradiction is that ARTD3 is modifying the H2B tail at a different position. Indeed, *in vitro* modification assays using an H2B mutant (E2A) revealed that ARTD3 does not target the E2 site, but rather a different site (Figure 13C).

PRM measurements can be used to analyze quantitative differences of specific acceptor sites present on the same peptide. In several cases, ADP-ribosylated peptides were eluting from the LC either in double-fused peaks or in two separate peaks. Usually, these peaks shared several common fragment ions [156]. Their shift of retention time indicates that they have various physical qualities, which potentially could be generated from differentially modified acceptor sites on the same peptide. Unfortunately, in many cases, the precise localization of the modification is difficult to define. By extracting characteristic fragment ions (i.e. just before and after the acceptor site), it would be possible to localize the modification. Furthermore, by knowing the quantitative differences of various acceptor sites, it would be possible to better understand the function of these specific sites. ARTD1 is known for its

extensive auto-ADP-ribosylation, especially when the protein is analyzed *in vitro*. However, it is not clear whether all identified sites play a functional role. By targeting all ARTD1 sites with PRM, it would be possible to correlate acceptor sites with specific stimuli, which trigger their modification.

One of the main problems of the ADP-ribosylation PRM measurements was the absence of suitable standards. At the moment, only one standard peptide is available [171]. Although it is a valuable tool to monitor the variability between analyzed samples after enrichment, it does not allow to perform proper normalization. Only fold changes greater than 2 can be reliably measured, leading to high variability. This is not a problem for the H_2O_2-induced ADP-ribosylome since the observed induced ADP-ribosylation levels are high (reaching up to 40-fold induction over basal levels) [156]. However, for other conditions, the changes might potentially be smaller. Thus, it would be critical to introduce additional standards. Nowadays, the chemical synthesis of ADP-ribosylated peptides is difficult. The way to bypass this might be to use protein glycation [19], which allows obtaining peptides with modified Ks. Moreover, many peptides contain more than one possible acceptor site. The PRM method targets and measures specific m/z of the precursor and the position of ADP-ribosylation is irrelevant for the method development. It would thus be possible to create peptides analogous to cellular peptides with E, D, and R sites if they have K in their sequence (which would be glycated). Unfortunately, for peptides with multiple K sites, this strategy does not work. The potential disadvantage of targeted proteomics methods lies in their data dependency. It is critical to know the fragmentation of a targeted peptide in advance. The information about fragmentation and LC behavior of the peptide is used to validate the identity of the target to avoid false identifications [149]. Recently, a new MS/MS approach that bypasses the aforementioned problems has been developed. The basic principle of this approach is the fragmentation of all peptide precursors within a pre-defined m/z mass range [138]. Since in this case, the instrument does not depend on the input data, i.e. the selection of most intense peaks in MS spectra, this approach was termed data-independent acquisition (DIA) [167]. DIA data analysis is complicated because the MS/MS spectra contain information not from one (like in shotgun) but from multiple precursors. Several strategies were developed to optimize the DIA data analysis [172, 173]. Since DIA spectra contain information about all peptides present in the sample, the data can potentially be re-analyzed to obtain new information. The retrospective aspect of this kind of analysis is

an important factor, especially in research fields with a limited amount of available information, e.g. ADP-ribosylation. With new targets identified every year, the possibility to re-analyze the data to obtain new insights into the molecular pathways of different conditions is extremely powerful. Thus, it would be important to test the applicability of DIA to a detection of ADP-ribosylated peptides.

4.5. Oxidative stress-induced ADP-ribosylome

Induction of PARylation during oxidative stress is well known [174]. Using the macrodomain Af1521 for the enrichment of ADP-ribosylated peptides, we were able to identify modified proteins and their acceptor sites in various cell lines. Independent of the cell line tested, a similar oxidative stress-induced ADP-ribosylome was present. The identified H_2O_2–induced ADP-ribosylome was mainly dependent on ARTD1. GO analysis revealed that identified ADP-ribosylated proteins are mainly nuclear proteins with DNA and RNA binding capacity. Moreover, the ADP-ribosylome is enriched for proteins that function as a part of macromolecular complex, which correlates with the ability of PAR to serve as a scaffold to induce complex formations.

The so far identified ADP-ribosylated proteins are among the most abundant proteins in the nucleus (e.g. ARTD1, HNRNPU, and NPC1). From this observation, the concern arises about the target specificity of ARTD1. If the only function of protein ADP-ribosylation was to negatively charge DNA-associated proteins, causing, for instance, chromatin relaxation, then ARTD1 could randomly modify any proteins in its proximity. However, our published ADPr-ChAP analysis identified the accumulation of ADP-ribosylation in heterochromatic regions upon oxidative stress [79]. The fact that all tested cells had a core ADP-ribosylome also indicates that ARTD1 specifically modifies proteins to regulate certain pathways upon H_2O_2 treatment. Moreover, the bias toward abundant proteins could be explained by the shortcomings of the shotgun MS/MS method. Due to the data-dependency of acquisition and the use of dynamic exclusion in the shotgun methods, low abundant proteins are rarely selected for fragmentation and thus are rarely identified in the samples. Nevertheless, to elucidate this “specificity“ aspect of oxidative stress-induced ADP-ribosylation, the functional consequence of ADP-ribosylation should be studied for every modified protein.

Although the number of identified ADP-ribosylated proteins in oxidative stress increases every year, it is still too early to conclude that the complete ADP-ribosylome

has been identified. First of all, the known biases of developed enrichment methods obstruct the complete ADP-ribosylome identification. Moreover, some known or expected ADP-ribosylation targets were not yet identified in cellular lysates. Despite the well-accepted theory that ARTD2 can functionally compensate for a lack of ARTD1 [71], only auto-modified ARTD1, but not ARTD2, was identified in the Af1521 pull-down. Interestingly, ARTD2 was detected when using the m-aminophenylboronic bead enrichment method and lysates from MEFs (Figure 10). Moreover, when the protein was modified *in vitro,* we detected several ARTD2 ADP-ribosylated auto-modification sites using m-aminophenylboronic bead. In contrast, similar experiments with Af1521 led to no assignment of ARTD2 modifications (data not shown). This discrepancy between enrichment methods indicates that the applied method protocol is biased towards some ADP-ribosylated targets. The PARG treatment could potentially be responsible for this loss of ARTD2 modification sites with Af1521. Although PARG is published to be unable to cleave the protein-bound ADP-ribose unit [175], our *in vitro* experiments indicate that this is not the case for all ADP-ribosylated proteins and that ARTD2 is completely demodified by PARG (personal observations by Jeannette Abplanalp). Treatment of the proteome with PARG is an important step to enable the detection of ADP-ribosylated peptides with MS/MS, since PARylated peptides have poor ionization capacity [125]. Thus, to avoid this bias but to still reduce complexity of the modification, an alternative to PARG treatment could be introduced. Ideally, this should be based on a chemical attack similar to the HA elution used in the m-aminophenylboronic beads enrichment [117] without a preference for certain acceptor sites. To our knowledge, such a treatment has yet to be developed.

An additional possible optimization of the protocol, which might increase the number of identified ADP-ribosylated proteins upon oxidative stress and other conditions, would be to increase the binding affinity of the domain used for the enrichment. Af1521 possesses the highest known affinity ($K_d \approx 130$ nM) among all known macrodomains [44]. However, this is not comparable to e.g. affinity of a specific antibody to its target. To identify ADP-ribosylated proteins, we currently process 15-20 mg of cell lysate [153]. The current enrichment method is unable to amplify enough modified peptides from less starting material. Although more sensitive methods such as PRM still perform well using only 5 mg of lysate [156], discovery proteomics methods need higher inputs to allow high confidence identifications [153,

160]. One of the possibilities to increase the affinity of the Af1521 domain used for enrichment is to perform a ribosomal display screen to detect mutants of the respective domain with increased binding affinity [176].

4.6. Identification of an ADP-ribosylation motif

Defining an ADP-ribosylation motif would be a step toward understanding the role of the modification in cells and linking it to specific writers. Such a motif would enable the search of ADP-ribosylated proteins using bioinformatics tools applied to protein databases. The identification and validation of novel ADP-ribosylation targets might help to predict the functional involvement of ADP-ribosylation in a specific pathway. However, the identification of a motif for ADP-ribosylation appeared to be a challenging task. Despite the identification of over 2000 mapped ADP-ribosylation sites to date [177], only a few motives have been proposed so far. Several aspects contribute to the failure of finding a motif.

First of all, the presence of four possible acceptor sites and thus potentially different motifs contributes to the complexity of the motif search problem. In total, 18 motifs were reported for E acceptor sites so far [117, 124]. Interestingly, the xxxxxxEPxxxxx motif was identified by two studies utilizing the m-aminophenylboronic beads enrichment [117, 124]. Gibson *et al*. also suggest several enzyme specific motifs [124]. However, the majority of the proposed motifs have several possible acceptor sites present in their sequence near the assigned main site (e.g. ExxxKxxK, one of the ARTD3 motifs reported by Gibson *et al.*, where E assigned to be the acceptor site). Indeed, we also frequently observed peptides with multiple possible ADP-ribosylation sites, which makes it difficult to precisely localize the site. Thus, careful assignment of the ADP-ribose acceptor site with a high confidence is critical in such cases. In general, the precise site assignment is difficult for bulky modifications like ADP-ribosylation due to the complete fragmentation of ADP-ribose and the usually poor peptide fragmentation upon HCD [125]. Nevertheless, advances in MS instrumentations drastically improved our ability to unambiguously assign ADP-ribose acceptor sites [155]. We recently reported three potential motives for K-acceptor sites (xxxxxxKSxxxxx, xxxxKSxxxxK, xxxxSKxxxxx). The motifs for R and D sites are still elusive due to the low number of identified proteins with these ADP-ribose acceptor sites.

A second aspect making identification of motif difficult relates to a potential redundancy in ARTD activities. Oxidative stress induces the activity of ARTD1, 2, and 3 [61]. Proteomics studies reveal that the targets of these ARTDs overlap [124]. Although they modify the same protein, it is not clear if they modify the same acceptor sites. Moreover, several cytoplasmic proteins were identified in our oxidative stress-induced ADP-ribosylome. These observations indicate that ARTDs from the cytoplasm modify targets identified in our dataset. These ARTDs might have their own recognition motif. The contribution of different ARTDs to the oxidative stress-induced ADP-ribosylome might obstruct the identification of ARTD1, ARTD2, and ARTD3 specific motifs. A possible method to prevent this kind of "contamination" would be to inhibit the activity of cytoplasmic ARTDs. However, there is still a lack of specific ARTD inhibitors. Furthermore, the question of substrate specificity is difficult to address based on the available enrichment methods since we are currently unable to distinguish between MARylation or PARylation.

The presence of several possible ADP-ribosylation sites close to each other identified in the same protein raises the question whether an ADP-ribosylation motif exists at all. In many cases, we observed that the validation of identified ADP-ribose acceptor site is difficult with standard *in vitro* methods (unpublished observations). The mutation of potential ADP-ribose acceptor sites in many cases only leads to a reduction but not a complete loss of ADP-ribosylation [21, 153]. This observation might indicate that ARTDs could "jump" to the next available acceptor site as described for ubiquitination [178]. ARTDs possibly might not recognize a specific sequence but rather a structural domain of a protein that is modified under certain conditions. To address this question, a systematic study aiming at understanding the substrate specificity of ARTDs is essential. Peptide screening methods utilizing peptide libraries might be applied for this purpose [179].

4.7. Crosstalk and interplay of ADP-ribosylation and other protein posttranslational modifications

K sites can not only be ADP-ribosylated, but can also be modified by methylation, acetylation, ubiquitination, SUMOylation and many other PTMs [180]. The identified K motif revealed the presence of an S adjacent (C-terminal or N-terminal) to the ADP-ribose acceptor site [155]. This potentially points at a crosstalk with serin phosphorylation. Indeed, ARTD1 activity is regulated by phosphorylation [78, 181].

However, the interplay between phosphorylation and ADP-ribosylation has not been studied so far. We observed a decrease in the level of ADP-ribosylation under low oxidative stress conditions (4-16 µM of H_2O_2) compared to untreated cells. One of the possible explanations might be that the targeted peptides are modified by another PTM, possibly phosphorylation. This would not allow us to detect the peptide with a targeted MS/MS approach due to a change in the m/z ratio. Potentially, low doses of H_2O_2 induce other signaling pathways and enzyme cascades to cope with the induced stress. This problem could be addressed on several levels. Firstly, transcriptome profiles of cells under low doses of H_2O_2 might reveal an upregulation of certain pathways, which could be regulated by known PTMs. Secondly, the peptides could be analysed for the presence of modification motifs (e.g. phosphorylation motif) in their sequence. Lastly, a DIA experiment with a subsequent data mining approach based on an educational guess could be performed inder the same oxidative stress conditions. A specific method containing the combination of the best-fitted PTMs for the ADP-ribosylated peptides (containing e.g. acetylation, methylation, and phosphorylation) should be generated. The analysis of this data might lead to the discovery of additional interfering modifications.

The crosstalk between acetylation is another possible yet unstudied field. We demonstrated that FEN1 K354 is an acceptor site for ADP-ribosylation in oxidative stress [153]. The same site is an acceptor of acetylation by p300 and thus inhibits FEN1 DNA binding and nuclease activity [182]. The potential regulation of FEN1 activity by ADP-ribosylation is an interesting question for further studies.

The interplay of ADP-ribosylation with ubiquitination was already demonstrated for RNF146, which can recognize ADP-ribosylated proteins and is also activated by ADP-ribosylation [183, 184]. Another example is ARTD9, which is predicted to be inactive, and interacts with the ubiquitin ligase DTX3L [185]. Recently, ARTD9 was identified as a binder of H2B E2 ADP-ribosylation (unpublished results, Roxane Feurer), which might indicate its functional involvement in epigenetic regulation. Recently, an interesting mechanism was suggested for bacterial ARTCs, which facilitates the ubiquitination reaction by bypassing E1 and E2 enzymes [186]. Working in a complex with an E3 ligase, ARTC was able to catalyze the addition of ubiquitin onto proteins. If the same mechanism occurred in eukaryotic cells, ARTD9 might be an ideal candidate fulfilling this function.

4.8. Investigating MARylated proteins

The majority of published studies identifying modified proteins use conditions under which PARylation is catalyzed by enzymes like ARTD1 and 2, e.g. oxidative stress. Taking into account that the number of MARylating ARTDs is higher than the PARylating ones, the ability to define the status of mono-ADP-ribosylation is a critical step to fully understand the function of the modification. Both published data and our data indicate several potential MARylated proteins, e.g. ER proteins (i.e. PDIA1 and PDIA3), which are modified under basal (untreated) conditions as well as after oxidative stress [156]. Their distinct localization indicates that they are not targets of nuclear ARTDs. However, due to the affinity of Af1521 toward both PARylated and MARylated proteins as well as considering the PARG digestion step in our workflow [153], it is impossible to distinguish between different modification statuses. Thus, several optimizations in the workflow could be considered to enable the discrimination between PAR and MAR. First, the binding properties of different existing ADP-ribose binding domains could be analyzed. Some of the ADP-ribose binding domains are able to discriminate between MARylated and PARylated proteins. E.g., the WWE domain only binds PARylated proteins [2]. Indeed, the WWE was successfully applied in an ADP-ribosylation-ChAP protocol [79]. Its applicability for the enrichment in an MS proteomics approach remains to be evaluated. Other macrodomains have been reported to specificaly bind MARylated proteins [187]. Moreover, MacroD1 and MacroD2 mutated to their enzymatic inactive state could be promising candidates as they show binding affinity toward MARylated E and D only [47]. Moreover, several MARylated ARTDs have macrodomains in their structure. The ARTD8 macrodomain e.g. is capable of binding MARylated ARTD10 [14]. The use of these domains for proteomics studies could thus fill a gap and allow discriminating between protein MARylation and PARylation.

REFERENCES

1. Hengel, S.M., et al., *Tandem mass spectrometry investigation of ADP-ribosylated kemptide.* J Am Soc Mass Spectrom, 2009. **20**(3): p. 477-83.
2. Teloni, F. and M. Altmeyer, *Readers of poly(ADP-ribose): designed to be fit for purpose.* Nucleic Acids Res, 2016. **44**(3): p. 993-1006.
3. Ong, S.E. and M. Mann, *Mass spectrometry-based proteomics turns quantitative.* Nat Chem Biol, 2005. **1**(5): p. 252-62.
4. Hottiger, M.O., *SnapShot: ADP-Ribosylation Signaling.* Mol Cell, 2015. **58**(6): p. 1134-1134 e1.
5. Consortium, I.H.G.S., *Finishing the euchtomatic sequence of the human genome.* Nature, 2004. **431**: p. 931-945.
6. Kim, M.S., et al., *A draft map of the human proteome.* Nature, 2014. **509**(7502): p. 575-81.
7. Wilhelm, M., et al., *Mass-spectrometry-based draft of the human proteome.* Nature, 2014. **509**(7502): p. 582-7.
8. Smith, L.M., N.L. Kelleher, and P. Consortium for Top Down, *Proteoform: a single term describing protein complexity.* Nat Methods, 2013. **10**(3): p. 186-7.
9. Roth, M.J., et al., *Precise and parallel characterization of coding polymorphisms, alternative splicing, and modifications in human proteins by mass spectrometry.* Mol Cell Proteomics, 2005. **4**(7): p. 1002-8.
10. Walsh, C.T., S. Garneau-Tsodikova, and G.J. Gatto, Jr., *Protein posttranslational modifications: the chemistry of proteome diversifications.* Angew Chem Int Ed Engl, 2005. **44**(45): p. 7342-72.
11. Cohen, P., *The origins of protein phosphorylation.* Nat Cell Biol, 2002. **4**(5): p. E127-30.
12. Jensen, O.N., *Modification-specific proteomics: characterization of post-translational modifications by mass spectrometry.* Curr Opin Chem Biol, 2004. **8**(1): p. 33-41.
13. Mann, M. and O.N. Jensen, *Proteomic analysis of post-translational modifications.* Nat Biotechnol, 2003. **21**(3): p. 255-61.
14. Yates, S.P., et al., *Stealth and mimicry by deadly bacterial toxins.* Trends Biochem Sci, 2006. **31**(2): p. 123-33.
15. Hottiger, M.O., et al., *Toward a unified nomenclature for mammalian ADP-ribosyltransferases.* Trends Biochem Sci, 2010. **35**(4): p. 208-19.
16. Hottiger, M.O., *Nuclear ADP-Ribosylation and Its Role in Chromatin Plasticity, Cell Differentiation, and Epigenetics.* Annu Rev Biochem, 2015. **84**: p. 227-63.
17. Hassa, P.O. and M.O. Hottiger, *The diverse biological roles of mammalian PARPS, a small but powerful family of poly-ADP-ribose polymerases.* Front Biosci, 2008. **13**: p. 3046-82.
18. Rosenthal, F. and M.O. Hottiger, *Identification of ADP-ribosylated peptides and ADP-ribose acceptor sites.* Front Biosci (Landmark Ed), 2014. **19**: p. 1041-56.
19. Jacobson, E.L., D. Cervantes-Laurean, and M.K. Jacobson, *Glycation of proteins by ADP-ribose.* Mol Cell Biochem, 1994. **138**(1-2): p. 207-12.
20. Seman, M., et al., *Ecto-ADP-ribosyltransferases (ARTs): emerging actors in cell communication and signaling.* Curr Med Chem, 2004. **11**(7): p. 857-72.

21. Vyas, S., et al., *Family-wide analysis of poly(ADP-ribose) polymerase activity.* Nat Commun, 2014. **5**: p. 4426.
22. Marsischky, G.T., B.A. Wilson, and R.J. Collier, *Role of glutamic acid 988 of human poly-ADP-ribose polymerase in polymer formation. Evidence for active site similarities to the ADP-ribosylating toxins.* J Biol Chem, 1995. **270**(7): p. 3247-54.
23. Ame, J.C., C. Spenlehauer, and G. de Murcia, *The PARP superfamily.* Bioessays, 2004. **26**(8): p. 882-93.
24. Schreiber, V., et al., *Poly(ADP-ribose): novel functions for an old molecule.* Nat Rev Mol Cell Biol, 2006. **7**(7): p. 517-28.
25. Kiehlbauch, C.C., et al., *High resolution fractionation and characterization of ADP-ribose polymers.* Anal Biochem, 1993. **208**(1): p. 26-34.
26. Tao, Z., P. Gao, and H.W. Liu, *Identification of the ADP-ribosylation sites in the PARP-1 automodification domain: analysis and implications.* J Am Chem Soc, 2009. **131**(40): p. 14258-60.
27. Alvarez-Gonzalez, R. and M.K. Jacobson, *Characterization of polymers of adenosine diphosphate ribose generated in vitro and in vivo.* Biochemistry, 1987. **26**(11): p. 3218-24.
28. Juarez-Salinas, H., et al., *Poly(ADP-ribose) has a branched structure in vivo.* J Biol Chem, 1982. **257**(2): p. 607-9.
29. Barkauskaite, E., G. Jankevicius, and I. Ahel, *Structures and Mechanisms of Enzymes Employed in the Synthesis and Degradation of PARP-Dependent Protein ADP-Ribosylation.* Mol Cell, 2015. **58**(6): p. 935-46.
30. Cook, B.D., et al., *Role for the related poly(ADP-Ribose) polymerases tankyrase 1 and 2 at human telomeres.* Mol Cell Biol, 2002. **22**(1): p. 332-42.
31. Steffen, J.D., et al., *Structural Implications for Selective Targeting of PARPs.* Front Oncol, 2013. **3**: p. 301.
32. Chi, N.W. and H.F. Lodish, *Tankyrase is a golgi-associated mitogen-activated protein kinase substrate that interacts with IRAP in GLUT4 vesicles.* J Biol Chem, 2000. **275**(49): p. 38437-44.
33. Callow, M.G., et al., *Ubiquitin ligase RNF146 regulates tankyrase and Axin to promote Wnt signaling.* PLoS One, 2011. **6**(7): p. e22595.
34. Loseva, O., et al., *PARP-3 is a mono-ADP-ribosylase that activates PARP-1 in the absence of DNA.* J Biol Chem, 2010. **285**(11): p. 8054-60.
35. Leger, K., et al., *ARTD2 activity is stimulated by RNA.* Nucleic Acids Res, 2014. **42**(8): p. 5072-82.
36. Langelier, M.F., A.A. Riccio, and J.M. Pascal, *PARP-2 and PARP-3 are selectively activated by 5' phosphorylated DNA breaks through an allosteric regulatory mechanism shared with PARP-1.* Nucleic Acids Res, 2014. **42**(12): p. 7762-75.
37. Gagne, J.P., et al., *Proteome-wide identification of poly(ADP-ribose) binding proteins and poly(ADP-ribose)-associated protein complexes.* Nucleic Acids Res, 2008. **36**(22): p. 6959-76.
38. Eustermann, S., et al., *Solution structures of the two PBZ domains from human APLF and their interaction with poly(ADP-ribose).* Nat Struct Mol Biol, 2010. **17**(2): p. 241-3.
39. Ahel, I., et al., *Poly(ADP-ribose)-binding zinc finger motifs in DNA repair/checkpoint proteins.* Nature, 2008. **451**(7174): p. 81-5.

40. Aravind, L., *The WWE domain: a common interaction module in protein ubiquitination and ADP ribosylation.* Trends Biochem Sci, 2001. **26**(5): p. 273-5.
41. Wang, Z., et al., *Recognition of the iso-ADP-ribose moiety in poly(ADP-ribose) by WWE domains suggests a general mechanism for poly(ADP-ribosyl)ation-dependent ubiquitination.* Genes Dev, 2012. **26**(3): p. 235-40.
42. Pehrson, J.R. and V.A. Fried, *MacroH2A, a core histone containing a large nonhistone region.* Science, 1992. **257**(5075): p. 1398-400.
43. Pehrson, J.R. and R.N. Fuji, *Evolutionary conservation of histone macroH2A subtypes and domains.* Nucleic Acids Res, 1998. **26**(12): p. 2837-42.
44. Karras, G.I., et al., *The macro domain is an ADP-ribose binding module.* EMBO J, 2005. **24**(11): p. 1911-20.
45. Allen, M.D., et al., *The crystal structure of AF1521 a protein from Archaeoglobus fulgidus with homology to the non-histone domain of macroH2A.* J Mol Biol, 2003. **330**(3): p. 503-11.
46. Dani, N., et al., *Combining affinity purification by ADP-ribose-binding macro domains with mass spectrometry to define the mammalian ADP-ribosyl proteome.* Proc Natl Acad Sci U S A, 2009. **106**(11): p. 4243-8.
47. Rosenthal, F., et al., *Macrodomain-containing proteins are new mono-ADP-ribosylhydrolases.* Nat Struct Mol Biol, 2013. **20**(4): p. 502-7.
48. Jankevicius, G., et al., *A family of macrodomain proteins reverses cellular mono-ADP-ribosylation.* Nat Struct Mol Biol, 2013. **20**(4): p. 508-14.
49. Min, W. and Z.Q. Wang, *Poly (ADP-ribose) glycohydrolase (PARG) and its therapeutic potential.* Front Biosci (Landmark Ed), 2009. **14**: p. 1619-26.
50. Oka, S., J. Kato, and J. Moss, *Identification and characterization of a mammalian 39-kDa poly(ADP-ribose) glycohydrolase.* J Biol Chem, 2006. **281**(2): p. 705-13.
51. Meyer-Ficca, M.L., et al., *Human poly(ADP-ribose) glycohydrolase is expressed in alternative splice variants yielding isoforms that localize to different cell compartments.* Exp Cell Res, 2004. **297**(2): p. 521-32.
52. Alvarez-Gonzalez, R. and F.R. Althaus, *Poly(ADP-ribose) catabolism in mammalian cells exposed to DNA-damaging agents.* Mutat Res, 1989. **218**(2): p. 67-74.
53. Gao, H., et al., *Altered poly(ADP-ribose) metabolism impairs cellular responses to genotoxic stress in a hypomorphic mutant of poly(ADP-ribose) glycohydrolase.* Exp Cell Res, 2007. **313**(5): p. 984-96.
54. Hengel, S.M. and D.R. Goodlett, *A Review of Tandem Mass Spectrometry Characterization of Adenosine Diphosphate-Ribosylated Peptides.* Int J Mass Spectrom, 2012. **312**: p. 114-121.
55. McLennan, A.G., *The Nudix hydrolase superfamily.* Cell Mol Life Sci, 2006. **63**(2): p. 123-43.
56. Daniels, C.M., et al., *Nudix hydrolases degrade protein-conjugated ADP-ribose.* Sci Rep, 2015. **5**: p. 18271.
57. Mehrotra, P., et al., *PARP-14 functions as a transcriptional switch for Stat6-dependent gene activation.* J Biol Chem, 2011. **286**(3): p. 1767-76.
58. Verheugd, P., et al., *Regulation of NF-kappaB signalling by the mono-ADP-ribosyltransferase ARTD10.* Nat Commun, 2013. **4**: p. 1683.
59. Takata, M., et al., *Homologous recombination and non-homologous end-joining pathways of DNA double-strand break repair have overlapping roles*

in the maintenance of chromosomal integrity in vertebrate cells. EMBO J, 1998. **17**(18): p. 5497-508.
60. O'Driscoll, M. and P.A. Jeggo, *The role of double-strand break repair - insights from human genetics.* Nat Rev Genet, 2006. **7**(1): p. 45-54.
61. Beck, C., et al., *Poly(ADP-ribose) polymerases in double-strand break repair: focus on PARP1, PARP2 and PARP3.* Exp Cell Res, 2014. **329**(1): p. 18-25.
62. Lindahl, T., et al., *Post-translational modification of poly(ADP-ribose) polymerase induced by DNA strand breaks.* Trends Biochem Sci, 1995. **20**(10): p. 405-11.
63. Langelier, M.F., et al., *Structural basis for DNA damage-dependent poly(ADP-ribosyl)ation by human PARP-1.* Science, 2012. **336**(6082): p. 728-32.
64. Haince, J.F., et al., *PARP1-dependent kinetics of recruitment of MRE11 and NBS1 proteins to multiple DNA damage sites.* J Biol Chem, 2008. **283**(2): p. 1197-208.
65. Messner, S. and M.O. Hottiger, *Histone ADP-ribosylation in DNA repair, replication and transcription.* Trends Cell Biol, 2011. **21**(9): p. 534-42.
66. El-Khamisy, S.F., et al., *A requirement for PARP-1 for the assembly or stability of XRCC1 nuclear foci at sites of oxidative DNA damage.* Nucleic Acids Res, 2003. **31**(19): p. 5526-33.
67. Breslin, C., et al., *The XRCC1 phosphate-binding pocket binds poly (ADP-ribose) and is required for XRCC1 function.* Nucleic Acids Res, 2015. **43**(14): p. 6934-44.
68. Haince, J.F., et al., *Ataxia telangiectasia mutated (ATM) signaling network is modulated by a novel poly(ADP-ribose)-dependent pathway in the early response to DNA-damaging agents.* J Biol Chem, 2007. **282**(22): p. 16441-53.
69. Shieh, W.M., et al., *Poly(ADP-ribose) polymerase null mouse cells synthesize ADP-ribose polymers.* J Biol Chem, 1998. **273**(46): p. 30069-72.
70. Menissier de Murcia, J., et al., *Functional interaction between PARP-1 and PARP-2 in chromosome stability and embryonic development in mouse.* EMBO J, 2003. **22**(9): p. 2255-63.
71. de Murcia, J.M., et al., *Requirement of poly(ADP-ribose) polymerase in recovery from DNA damage in mice and in cells.* Proc Natl Acad Sci U S A, 1997. **94**(14): p. 7303-7.
72. Yang, Y.G., et al., *Ablation of PARP-1 does not interfere with the repair of DNA double-strand breaks, but compromises the reactivation of stalled replication forks.* Oncogene, 2004. **23**(21): p. 3872-82.
73. D'Amours, D., et al., *Poly(ADP-ribosyl)ation reactions in the regulation of nuclear functions.* Biochem J, 1999. **342 (Pt 2)**: p. 249-68.
74. Tong, W.M., et al., *Synergistic role of Ku80 and poly(ADP-ribose) polymerase in suppressing chromosomal aberrations and liver cancer formation.* Cancer Res, 2002. **62**(23): p. 6990-6.
75. Menisser-de Murcia, J., et al., *Early embryonic lethality in PARP-1 Atm double-mutant mice suggests a functional synergy in cell proliferation during development.* Mol Cell Biol, 2001. **21**(5): p. 1828-32.
76. Betteridge, D.J., *What is oxidative stress?* Metabolism, 2000. **49**(2 Suppl 1): p. 3-8.

77. Collins, A.R., *Oxidative DNA damage, antioxidants, and cancer.* Bioessays, 1999. **21**(3): p. 238-46.
78. Andersson, A., et al., *PKCalpha and HMGB1 antagonistically control hydrogen peroxide-induced poly-ADP-ribose formation.* Nucleic Acids Res, 2016.
79. Bartolomei, G., et al., *Analysis of Chromatin ADP-Ribosylation at the Genome-wide Level and at Specific Loci by ADPr-ChAP.* Mol Cell, 2016. **61**(3): p. 474-85.
80. Krishnakumar, R., et al., *Reciprocal binding of PARP-1 and histone H1 at promoters specifies transcriptional outcomes.* Science, 2008. **319**(5864): p. 819-21.
81. Chou, D.M., et al., *A chromatin localization screen reveals poly (ADP ribose)-regulated recruitment of the repressive polycomb and NuRD complexes to sites of DNA damage.* Proc Natl Acad Sci U S A, 2010. **107**(43): p. 18475-80.
82. Kim, M.Y., et al., *NAD+-dependent modulation of chromatin structure and transcription by nucleosome binding properties of PARP-1.* Cell, 2004. **119**(6): p. 803-14.
83. Ju, B.G., et al., *Activating the PARP-1 sensor component of the groucho/ TLE1 corepressor complex mediates a CaMKinase IIdelta-dependent neurogenic gene activation pathway.* Cell, 2004. **119**(6): p. 815-29.
84. Bai, P., et al., *PARP-2 regulates SIRT1 expression and whole-body energy expenditure.* Cell Metab, 2011. **13**(4): p. 450-60.
85. Rouleau, M., et al., *A key role for poly(ADP-ribose) polymerase 3 in ectodermal specification and neural crest development.* PLoS One, 2011. **6**(1): p. e15834.
86. Lehmann, M., et al., *ARTD1-induced poly-ADP-ribose formation enhances PPARgamma ligand binding and co-factor exchange.* Nucleic Acids Res, 2015. **43**(1): p. 129-42.
87. Purnell, M.R. and W.J. Whish, *Novel inhibitors of poly(ADP-ribose) synthetase.* Biochem J, 1980. **185**(3): p. 775-7.
88. Wahlberg, E., et al., *Family-wide chemical profiling and structural analysis of PARP and tankyrase inhibitors.* Nat Biotechnol, 2012. **30**(3): p. 283-8.
89. Papeo, G., et al., *Poly(ADP-ribose) polymerase inhibition in cancer therapy: are we close to maturity?* Expert Opin Ther Pat, 2009. **19**(10): p. 1377-400.
90. Kaelin, W.G., Jr., *The concept of synthetic lethality in the context of anticancer therapy.* Nat Rev Cancer, 2005. **5**(9): p. 689-98.
91. Ashworth, A., *A synthetic lethal therapeutic approach: poly(ADP) ribose polymerase inhibitors for the treatment of cancers deficient in DNA double-strand break repair.* J Clin Oncol, 2008. **26**(22): p. 3785-90.
92. Murai, J., et al., *Trapping of PARP1 and PARP2 by Clinical PARP Inhibitors.* Cancer Res, 2012. **72**(21): p. 5588-99.
93. Hopkins, T.A., et al., *Mechanistic Dissection of PARP1 Trapping and the Impact on In Vivo Tolerability and Efficacy of PARP Inhibitors.* Mol Cancer Res, 2015. **13**(11): p. 1465-77.
94. Bai, P., et al., *PARP-1 inhibition increases mitochondrial metabolism through SIRT1 activation.* Cell Metab, 2011. **13**(4): p. 461-8.
95. Devic, S., *Warburg Effect - a Consequence or the Cause of Carcinogenesis?* J Cancer, 2016. **7**(7): p. 817-22.

96. Mouchiroud, L., R.H. Houtkooper, and J. Auwerx, *NAD(+) metabolism: a therapeutic target for age-related metabolic disease.* Crit Rev Biochem Mol Biol, 2013. **48**(4): p. 397-408.
97. Farmer, H., et al., *Targeting the DNA repair defect in BRCA mutant cells as a therapeutic strategy.* Nature, 2005. **434**(7035): p. 917-21.
98. Bryant, H.E., et al., *Specific killing of BRCA2-deficient tumours with inhibitors of poly(ADP-ribose) polymerase.* Nature, 2005. **434**(7035): p. 913-7.
99. Helleday, T., *PARP inhibitor receives FDA breakthrough therapy designation in castration resistant prostate cancer: beyond germline BRCA mutations.* Ann Oncol, 2016. **27**(5): p. 755-7.
100. Chen, S. and G. Parmigiani, *Meta-analysis of BRCA1 and BRCA2 penetrance.* J Clin Oncol, 2007. **25**(11): p. 1329-33.
101. Risch, H.A., et al., *Prevalence and penetrance of germline BRCA1 and BRCA2 mutations in a population series of 649 women with ovarian cancer.* Am J Hum Genet, 2001. **68**(3): p. 700-10.
102. Alsop, K., et al., *BRCA mutation frequency and patterns of treatment response in BRCA mutation-positive women with ovarian cancer: a report from the Australian Ovarian Cancer Study Group.* J Clin Oncol, 2012. **30**(21): p. 2654-63.
103. Lim, D. and J. Ngeow, *Evaluation of the methods to identify patients who may benefit from PARP inhibitor use.* Endocr Relat Cancer, 2016. **23**(6): p. R267-85.
104. Rajan, A., et al., *A phase I combination study of olaparib with cisplatin and gemcitabine in adults with solid tumors.* Clin Cancer Res, 2012. **18**(8): p. 2344-51.
105. Khan, O.A., et al., *A phase I study of the safety and tolerability of olaparib (AZD2281, KU0059436) and dacarbazine in patients with advanced solid tumours.* Br J Cancer, 2011. **104**(5): p. 750-5.
106. Dent, R.A., et al., *Phase I trial of the oral PARP inhibitor olaparib in combination with paclitaxel for first- or second-line treatment of patients with metastatic triple-negative breast cancer.* Breast Cancer Res, 2013. **15**(5): p. R88.
107. Bajrami, I., et al., *Synthetic lethality of PARP and NAMPT inhibition in triple-negative breast cancer cells.* EMBO Mol Med, 2012. **4**(10): p. 1087-96.
108. Sistigu, A., et al., *Trial watch - inhibiting PARP enzymes for anticancer therapy.* Mol Cell Oncol, 2016. **3**(2): p. e1053594.
109. Kahn, P., *From genome to proteome: looking at a cell's proteins.* Science, 1995. **270**(5235): p. 369-70.
110. Zhang, Y., et al., *Protein analysis by shotgun/bottom-up proteomics.* Chem Rev, 2013. **113**(4): p. 2343-94.
111. Perkins, D.N., et al., *Probability-based protein identification by searching sequence databases using mass spectrometry data.* Electrophoresis, 1999. **20**(18): p. 3551-67.
112. Cox, J., et al., *Andromeda: a peptide search engine integrated into the MaxQuant environment.* J Proteome Res, 2011. **10**(4): p. 1794-805.
113. Cristobal, A., et al., *In-house construction of a UHPLC system enabling the identification of over 4000 protein groups in a single analysis.* Analyst, 2012. **137**(15): p. 3541-8.

114. Hebert, A.S., et al., *The one hour yeast proteome.* Mol Cell Proteomics, 2014. **13**(1): p. 339-47.
115. Okayama, H., K. Ueda, and O. Hayaishi, *Purification of ADP-ribosylated nuclear proteins by covalent chromatography on dihydroxyboryl polyacrylamide beads and their characterization.* Proc Natl Acad Sci U S A, 1978. **75**(3): p. 1111-5.
116. Hottiger, M.O., *ADP-ribosylation of histones by ARTD1: an additional module of the histone code?* FEBS Lett, 2011. **585**(11): p. 1595-9.
117. Zhang, Y., et al., *Site-specific characterization of the Asp- and Glu-ADP-ribosylated proteome.* Nat Methods, 2013. **10**(10): p. 981-4.
118. Rosenqvist, H., J. Ye, and O.N. Jensen, *Analytical strategies in mass spectrometry-based phosphoproteomics.* Methods Mol Biol, 2011. **753**: p. 183-213.
119. Matic, I., I. Ahel, and R.T. Hay, *Reanalysis of phosphoproteomics data uncovers ADP-ribosylation sites.* Nat Methods, 2012. **9**(8): p. 771-2.
120. Daniels, C.M., S.E. Ong, and A.K. Leung, *Phosphoproteomic approach to characterize protein mono- and poly(ADP-ribosyl)ation sites from cells.* J Proteome Res, 2014. **13**(8): p. 3510-22.
121. Jungmichel, S., et al., *Proteome-wide identification of poly(ADP-Ribosyl)ation targets in different genotoxic stress responses.* Mol Cell, 2013. **52**(2): p. 272-85.
122. Zhang, J., *Use of biotinylated NAD to label and purify ADP-ribosylated proteins.* Methods Enzymol, 1997. **280**: p. 255-65.
123. Jiang, H., et al., *Clickable NAD analogues for labeling substrate proteins of poly(ADP-ribose) polymerases.* J Am Chem Soc, 2010. **132**(27): p. 9363-72.
124. Gibson, B.A., et al., *Chemical genetic discovery of PARP targets reveals a role for PARP-1 in transcription elongation.* Science, 2016. **353**(6294): p. 45-50.
125. Rosenthal, F., et al., *Optimization of LTQ-Orbitrap Mass Spectrometer Parameters for the Identification of ADP-Ribosylation Sites.* J Proteome Res, 2015. **14**(9): p. 4072-9.
126. Tao, W.A. and R. Aebersold, *Advances in quantitative proteomics via stable isotope tagging and mass spectrometry.* Curr Opin Biotechnol, 2003. **14**(1): p. 110-8.
127. Hunter, T.C., et al., *Peptide mass mapping constrained with stable isotope-tagged peptides for identification of protein mixtures.* Anal Chem, 2001. **73**(20): p. 4891-902.
128. Munchbach, M., et al., *Quantitation and facilitated de novo sequencing of proteins by isotopic N-terminal labeling of peptides with a fragmentation-directing moiety.* Anal Chem, 2000. **72**(17): p. 4047-57.
129. Ong, S.E., et al., *Stable isotope labeling by amino acids in cell culture, SILAC, as a simple and accurate approach to expression proteomics.* Mol Cell Proteomics, 2002. **1**(5): p. 376-86.
130. Gygi, S.P., et al., *Quantitative analysis of complex protein mixtures using isotope-coded affinity tags.* Nat Biotechnol, 1999. **17**(10): p. 994-9.
131. Choe, L., et al., *8-plex quantitation of changes in cerebrospinal fluid protein expression in subjects undergoing intravenous immunoglobulin treatment for Alzheimer's disease.* Proteomics, 2007. **7**(20): p. 3651-60.

132. Oda, Y., T. Nagasu, and B.T. Chait, *Enrichment analysis of phosphorylated proteins as a tool for probing the phosphoproteome.* Nat Biotechnol, 2001. **19**(4): p. 379-82.
133. Goshe, M.B., et al., *Phosphoprotein isotope-coded affinity tag approach for isolating and quantitating phosphopeptides in proteome-wide analyses.* Anal Chem, 2001. **73**(11): p. 2578-86.
134. Bakalarski, C.E. and D.S. Kirkpatrick, *A Biologist's Field Guide to Multiplexed Quantitative Proteomics.* Mol Cell Proteomics, 2016. **15**(5): p. 1489-97.
135. Clough, T., et al., *Statistical protein quantification and significance analysis in label-free LC-MS experiments with complex designs.* BMC Bioinformatics, 2012. **13 Suppl 16**: p. S6.
136. Griffin, N.M., et al., *Label-free, normalized quantification of complex mass spectrometry data for proteomic analysis.* Nat Biotechnol, 2010. **28**(1): p. 83-9.
137. Cox, J., et al., *Accurate proteome-wide label-free quantification by delayed normalization and maximal peptide ratio extraction, termed MaxLFQ.* Mol Cell Proteomics, 2014. **13**(9): p. 2513-26.
138. Hu, A., W.S. Noble, and A. Wolf-Yadlin, *Technical advances in proteomics: new developments in data-independent acquisition.* F1000Res, 2016. **5**.
139. Lesur, A. and B. Domon, *Advances in high-resolution accurate mass spectrometry application to targeted proteomics.* Proteomics, 2015. **15**(5-6): p. 880-90.
140. Domon, B. and R. Aebersold, *Options and considerations when selecting a quantitative proteomics strategy.* Nat Biotechnol, 2010. **28**(7): p. 710-21.
141. Wolf-Yadlin, A., et al., *Multiple reaction monitoring for robust quantitative proteomic analysis of cellular signaling networks.* Proc Natl Acad Sci U S A, 2007. **104**(14): p. 5860-5.
142. Yost, R.A. and C.G. Enke, *Triple quadrupole mass spectrometry for direct mixture analysis and structure elucidation.* Anal Chem, 1979. **51**(12): p. 1251-64.
143. Stahl-Zeng, J., et al., *High sensitivity detection of plasma proteins by multiple reaction monitoring of N-glycosites.* Mol Cell Proteomics, 2007. **6**(10): p. 1809-17.
144. Lange, V., et al., *Selected reaction monitoring for quantitative proteomics: a tutorial.* Mol Syst Biol, 2008. **4**: p. 222.
145. Titz, B., et al., *Proteomics for systems toxicology.* Comput Struct Biotechnol J, 2014. **11**(18): p. 73-90.
146. Cox, D.M., et al., *Multiple reaction monitoring as a method for identifying protein posttranslational modifications.* J Biomol Tech, 2005. **16**(2): p. 83-90.
147. Lill, J., *Proteomic tools for quantitation by mass spectrometry.* Mass Spectrom Rev, 2003. **22**(3): p. 182-94.
148. Sherman, J., et al., *How specific is my SRM?: The issue of precursor and product ion redundancy.* Proteomics, 2009. **9**(5): p. 1120-3.
149. Peterson, A.C., et al., *Parallel reaction monitoring for high resolution and high mass accuracy quantitative, targeted proteomics.* Mol Cell Proteomics, 2012. **11**(11): p. 1475-88.

150. Tsuchiya, H., K. Tanaka, and Y. Saeki, *The parallel reaction monitoring method contributes to a highly sensitive polyubiquitin chain quantification.* Biochem Biophys Res Commun, 2013. **436**(2): p. 223-9.
151. Tang, H., et al., *Multiplexed parallel reaction monitoring targeting histone modifications on the QExactive mass spectrometer.* Anal Chem, 2014. **86**(11): p. 5526-34.
152. Gagne, J.P., et al., *Quantitative site-specific ADP-ribosylation profiling of DNA-dependent PARPs.* DNA Repair (Amst), 2015. **30**: p. 68-79.
153. Martello, R., et al., *Proteome-wide identification of the endogenous ADP-ribosylome of mammalian cells and tissue.* Nature Communications, in press, 2016.
154. Messner, S., et al., *PARP1 ADP-ribosylates lysine residues of the core histone tails.* Nucleic Acids Res, 2010. **38**(19): p. 6350-62.
155. Bilan, V., et al., *Combining HCD and EThcD fragmentations in a product dependent manner provides in-depth characterization of the cellular ADP-ribosylome* manuscript submitted, 2016.
156. Bilan, V., et al., *Quantitative analysis of protein ADP-ribosylated during oxidative stress by a label-free PRM approach.* manuscript submitted, 2016.
157. Leutert, M., D.M. Pedrioli, and M.O. Hottiger, *Identification of PARP-Specific ADP-Ribosylation Targets Reveals a Regulatory Function for ADP-Ribosylation in Transcription Elongation.* Mol Cell, 2016. **63**(2): p. 181-3.
158. Tabb, D.L., et al., *Repeatability and reproducibility in proteomic identifications by liquid chromatography-tandem mass spectrometry.* J Proteome Res, 2010. **9**(2): p. 761-76.
159. Ray Chaudhuri, A., et al., *Poly(ADP-ribosyl) glycohydrolase prevents the accumulation of unusual replication structures during unperturbed S phase.* Mol Cell Biol, 2015. **35**(5): p. 856-65.
160. Martello, R., et al., *Proteome-wide identification of the endogenous ADP-ribosylome of mammalian cells and tissue.* Nature Communications, 2016. **in press**.
161. Kistemaker, H.A., et al., *Synthesis and Macrodomain Binding of Mono-ADP-Ribosylated Peptides.* Angew Chem Int Ed Engl, 2016. **55**(36): p. 10634-8.
162. Cooke, M.S., et al., *Oxidative DNA damage: mechanisms, mutation, and disease.* FASEB J, 2003. **17**(10): p. 1195-214.
163. Smith, J.A., et al., *Oxidative stress, DNA damage, and the telomeric complex as therapeutic targets in acute neurodegeneration.* Neurochem Int, 2013. **62**(5): p. 764-75.
164. Endres, M., et al., *Ischemic brain injury is mediated by the activation of poly(ADP-ribose)polymerase.* J Cereb Blood Flow Metab, 1997. **17**(11): p. 1143-51.
165. Rabenau, K. and E. Hofstatter, *DNA Damage Repair and the Emerging Role of Poly(ADP-ribose) Polymerase Inhibition in Cancer Therapeutics.* Clin Ther, 2016.
166. Strimbu, K. and J.A. Tavel, *What are biomarkers?* Curr Opin HIV AIDS, 2010. **5**(6): p. 463-6.
167. Sajic, T., Y. Liu, and R. Aebersold, *Using data-independent, high-resolution mass spectrometry in protein biomarker research: perspectives and clinical applications.* Proteomics Clin Appl, 2015. **9**(3-4): p. 307-21.

168. Huttenhain, R., et al., *Reproducible quantification of cancer-associated proteins in body fluids using targeted proteomics.* Sci Transl Med, 2012. **4**(142): p. 142ra94.
169. Issaq, H.J., Z. Xiao, and T.D. Veenstra, *Serum and plasma proteomics.* Chem Rev, 2007. **107**(8): p. 3601-20.
170. Zolotarjova, N., et al., *Differences among techniques for high-abundant protein depletion.* Proteomics, 2005. **5**(13): p. 3304-13.
171. Kistemaker, H.A., et al., *Stereoselective ribosylation of amino acids.* Org Lett, 2013. **15**(9): p. 2306-9.
172. Gillet, L.C., et al., *Targeted data extraction of the MS/MS spectra generated by data-independent acquisition: a new concept for consistent and accurate proteome analysis.* Mol Cell Proteomics, 2012. **11**(6): p. O111 016717.
173. Carvalho, P.C., et al., *XDIA: improving on the label-free data-independent analysis.* Bioinformatics, 2010. **26**(6): p. 847-8.
174. Luo, X. and W.L. Kraus, *On PAR with PARP: cellular stress signaling through poly(ADP-ribose) and PARP-1.* Genes Dev, 2012. **26**(5): p. 417-32.
175. Slade, D., et al., *The structure and catalytic mechanism of a poly(ADP-ribose) glycohydrolase.* Nature, 2011. **477**(7366): p. 616-20.
176. Lipovsek, D. and A. Pluckthun, *In-vitro protein evolution by ribosome display and mRNA display.* J Immunol Methods, 2004. **290**(1-2): p. 51-67.
177. Vivelo, C.A., et al., *ADPriboDB: The database of ADP-ribosylated proteins.* Nucleic Acids Res, 2016.
178. Kirkpatrick, D.S., C. Denison, and S.P. Gygi, *Weighing in on ubiquitin: the expanding role of mass-spectrometry-based proteomics.* Nat Cell Biol, 2005. **7**(8): p. 750-7.
179. Hutti, J.E., et al., *A rapid method for determining protein kinase phosphorylation specificity.* Nat Methods, 2004. **1**(1): p. 27-9.
180. Azevedo, C. and A. Saiardi, *Why always lysine? The ongoing tale of one of the most modified amino acids.* Adv Biol Regul, 2016. **60**: p. 144-50.
181. Bauer, P.I., et al., *Inhibition of DNA binding by the phosphorylation of poly ADP-ribose polymerase protein catalysed by protein kinase C.* Biochem Biophys Res Commun, 1992. **187**(2): p. 730-6.
182. Hasan, S., et al., *Regulation of human flap endonuclease-1 activity by acetylation through the transcriptional coactivator p300.* Mol Cell, 2001. **7**(6): p. 1221-31.
183. DaRosa, P.A., et al., *Allosteric activation of the RNF146 ubiquitin ligase by a poly(ADP-ribosyl)ation signal.* Nature, 2015. **517**(7533): p. 223-6.
184. Zhou, Z.D., et al., *Ring finger protein 146/Iduna is a poly(ADP-ribose) polymer binding and PARsylation dependent E3 ubiquitin ligase.* Cell Adh Migr, 2011. **5**(6): p. 463-71.
185. Yan, Q., et al., *BAL1 and its partner E3 ligase, BBAP, link Poly(ADP-ribose) activation, ubiquitylation, and double-strand DNA repair independent of ATM, MDC1, and RNF8.* Mol Cell Biol, 2013. **33**(4): p. 845-57.
186. Qiu, J., et al., *Ubiquitination independent of E1 and E2 enzymes by bacterial effectors.* Nature, 2016. **533**(7601): p. 120-4.
187. Forst, A.H., et al., *Recognition of mono-ADP-ribosylated ARTD10 substrates by ARTD8 macrodomains.* Structure, 2013. **21**(3): p. 462-75.

ACKNOWLEDGMENTS

First of all, I would like to thank Prof. Michael Hottiger for provided this excellent opportunity to work on this challenging interdisciplinary project. My committee members Prof. Bernd Wollscheid, Prof. Gerard Hopfgartner, and Prof. Thierry Hennet, whose advices and ideas contributed a lot to the project development. I also want to thank Prof. Myron Jacobson, who kindly agreed to review this thesis. Additionally, I am grateful to Dr. Stephan Christian for the editorial support and to Dr. Deena Leslie Pedrioli for her great help with revising the manuscripts in very tight deadlines.

Special thanks to the team of FGCZ, specifically to Dr. Paolo Nanni and Dr. Natalie Selevsek for their technical support during the entire project and high tolerance toward our not always ideal samples.

Thanks to the Hottiger group, all new and old members. It was always fun to work with you, to discuss science during our productive group meetings, and to have group outings. Special thanks to Dr.Florian Rosenthal and Mario Leutert for making a task “to hack ADP-ribosylome” a bit easier and way more fun. Also, thanks to all DMMD and CABMM members for an amazing working environment.

A big thank goes to Jeannette Abplanalp for an incredible support in all aspects of my life, for always being ready to help and for all the crazy time we spend together at work and outside. Thanks to my scientific “baby” Roxane Feurer for her humor and endless energy, which were always able to make me laugh. Another big thank goes to Dr. Ali Mirsaidi. His incredible optimism always calmed down my worries. The great support during my PhD time was coming from my friends in Germany and Russia. They always had time to talk to me, to travel with me and they always believed in my success.

Finally, the special gratitude and love go to my family. Their constant support motivated me to go and try all my ideas. All of these is only possible because I knew they would always be by my side.

CURRICULUM VITAE

Personal information

Surname:	BILAN
Name:	Vera
Address:	Hugostrasse 2, CH-8050 Zurich
Phone:	+41-78 832 6567
Email:	vera.bilan@uzh.ch
Date of Birth:	2nd October 1986
Place of Birth:	Arkhangelsk, Russian Federation
Nationality:	Russian

Education

November 2012 – present **Doctoral Studies in Molecular Biology**

- Department of Molecular Mechanisms of Diseases, University of Zürich, Switzerland
- Ph.D Program in Molecular Life Sciences, LSZGS
- Thesis title: "Mass Spectrometry-Based Methods for Analyzing Oxidative Stress-Mediated Cellular ADP-Ribosylation"

September 2009 – September 2011 **Master of Science**

- Humboldt University, Charite Berlin, Germany
- Field of study: Molecular Medicine
- Degree: Master of Science
- Thesis title: "Molecular mechanisms of embryonic and adult cardiac stress response"

September 2003 – July 2009 **Diploma**

- Northern State Medical University, Russia
- Field of study: Biochemistry
- Degree: Diploma
- Diploma title: „Genetic variants in disturbances of β oxidation of fatty acids"

September 2001 – June 2003 **Secondary School**

- Gymnasium of general secondary education №6, Arkhangelsk, Russia